# Decadal to Interdecadal Variability of the North Atlantic Oscillation: A Paleoclimatic Index Reconstruction

Dissertation
zur Erlangung des Doktorgrades
der Mathematisch-Naturwissenschaftlichen Fakultät
der Christian-Albrechts-Universität
vorgelegt von

Oliver Timm


Kiel 2003

Referent: .....

Korreferent: .....

Tag der mündlichen Prüfung: .....

Zum Druck genehmigt: .....

# Contents

# Zusammenfassung

In dieser Arbeit wird der Winter-Index der Nordatlantischen Oszillation (NAO) mit Hilfe von paläoklimatischen Daten erweitert. Der Schwerpunkt liegt dabei auf der niederfrequenten (dekadischen und interdekadischen) Variabilität. Dieser Frequenzbereich ist in doppelter Hinsicht von besonderem Interesse für die Klimaforschung. Zum einen ist die dekadische und interdekadische Variabilität der NAO wichtig für das Verständnis der Wechselwirkung zwischen der Atmosphäre außerhalb der Tropen und den Ozeanen. Zum anderen bedarf es einer Abschätzung der natürlichen Variabilität, um vom Menschen hervorgerufene Klimaschwankungen in dem niederfrequenten Frequenzspektrum der NAO zu erfassen.

Es existieren zahlreiche natürliche Archive über die Geschichte des Erdklimas. Diese Archive enthalten sogenannte Proxy-Daten mit einer jährlichen, teils noch höheren Auflösung. In der vorliegenden Arbeit werden Isotopenkonzentrationen und Akkumulationsraten aus Eiskernen sowie Zeitreihen der Jahresringweiten von Bäumen genutzt. Diese Proxies stellen die Basis zur Rekonstruktion des NAO-Indexes dar. Die Untersuchung der Beziehungen zwischen den Proxies und der NAO verdeutlicht, dass komplexe Zusammenhänge zwischen den Proxies und den lokalen Klimaverhältnissen bestehen können. Da ferner die Beziehung zwischen den lokalen Klimaverhältnissen und der NAO durch stochastisches Rauschen überlagert wird, ist es erforderlich das NAO-Signal mittels statistischer Rekonstruktionsansätze zurückzugewinnen.

Die genauere statistische Betrachtung des Rekonstruktionsproblems geht auf die einzelnen Aspekte der statistischen Rekonstruktion ein. Nachfolgend werden zwei Strategien vorgestellt, die die Rekonstruktion auf dekadischen und interdekadischen Zeitskalen erlauben. Bei der ersten Methode wird den Standardverfahren folgend der NAO-Index zuerst aus ungefilterten Daten rekonstruiert und anschließend gefiltert. Die zweite Strategie besteht darin, erst die inter-/dekadischen Zeitskalen durch Filtern aus den Daten zu erhalten. Dadurch fließt in dieser NAO-Index Rekonstruktion ausschließlich die Proxy-NAO Beziehung der (inter-)dekadischen Zeitskalen ein. Weiterhin werden verschiedene Rekonstruktionsmethoden verglichen: die Hauptkomponenten-Regression, die Methode des besten unverzerrten linearen Schätzers und die Regression über gewichtete Mittelwerte. Letztere wird in dieser Studie entwickelt und es wird gezeigt, dass diese eine geeignete Methode für die NAO-Index Rekonstruktion ist.

Die dekadische Variabilität wird für den Zeitraum 1700–1978 mit grönländischen Eiskern-Proxies und den Jahresringweiten europäischer Bäume rekonstruiert. Die Rekonstruktion, in der zuvor gefilterte Daten verwendet werden, übertrifft dabei in ihrer Güte die der nachträglich gefilterten Rekonstruktion. Beim Vergleich mit zwei unabhängigen Rekonstruktionen anderer Forschergruppen zeigt sich, dass trotz der erfolgreichen Verifikation systematische Unterschiede zwischen den Rekonstruktionen im frühen 18. Jahrhundert bestehen. Die Ergebnisse deuten darauf hin, dass im Nordatlantik-Sektor anomale Muster in der atmosphärischen Variabilität im frühen 18. Jahrhundert auftraten, die in dieser Art nicht im 19. sowie bis Mitte des 20. Jahrhunderts auftraten. Die Variabilität war in der Anfangsphase des 18. Jahrhunderts wahrscheinlich durch solaren Antrieb und vulkanische Aktivität verstärkt worden.

Die interdekadische Variabilität wird für den Zeitraum 1623–1966 rekonstruiert, wobei ein Netz von Proxy-Daten bestehend aus Eiskernen von Grönland und Kanada sowie Baumringzeitreihen aus Europa, Nordafrika und Nordamerika verwendet wird. Dabei wird deutlich, dass die Rekonstruktion basierend auf vorgefilterten Daten gegenüber der nachträglich gefilterten Rekonstruktion ihre Vorteile aufgrund des eingeschränkten Stichprobenumfangs einbüßt. Ein Vergleich der hier erstellten Rekonstruktion mit unabhängigen Rekonstruktionen deckt signifikante Unterschiede auf. Jedoch zeigen alle drei Rekonstruktionen eine verstärkte Variabilität auf Skalen von 32–64 Jahren

während des 17. und frühen 18. Jahrhunderts. Falls weitere Anzeichen gefunden werden, die diese Resultate bestätigen, dann läge der Trend des NAO Indexes von negativen Werten in den 1960/70er Jahren zu anhaltend positiven seit den 80ern im Bereich der natürlichen Klimavariabilität.

# Abstract

The study aims to extend the wintertime index of the North Atlantic Oscillation (NAO) using paleoclimatic data. The primary interest lies in the low-frequent (decadal and interdecadal) variability. Two reasons should be mentioned to stress the importance of this frequency band for climate research. First, decadal and interdecadal NAO variability is important for the understanding of coupling mechanisms between the extratropical atmosphere and the oceans. Second, estimates of preindustrial natural variability are important for detecting anthropogenically induced climate changes in the low-frequency spectrum of the NAO.

Various natural archives of the earth's climate history exist, which provide so-called proxy data with annual to subannual temporal resolution. In this study isotopic concentrations and accumulation rates measured in ice cores, and tree-ring widths chronologies form the proxy basis for the reconstruction of the NAO index. The relationships between these types of proxies and the NAO are investigated. It is reasoned that complex relations between the proxies and the climate at the proxies' locations exist. Since the linkage between the local climate factors and the NAO is obscured by stochastic noise, statistical reconstruction methods are required to recover the NAO signal.

The statistical treatment of the reconstruction problem is discussed in detail. Two different reconstruction strategies are presented for the decadal to interdecadal time scales. The first follows the standard procedures and reconstructs the NAO index from unfiltered data. The reconstructed NAO index is filtered afterwards (post-filtered reconstruction). The second pre-filters the data on the (inter-)decadal time scales. Thus, the latter NAO index reconstruction is exclusively based on the proxy-NAO relationships in the (inter-)decadal range of variability. Different reconstruction methods are compared with each other: the principal component regression, the best linear unbiased estimate, and the weighted average regression. The latter is developed in this study. It is shown that the weighted average regression is an adequate method for the NAO index reconstruction.

The decadal variability is reconstructed over the period 1700–1978 using ice-core proxies from Greenland and European tree-ring width data. It is found that the pre-filtered reconstruction is statistically more skillful than the post-filtered index. The reconstruction is compared with two independent reconstructions of other research groups. Despite the successful verification of the reconstructions, systematic differences exist among the reconstructions in the early 18th century. The results hint at an anomalous pattern of atmospheric variability in the North Atlantic sector in the early 18th century; a pattern which was not observed in the 19th to mid-20th century. In the early 18th century the magnitude of the variance was probably increased by solar or volcanic forcing, but the uncertainty in the estimates is too large for a quantitative analysis.

The interdecadal (16–64 years) variability is reconstructed over the period 1623–1966. The used multiproxy data set includes ice cores from Greenland and Canada, and tree-ring width chronologies from Europe, North Africa and North America. It is shown that the pre-filtering reconstruction loses its advantages over the post-filtering on interdecadal time scales due to sampling limitations. The comparison with the independent reconstructions reveals that the reconstruction of this study is significantly different. However, the three reconstructions indicate an increased 32–64 year variability in the 17th and early 18th century. If further indicators supported these findings, then the recent trend in the NAO index, from negative values in the 1960-70s to prolonged positive values since the 1980s, would be in the range of natural variability.

# Acronyms

| | |
|---|---|
| AR(1) | Auto-regressive [process] of order 1 |
| BB | British Isles and Belgium [proxy data set] |
| BLUE | Best Linear Unbiased Estimate |
| CET | Central England Temperature |
| CGCM | Coupled General Circulation Model |
| CLIVAR | Climate Variability and Predictability |
| CO6 | Coiflet filter of width 6 |
| DJFM | December, January, February, March |
| ECMWF | European Centre for Medium-Range Weather Forecasts |
| EOF | Empirical Orthogonal Function |
| EUR | Europe inclusive Morroco [proxy data set] |
| FT | Fourier Transform |
| GCM | General Circulation Model |
| GISP2 | Greenland Ice Sheet Project Two |
| GR | Greenland [proxy data set] |
| GRIP | Greenland Ice Core Project |
| IICC | International Ice-Core Cooperative |
| ITRDB | International Tree Ring Data Bank |
| JFM | January, February, March |
| LA8 | Least Asymmetric filter of width 8 |
| MLR | Multiple Linear Regression |
| MOC | Meridional Overturning Circulation |
| MODWT | Maximum Overlap Discrete Wavelet Transform |
| NA | North America [proxy data set] |
| NAO | North Atlantic Oscillation |
| NCAR | National Center of Atmospheric Research |
| NCEP | National Centers for Environmental Prediction |
| NDJFM | November, December, January, February, March |
| PC | Principal Component |
| PCA | Principal Component Analysis |
| PCR | Principal Component Regression |
| PDF | Probability Density Function |
| PDSI | Palmer Drought Severity Index |
| S3 | Scale [coefficients] of level 3 |
| SLP | Sea Level Pressure |
| S/N | Signal-to-Noise |
| SP | Spain [proxy data set] |
| SSD | Sum of Squared Differences |
| SST | Sea Surface Temperature |
| STDDEV | Standard Deviation |
| THC | Thermohaline Circulation |
| W3, W4, W5 | Wavelet [coefficients] of level 3, 4, 5 |
| WAVER | Weighted Average Regression |
| WDC | World Data Center |

# List of Figures

# List of Tables

# Chapter 1

# Introduction

An increasing body of evidence indicates that human activity influences the world's climate. The observed warming of the surface temperature over the last 50 years is very likely attributable to human activities (Houghton et al., 2001). Climate models result in an increase in global surface temperatures of 1.4–5.8 K over the next century. However, there is less agreement concerning the changes in the variability of the natural modes in the coupled ocean-atmosphere system. Although much efforts have been put into the development of climate models, the models' credibility relies on their successful validation against observational evidence. Most observational records are too short for a faithful validation on time scales relevant to climate change studies. On decadal to century time scales, paleoclimatic data provide invaluable information for the understanding of natural climate variability (CLIVAR, 1997). This study is a contribution towards a deeper understanding of the natural climate variability over the last 300 to 400 years. The particular climate phenomenon to be investigated is the North Atlantic Oscillation.

Variations of the North Atlantic climate are orchestrated by two major actors during the boreal winter season: the Iceland low and the Azores high. The Iceland low and Azores high have long been known for their synchronous intensification and weakening, termed 'North Atlantic Oscillation' (NAO) (Walker, 1924; Walker and Bliss, 1932). It is well documented that the NAO dominates the winter climate variability over the North Atlantic and its surrounding continents (Hurrell and van Loon, 1997). For example, over the North Atlantic the strength of the zonal wind depends on the intensity of the pressure gradient between both systems. In the case of large gradients, the intensified zonal winds advect more heat and moisture towards northern Europe. Mild and wet winters accompany the strong zonal winds. At the same time, cyclones less frequently move into the Mediterranean area, and dry winters prevail in southern Europe and northern Africa. In North America and Greenland, anomalies in temperature and precipitation are also related to the NAO (see Fig. 1.1). The atmospheric changes accompanying the NAO also drive variability patterns in the North Atlantic Ocean. The strength of the wind controls the exchange of heat and momentum (and in parts the fresh water flux, which is given by the evaporation and precipitation) between ocean and atmosphere [see also the reviews of Marshall et al. (2001) and Visbeck et al. (2003)].

Despite these well-known facts, the dynamics of the NAO are not well understood. Especially, the behaviour in the low-frequency range and the question what causes the variability on time scales longer than 10 years is subject to intense debates (Greatbatch, 2000; Delworth and Greatbatch, 2000; Wanner et al., 2001; Marshall et al., 2001). The overall spectral characteristics of the

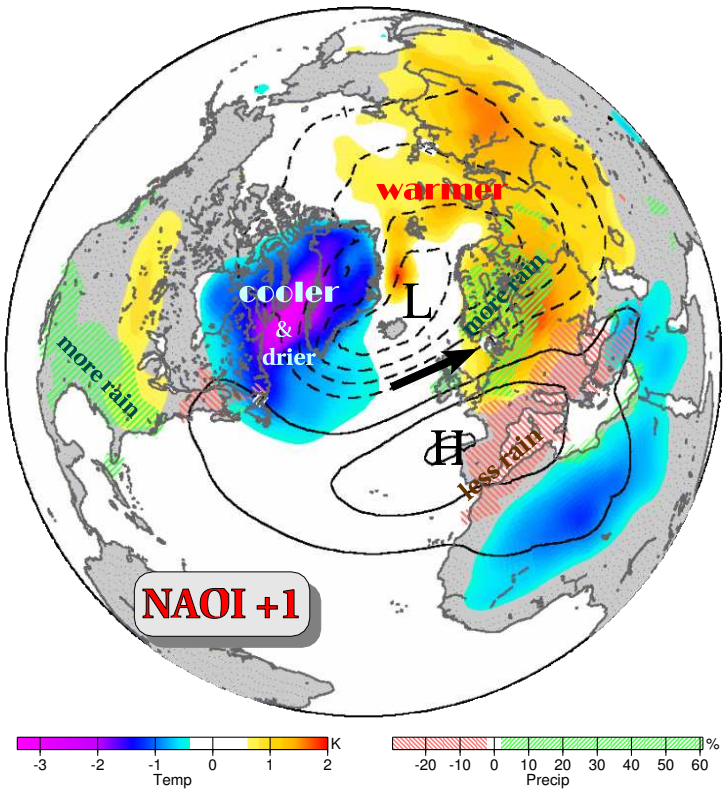


Figure 1.1: *Illustration of the wintertime climate anomalies associated with a positive (+1 standard deviation) NAO index: sea level pressure (contours in hPa), air temperature (colours), and precipitation (hatched areas). Note that a negative NAO index is associated with the same pattern but signs reversed.*

NAO index[1], defined as the difference between the normalised pressure anomalies of the southern high and northern low [see Jones et al. (1997), Hurrell (1995), Rogers (1984) for definitions], are consistent with a weakly red spectrum. However, in the late 20th century the NAO spectrum approached a red spectrum with an enhancement of the low-frequency variability (Hurrell and van Loon, 1997; Jung, 2000; Pozo-Vázquez et al., 2001). A lot of attention has been paid to the recent trend from a negative to a prolonged positive NAO index (Fig. 1.2), which contributed to the observed increase of temperatures in northern Europe (Hurrell, 1996). There is an ongoing discussion whether this trend is an early indication of anthropogenic greenhouse gas warming (Gillett et al., 2000; Feldstein, 2002; Gillett et al., 2003). A clear solution to this question is difficult to obtain due to limited sampling (Wunsch, 1999). At the moment, climate model simulations provide the best possibility to address this important issue (Osborn et al., 1999; Paeth et al., 1999; Gillett et al., 2003). State-of-the-art coupled ocean-atmosphere general circulation models (CGCM) show a significant difference between unforced (control) runs and anthropogenic greenhouse warming scenarios. However, an extended comparison between observed and modelled low-frequency NAO variability is needed to assess the credibility of the modelling results.

[1]A positive NAO index means a large pressure difference and thus strong zonal winds and mild winters in northern Europe.

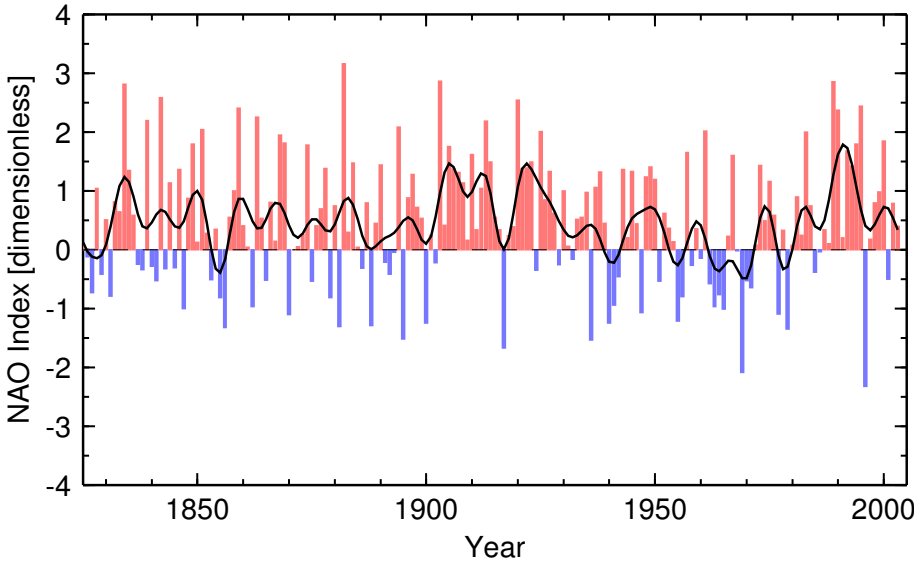


Figure 1.2: *Time series of the winter season (DJFM) NAO index (after Jones et al., 1997): annual index values (bars), low-pass filtered variability (periods <8 yr removed) time series (solid line). The index is available at http://www.cru.uea.ac.uk/~timo/projpages/nao_update.htm.*

The low-frequency variations of the NAO on decadal and interdecadal time scales are considered to be influenced by the dynamics and thermodynamics in the North Atlantic Ocean. It is broadly accepted that the *passive* response of the sea surface temperature (SST) is in agreement with the statistical climate model concept of Hasselmann (1976), but the *active* role of the ocean on the NAO dynamics is still uncertain (Kushnir et al., 2002). Studies based on observational data have shown that extratropical SST anomalies could force atmospheric circulation anomalies (Czaja and Frankignoul, 2002). Various climate model simulations revealed that the ocean feeds back onto the atmospheric circulation (for example Rodwell et al., 1999; Metha et al., 2000; Latif et al., 2000; Kushnir et al., 2002). One possible result is an enhanced atmospheric low-frequency variability (Hasselmann, 1976; Kushnir et al., 2002; Czaja et al., 2003). Barsugli and Battisti (1998) suggested a negative local thermodynamic feedback, in which the oceanic temperature adjustment reduces the air-sea fluxes. This leads to increased low-frequency variance of extratropical atmospheric variability (Czaja et al., 2003). Other hypotheses have been put forward calling for a more active role of the ocean. The gyre circulation is conceived to enhance the decadal variability of the NAO (Sutton and Allen, 1997; Grötzner and Latif, 1998; Czaja et al., 2003; Paeth et al., 2003). The thermohaline circulation (THC) has been suggested to increase the interdecadal variability of the atmospheric circulation anomalies (Timmermann et al., 1998; Eden and Jung, 2001; Wu and Gordon, 2002). Sensitivity tests have further brought up the debate about the role of the tropical ocean-atmosphere interaction for the trend in the NAO (Hoerling et al., 2001, 2003; Hurrell et al., 2003a; Bader and Latif, 2003). A more detailed knowledge of the processes governing the ocean-atmosphere interactions is of fundamental importance for the understanding of the NAO on long time scales. Realistic low-frequency modelling of the NAO depends on whether the model can adequately simulate the involved processes.

There are two major reasons why an extended knowledge about the NAO's history is essential. First, producing a longer NAO index will help to characterise the low frequency behaviour of the

NAO and thus the mechanisms of interdecadal variability. Second, the reconstruction into the preindustrial age will contribute to an improved detection of climate change signals (Barnett et al., 1999; Bradley et al., 2000; Barnett and Jones, 2000).
Paleoclimatic reconstructions make use of so-called proxies. Proxies provide indirect information about some climatic variables like temperature, precipitation or wind. For example, ice cores, corals, and trees are natural archives (among a variety of geochemical data) that provide a wealth of climatic information. Together with historical and documentary records they are invaluable archives of the the earth's climate history. An appropriate selection of such proxies can provide indirect information about the state of the NAO. The reconstruction process transforms the proxy data into an NAO index. Several NAO index reconstructions have been established, derived from various proxies using different reconstruction methods (Cook et al., 1998; Appenzeller et al., 1998b; Luterbacher et al., 1999, 2002a; Garcia et al., 2000; Cullen et al., 2000; Proctor et al., 2000; Glueck and Stockton, 2001; Rodrigo et al., 2001; Vinther et al., 2003). However, Schmutz et al. (2000) raised some doubts about the reliability of many of the reconstructions that were based on natural proxies. Their correlation analysis has revealed that the reconstructions failed to be verified in the 18th and early 19th century. Cook et al. (2002) obtained the same results using a more objective Kalman filter method. Recently, optimised reconstructions have been published by Luterbacher et al. (2002a) and Cook et al. (2002) [see also Cook (2003)]. These new time series are significantly correlated throughout the entire common period back to AD 1500, at least on interannual time scales. In the low-frequency range the reconstructions show larger discrepancies (Jones et al., 2001). All of these reconstructions have in common that unfiltered time series were used to calibrate and validate the statistical transfer models and to reconstruct the NAO signal from the proxies. These models provide 'best' estimates for individual annual (winter) or even monthly index values (Luterbacher et al., 1999, 2002a). The spectral characteristics of the reconstructed time series are estimated after the reconstruction procedure. This kind of transfer function in time-space is equivalent to a corresponding filter function in frequency-space that is constant for all frequencies. When proxies have a signal-to-noise ratio independent of the frequency this is an adequate choice. In other cases this choice could bias the spectral power characteristics of the reconstruction. In practice, the paleoclimatic reconstruction should follow a strategy that meets the requirements of the climatic research objectives. The primary goal of this study is to provide a detailed view onto the decadal and interdecadal variability of the NAO in preindustrial times. In order to overcome the problems of the frequency dependence, two reconstruction strategies will be applied. The first one follows the ideas of the previous studies and filters the reconstructed time series (the 'post-filtering' technique). The second applies the filter to the proxies and the NAO index prior to the reconstruction process (the 'pre-filtering' technique). This concept was already introduced into the field of paleoclimatic reconstruction by Guiot (1985). Only a few studies have followed similar strategies yet (e.g. Osborn and Briffa, 2000).
This study is organised as follows. In chapter 2 a brief description of the proxies and their general relationship to the climate is presented. Two sources of paleoclimatic data, ice cores and tree-ring proxies, are introduced. The basic facts about the proxy-climate relationships, the sources of noise that mask the climate signal, and the dating accuracy are summarised. Chapter 3 formulates the statistical concepts which are essential for a proper design of the reconstruction strategy. Three reconstruction methods are introduced. The *principal component regression* and the *best linear unbiased estimate* are compared with each other and a simplified *weighted average method* is developed. A detailed analysis of the relationship between the climate of Greenland and the NAO follows in chapter 4. The potential consequences for the proxy-NAO relationship are highlighted. A preliminary NAO index reconstruction is presented based on ice-core proxies. The skill of the

three reconstruction methods is investigated and the effect of the pre-filtering and post-filtering technique is analysed. Chapter 5 presents the reconstructions of the NAO index derived from multiproxy data sets. In section 5.1 the decadal variability is reconstructed from proxies comprising Greenland ice cores and European tree rings. The reconstruction interval is 1700–1978. Section 5.2 presents the reconstruction of the interdecadal variability in the interval 1623–1966. Both sections provide a description of the proxy-climate relationships and a detailed presentation of the reconstructions. The discussion of the results is focused on the comparison with two independent reconstructions of Cook et al. (2002) and Luterbacher et al. (2002a) and the climatic interpretation. Concluding remarks follow the discussion. The last chapter summarises the basic results of this study and final conclusions are drawn.

# Chapter 2

# Natural Climate Proxies

This chapter gives a brief description of the climate proxy data used in the following chapters. It is stated below what is meant by the expression *natural climate proxy* (later the short term proxy will be used) in this study.

**Definition 2.1 (Natural climate proxy)** *A physical or chemical property of a given medium which is influenced by one or more components of the climate system.*

This is a rather general definition but does not include all types of indirect climate information[1]. The medium has the function of an 'archive'. For example, trees, ice cores or corals are valuable archives. The definition does not take further requirements into account which make a proxy suitable for climate reconstructions. These are:

- an archive with a longterm memory capability
- an unambiguous age assignment of the measured property (within a tolerable uncertainty range).

For a better illustration of these factors one can consider a proxy to be a rather perfect indicator for local temperatures. Unless the medium ('archive') is capable of storing these climatic information it will be useless for regional temperature reconstructions. The second point is that even a good climate sensitivity and memory capability are insufficient for climate reconstructions if no temporal assignment of the measured signal is possible. Beyond these necessary conditions there are other essential items making some proxies preferable to others (simple relationship proxy–climate, stable or stationary proxy-climate relation).
It is beyond the scope of this study to describe the proxies used in detail (e.g. the laborious procedures of field work needed for collecting the proxy material and the measurement techniques) but the key facts about the quality of measurements (especially temporal resolution and dating) are given. The most important aspect for this study is the link between the proxy and the climate. This is the central topic to be discussed in this chapter. However, it is impossible to draw attention to all kind of proxies used in similar climate reconstructions so far. The following studies are based on two different groups of proxy sources, namely ice cores and tree rings. They are described in the next sections.

[1] for example documentary data like phenological records

## 2.1 Proxies from Ice Cores

The Greenland ice sheet is an inexhaustible source of paleoclimate information. In the 1960–70s the first ice cores were recovered from the ice sheet and analysed (Johnsen et al., 1970; Dansgaard et al., 1975). Prominent examples of recent ice core drilling projects are GISP2 and GRIP.[2] The most commonly used proxies, accumulation and $\delta^{18}$O, are described in detail in the next section. Deuterium excess, which is of less importance in this study, will be introduced in a subsequent section.

### 2.1.1 Accumulation and $\delta^{18}$O

There are two types of proxies that are routinely measured in ice cores: the accumulation rate and isotopic concentration of oxygen $^{18}$O. The accumulation rate is the mass of equivalent water in a given layer of the ice core. Usually, the accumulation rate of annual layers is measured. Annual accumulation rates represent the annual amount of precipitation minus evaporation. The water molecules of the ice consist of $H_2^{16}O$, $HD^{16}O$ and $H_2^{18}O$. In paleoclimatic studies, the ratio of $^{18}$O to $^{16}$O (or equivalently D to $^{16}$O, but this is not treated in this study) is used as a proxy for local temperatures. Since measurements are not absolute but relative to a given standard [V-SMOW, Vienna-Standard Mean Ocean Water, (Craig, 1961b)] the quantity

$$\delta^{18}\mathrm{O} = \frac{R_s - R_0}{R_0} \times 1000 \tag{2.1}$$

is used (unit ‰), where $R_s$ is the ratio of $^{18}$O to $^{16}$O of the sample and $R_0$ the given standard ratio. Due to the differences in the atomic masses, the volatility of the lighter isotope $H_2^{16}O$ is higher. During evaporation the $H_2^{16}O$ preferably changes from the liquid to the vapour phase. The condensation process favours the heavy components to change from the vapour phase to the liquid phase. This mechanism is called *isotopic fractionation*. The effectivity of the isotopic fractionation depends on the ambient temperature. Evaporation and condensation at lower temperature leads to more pronounced fractionation in the vapour (Dansgaard, 1964). Dansgaard (1964) analysed $\delta^{18}$O in precipitation from a global observation network. He was able to establish a linear relationship between the local air temperature and $\delta^{18}$O. This laid the foundation for the use of $\delta^{18}$O in paleoclimate reconstructions.

Several problems arise with the simple interpretation of $\delta^{18}$O representing local temperature variations. The basic processes influencing the $\delta^{18}$O-signal in ice cores are sketched in Fig. 2.1. They are described below. Dansgaard (1964) has emphasised that the trajectories of the precipitating air masses have to remain unchanged. Any change in the major pathways of the air masses, which are contributing to the precipitation at the ice core location, can interfere with the local temperature signal. Additionally, if pathways reorganise during the time the change is likely accompanied with changes in the source regions of the precipitating waters (to be discussed in section 4.1.2).

Once the snow reached the ground (ice shield) it is exposed to wind scouring. The wind scouring effect is strong in regions with rough topography (Fisher et al., 1983) and disturbs both the accumulation and the isotopic concentration. Drifting snow shapes the snow surface in ripples. The undulation is preserved during subsequent snow events. Its prevalence in the ice cores is well known to cause specific *noise* in the ice cores (Fisher et al., 1985, 1996). This type of noise contaminates the accumulation measurements. Fisher et al. (1985) has shown that the irregular deposition effects produce a ‘blue’ noise spectrum. For example, a sequence of annual accumulation

[2] see the special issue of the J. Geophys. Res., Vol. 102(C12), 1997.

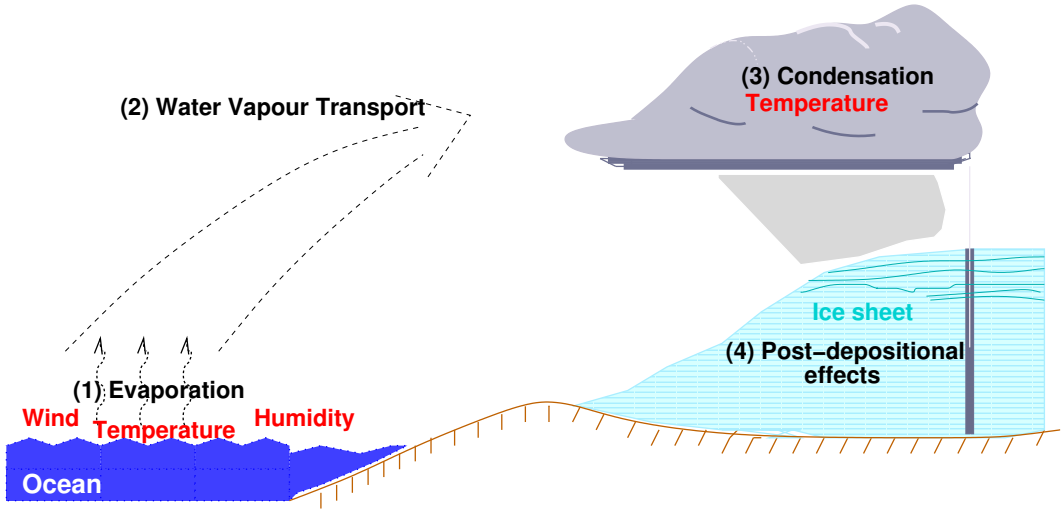


Figure 2.1: *Sketch of the basic processes affecting the $\delta^{18}O$ signal in ice cores: (1) Evaporation in the oceanic source region, (2) water vapour transport in the atmosphere, (3) condensation processes forming clouds and precipitation, and (4) post-depositional effects in the ice.*

rates would have a larger noise component in the year-to-year variability than in the more gradual variations on time scales of decades to centuries.

The signal in isotopic concentrations is subject to another source of noise. Diffusion of volatile species in snow and firn dilutes existing gradients of the volatile substance in the upper layers of the firn. The diffusion process effectively redistributes the substance in the vertical direction, where the gradients are strong. Thus, rapid changes (e.g. from winter to summer or between individual snowfall events) are reduced in their amplitude. Fisher et al. (1985, 1996) analysed the influence of the diffusion on the noise component and found a red noise character.[3] Diffusion models have been developed based on theoretical concepts of diffusion combined with empirical evidence. These models simulate the processes in firn and snow (Whillans and Grootes, 1985; Cuffey and Steig, 1998). Some studies employed reverse models in order to transform the diffused $\delta^{18}$O-signal back to its original shape. In this study the diffused $\delta^{18}$O information is used in the reconstructions.

Another source of noise may be present in regions where summer melt events occur. This is rarely observed in central Greenland ice cores, nevertheless it causes some problems in the climatic interpretation of accumulation and $\delta^{18}$O of ice cores in other regions of Greenland (Johnsen et al., 1972). Melting water invades the underlying layers of the ice, causing redistribution of mass and isotopes therein. Moreover, melting surface snow might coincide with anomalous high evaporation rates, which could again change the proxy signals. There are conceivably more difficulties in interpreting the $\delta^{18}$O-signal as a local temperature signal. More information can be found in Dansgaard (1964), Merlivat and Jouzel (1979), Fisher (1991) and White et al. (1997).

The difficulties with ice core proxies described so far concerned the physical relationship between the proxy measurements and the potential climate signals therein. A secondary source of error,

[3] However, it is not strictly intuitive why it should lead to higher disturbances in the low frequency part. Diffusion is constraint to regions of large gradients. Large gradients are typical of small vertical scale (i.e. short temporal periods) and diffusion should effectively diminish the high-frequency fluctuations.

which is of utmost importance, is the dating of the ice core samples. More and more sophisticated methods have been developed during the course of ice core research activities. In early investigations rather simple depth-time scale relationships were proposed. The underlying assumption was a constant annual accumulation rate on the ice core drilling site. This boundary condition entered into simple ice flow models (Johnsen et al., 1970), which translated a given depth from the core to a temporal date. This dating method was only applicable for climatic interpretations on glaciological time scales ($> 100$ years). The possibility of counting annual layers by the use of the seasonal variations of the $\delta^{18}$O was soon recognised (Johnsen et al., 1972). Dansgaard et al. (1975) exploited the annual cycle of the $\delta^{18}$O from detailed profiles. The dating accuracy was assumed to range from single years to 10 years in the earliest part of their 1000 yr chronologies. The visual stratification of annual layers provides access to high resolution time scales (Alley et al., 1997, and reference therein). The tedious work guarantees an accuracy of probably 1 yr per century (Alley et al., 1997). More complex analyses of the ice core properties allow for combining various dating methods that can further reduce the dating error (Meese et al., 1997). Today, dating accuracy is between one to ten years for Holocene ice core records. However, a shift by one year could cause severe problems in statistical analysis techniques when annual proxy data are used.

### 2.1.2 Deuterium Excess

A second order proxy can be obtained if both $\mathrm{HD}^{16}\mathrm{O}$ and $\mathrm{H}_2^{18}\mathrm{O}$ are measured in the ice core samples. The isotopic concentrations show a strong linear relationship, known as the *meteoric water line* (Craig, 1961a). The residual, *deuterium excess*, is defined as (Dansgaard, 1964)

$$\mathrm{d} = \delta\mathrm{D} - 8\,\delta^{18}\mathrm{O} \quad . \tag{2.2}$$

Deuterium excess is believed to provide insight into moisture source regions of Greenland's precipitation. This non-local signal is the result of kinetic fractionation effects over the oceanic source regions during evaporation (Dansgaard, 1964; Merlivat and Jouzel, 1979; Johnsen et al., 1989) . The kinetic effects depend on relative humidity, temperature and wind speed at the evaporating ocean surface. However, the resulting deuterium excess in the precipitation over Greenland can be modified during phase transitions in polar clouds (Jouzel and Merlivat, 1984; Johnsen et al., 1989; Fisher, 1991). The relevant processes that form the deuterium excess signal in precipitating waters are illustrated in Fig. 2.2.

Johnsen et al. (1989) used a Rayleigh-model, including the isotopic kinetic effects during evaporation and formation of precipitation, to simulate the observed deuterium excess values in Greenland ice cores. The model reproduced the characteristic features only in cases where the evaporation conditions (relative humidity and temperature) coincided with the prevailing subtropical North Atlantic Ocean conditions. In other studies GCMs were used for 'tagging' precipitation (Koster et al., 1986; Charles et al., 1994; Armengaud et al., 1998; Werner, 2000). In those studies, the oceans and continents were divided into several areas and the evaporating waters were tagged according to their location. Each moisture element in the model is linked to one of the defined areas, and any precipitation is attributable to one of these source regions. The models revealed that the composition of the precipitation is a mixture of several regions. The subtropical North Atlantic is a major source region for precipitation over Greenland. Moreover, the model results showed that seasonal variations in the major source region might exist. The North American continent is important for Greenland's precipitation during summer. In winter, the evaporation over North America is a negligible precipitation source for Greenland. Source region variations on interannual time scales, which could cause severe problems in the paleoclimatic interpretation of

deuterium excess variability, have not been studied in detail yet. The model results demonstrate that deuterium excess in Greenland ice cores represents the climate conditions of several source areas rather than of one single site.
The intricate deuterium excess signal is even more complex due to the kinetic fractionation effect in clouds during the formation of snow. This process can be very important (Jouzel and Merlivat, 1984; Fisher, 1991). It is questionable to what extend these effects mask the recorded signals from the source regions. Therefore, deuterium excess should be handled with much more care than the well-understood $\delta^{18}$O and accumulation proxies.

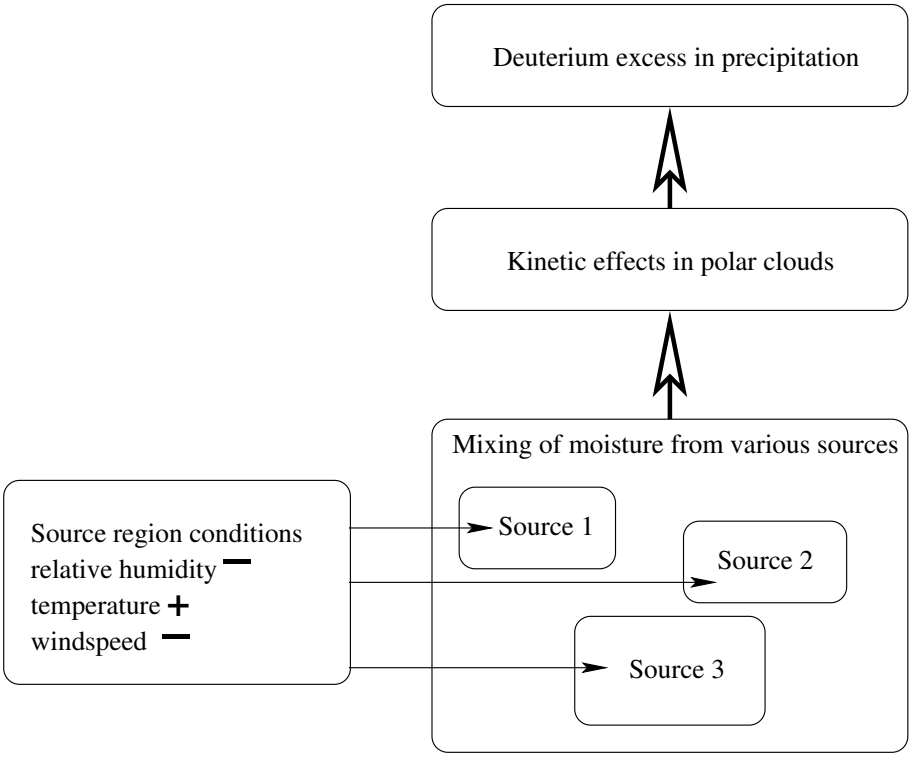


Figure 2.2: *Scheme of climatic influences on deuterium excess in precipitating waters over Greenland. Positive (negative) relationships between source region climate parameters and deuterium excess are marked with + (-).*

## 2.2 Tree-Ring Width

Trees have proved to be extremely useful for paleoclimatic studies for at least two reasons: first, the habitat of trees extends over large parts of the earth's continents and islands which allows paleoclimatic analyses in many parts of the world. Second, dendroclimatology (i.e. the study of climate on the basis of trees) is a mature discipline which has gradually been established over nearly one century now. A huge archive of tree-based proxies exist and sophisticated analysis methods have been developed. Two types of proxies are commonly used in practise: the width of the tree rings and the density of the wood that forms the ring. In this study, the ring width is used as a climate proxy. The basic concepts of dendroclimatology, which are essential for applying the tree rings in the paleoclimatic reconstructions of the following chapters, are listed below. It is by no means possible to discuss all aspects of the relationship between climate and tree rings. The interested reader can find comprehensive information about dendroclimatology in the textbooks of Fritts (1976), Schweingruber (1988) and Bradley (1999).

Most of the extratropical trees produce rings of annual growth in their stems. In spring, the beginning of the growing season, the trees produce less dense wood than in the end of the growing period in autumn. The differences in density are visually detectable because the denser latewood (i.e. produced in autumn) is darker than the earlywood that is produced in the next spring. Due to the radial growth the contrast in the wood's colour forms a ring in the stem. The width of such a ring can be influenced by the climate.

Two important steps are required before a ring width signature is accessible for climatic interpretations: a precise dating of the annual ring width is most important. This is accomplished by means of *crossdating*. The crossdating procedures compare ring width patterns among samples from different trees (note that more than one sample from a single tree is common in practise). It allows to identify and correct missing or false rings[4] in certain samples. It suffices to date one ring in a continuous sequence of ring measurements. Usually, the outmost ring of a living tree can be dated to obtain an accurate time scale. The laborious crossdating methods produce time scales which are superior to those of the ice-core proxies (and other proxies).

In a second step, the time series of ring-width measurements are standardised and averaged into a single site chronology. Standardisation is a crucial factor in processing the tree ring data. It is necessary because trees show a biological growth structure that depends on the tree age: generally, young trees produce thicker rings than old trees. Therefore, an intrinsic feature of any tree-ring width time series is a nonlinear age trend. The statistical properties of the ring widths (the mean and the variance) are affected by this trend. Various methods are applied to reduce the biological growth trends. Polynomial or exponential curve fitting is widely used.

A major drawback of this standardisation technique is that biological trends cannot be distinguished from slowly varying climate conditions. The essential implication of this detrending procedure is that it limits the range of climate variations which can be estimated from such chronologies. It is still an open question how to circumvent this problem. Methods like regional curve standardisation (RCS) (Mitchell, 1967; Briffa et al., 1992; Esper et al., 2002) or age band decomposition (ABD) (Briffa et al., 2001) have been invented, but they require large sample sizes The ring width chronologies, which will be used later for the reconstruction, were standardised by means of polynomial (exponential) curve fits. Thus, the established reconstructions must carefully be interpreted on the lowest part of the frequency range[5]. However, decadal to interdecadal

[4] False rings can be formed when the growing period is interrupted and continued later in the same year.

[5] This frequency range is not well known, because it requires detailed knowledge of each standardisation. However, climate variability on centennial and longer time scales is strongly damped (Briffa et al., 1992, 2001; Esper et al., 2002).

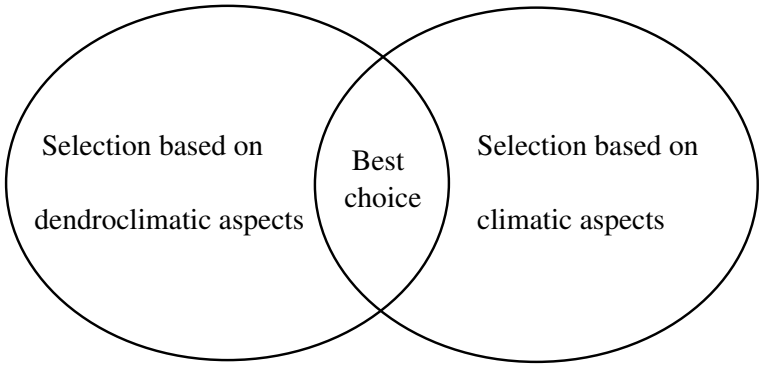


Figure 2.3: *The problem of selecting the best tree-ring proxies. Depending on the point of view there are two different criteria: dendroclimatological or climatic reasons. The optimal tree-ring proxies should match both criteria.*

climate variability should be well represented in the standardised chronologies.

So far, it has always been assumed that the tree-ring width depends to some extend on climatic factors, although the width of a tree ring is the result of very complex biological processes within the tree. But, external stress factors regulate the tree growth and some of these external factors like temperature or precipitation determine the climatic conditions at the tree's location. The causal connections between climate and tree-ring width is very complex and dendroclimatologists are compelled to apply various statistical methods in order to extract climatic signals from tree rings (for example Fritts, 1976; Guiot, 1985; Cook et al., 1994; Briffa, 1995; Meko, 1997; Cook et al., 1999; D'Odorico et al., 2000). It should be noted that not only the climatic conditions during the growing season but also climate factors from preceding seasons, including winter, are relevant. Winter climate can be an important factor because it could determine the preconditions of tree's growth rates. It is important to realize that trees can 'feel' winter climate conditions and 'remember' them. It is not necessary that the climate system itself has a memory of several month in order to reconstruct winter climate from summer tree growth rates.

Dendroclimatologists are fully aware of the difficulties in climatic interpretations of tree-ring proxies. A careful site selection helps to obtain proxies from trees that are *sensitive*, i.e. the tree growth responds to specific climate variations. For example, in semi-arid regions maximum tree growth rates will be limited by precipitation. Temperature will presumably be the limiting factor in arctic regions close to the tree line. Dendroclimatologists can try to optimise the climatic signal information of their selected trees. For the reconstruction of the wintertime NAO index, it is clear that an optimal tree selection, from the perspective of a dendroclimatologist, would prefer trees which are sensitive to either temperature or precipitation during the winter month. A selection of a climatologist instead would preferably require trees from regions where the impact of the NAO is most strongly pronounced in local climate variability. The application of both criteria would select the most promising tree-ring proxies (Fig. 2.3).

The strategy that is followed in this study is based on the climatic aspects. Trees from Europe (Scandinavia, Iberian peninsula, British Isles, and central Europe) North Africa, and from the northeastern part of North America are chosen. Comparison with Fig. 1.1 shows that the climate variability of these regions is under the influence of the NAO during winter. The standardised tree-ring chronologies are taken from the 'International Tree Ring Data Bank' (ITRDB). This

huge archive of tree rings is a collection of contributions from numerous investigators.[6] The ITRDB includes chronologies of different standardisation types. More detailed information about the tree-ring chronologies used (including their original file names for unequivocal identifications) are tabulated in the appendix (A.2, A.3). Their geographical distribution is depicted in the sections where the reconstructions are presented. Two groups are used. One group of tree-ring chronologies comprises the period 1700–1978, the other group the period 1623-1966.

[6] This archive is accessible at *http://www.ngdc.noaa.gov/paleo/treering.html*.

# Chapter 3

# Statistical Methods

The paleoclimatic time series reconstruction methods which are used in the next chapters are statistical methods. The statistical treatment of the proxy data is often the best way to deal with the large uncertainties concerning the physical linkage between the proxies and the climate signal. It cannot be fully answered which of all existing statistical techniques is presumably the optimal tool for the reconstruction problem. Even a theoretically optimal method for this type of problem could fail in practise. This chapter is organised as follows. The relationship between a climate signal and a proxy in terms of linear response functions is investigated with respect to its spectral (frequency domain) characteristics. The effect of noise and the importance of its covariance structure among several proxies are highlighted. Some comments are made on the problem of nonstationarity in the response functions and the noise before the applied reconstruction methods are introduced. A brief description of the applied filtering method (the *maximum overlap discrete wavelet transform*) is presented. The mathematical typesetting convention in this chapter is: a scalar variable is set as italic (e.g. $X, x_i$), vectors are set as bold roman (e.g., $\mathbf{X}$), and matrices are set as bold sans serif (e.g., $\mathsf{\mathbf{X}}$). The transpose of a vector or a matrix is indicated with $^T$. Other symbols are explained when they are first used in the text.

## 3.1 Specifying the Reconstruction Problem

A precise understanding of the reconstruction problem is the key to an applicable reconstruction method. The reconstruction problem in this work can be defined through the following question.

**Definition 3.1 (Time series reconstruction problem)** *Given a number of proxy time series and a climate signal time series that partly overlap in time. What is the optimum combination of the proxies in order to obtain a realistic estimate of the climate signal?*

Intuitively, one would first try to figure out which proxy time series fit best with the climate signal in the overlapping period. The proxies that show clear resemblance with the climate signal are more trustworthy than those with weak similarities. That is, a proper weighting of the individual proxies is the centre of the statistical reconstruction technique.
The first step is to make some assumptions about the response functions. The response function is barely known from physical considerations (see Chapter 2) and has to be estimated from the data. The definition below describes the proxy-climate relationship. For convenience, it is assumed that the climate signal (i.e. that part of the climate variability which will be reconstructed) is represented by a single index time series.

**Definition 3.2 (Response function)** *Let* $\mathbf{X}$ *be a vector of length* $N + 2K$ *representing the climate signal time series* $x_t, t = -K, \ldots, -1, 0, \ldots N - 1 + K$*, and* $\mathbf{P}$ *the proxy time series* $p_t, t = 0, \ldots, N - 1$*. The vector* $\mathbf{N}$ *(*$n_t, t = 0, \ldots, N - 1$*) represents the variations in the proxy time series independent of the climate signal. A response function* $\mathcal{H}$ *describes the impact of the climate signal* $\mathbf{X}$ *on the proxy:* $\mathbf{P} = \mathcal{H}(\mathbf{X}) + \mathbf{N}$.

The inclusion of a sufficient number of $2K$ additional time steps in $\mathbf{X}$ takes into account that the proxy response at time $t$ could be the sum of some preceeding and following[1] climate states. The response function $\mathcal{H}$ can be nonlinear. For example, it is shown in section 2.1 that the response function of $\delta^{18}$O from Greenland ice cores might be the product of several factors. Throughout this study restriction is made to linear response functions $\mathcal{H}(\mathbf{X}) = \mathbf{H}\mathbf{X}$, with $\mathbf{H}$ a $N \times (N + 2K)$-matrix. Note, that this formulation also allows nonstationary responses. In case of a stationary response, each row contains a circularly shifted sequence of coefficients, and the matrix has the form:

$$\mathbf{H} = \begin{pmatrix} h_{-K} & h_{-K+1} & \cdots & h_0 & \cdots & h_K & & 0 & & \\ 0 & h_{-K} & h_{-K+1} & \cdots & h_0 & \cdots & h_K & & 0 & \\ \vdots & & & & & \vdots & & & & \\ & & & 0 & & & h_{-K} & \cdots & h_0 & \cdots & h_K \end{pmatrix} .$$

The first row describes the linear response of the proxy at time $t = 0$. As a result, the proxy contains a weighted sum of $K$ preceeding climate states, the instantaneous response at time $t = 0$ and $K$ following climate states. The second row represents the response for the time step $t = 1$. The row elements are shifted to the right by one position. The rightmost coefficient enters the matrix again from the left. For a given point $t$, the proxy time series is given by

$$p_t = \sum_{j=-K}^{K} h_j \, x_{t+j} + n_t \, . \tag{3.1}$$

Throughout this study the assumption of a stationary response function is made. The problems with nonstationarity are briefly discussed in Sec. 3.1.3.

### 3.1.1 Spectral Characteristics

The net effect of the response function given in Eq. 3.1 is that at any point $t$ the proxy contains a weighted average signal of the climate history. The response function could equivalently be expressed as a convolution of the climate signal with a corresponding function. The theoretical formalism requires infinite time series[2]

$$p_t = \sum_{j=-\infty}^{\infty} \tilde{h}_j \, x_{t-j} + n_t \quad . \tag{3.2}$$

In Eq. 3.2, $\tilde{h}_j$ contains the response function in reverse order ($\tilde{h}_j = h_{-j}$). It is known that the convolution of two functions in time domain is equivalent to the product of their corresponding Fourier transforms (FT). Therefore, Eq. 3.2 becomes

$$p_\omega^{FT} = \tilde{h}_\omega^{FT} \, x_\omega^{FT} + n_\omega^{FT}, \tag{3.3}$$

[1] e.g. caused by the post-depositional diffusion effects in ice cores

[2] To achieve this, the time series $x_t$ and the response function $h_j$ can be padded with zero elements.

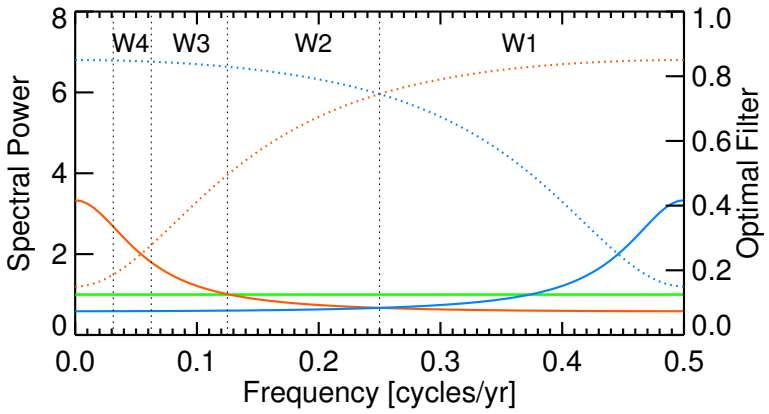


Figure 3.1: *Illustration of the optimal filter problem. The white noise process represents the climate signal (green). Two proxies are contaminated with red noise (solid red line) and blue noise (solid blue line). The optimal filter weights for the first (second) proxy are plotted with red (blue) dotted lines.*

where $^{FT}$ denotes the FT of a time series and $\omega$ is the frequency index ($-2^{-1} \leq \omega \leq 2^{-1}$). Equations 3.1–3.3 demonstrate that a stationary linear response function can change the spectral characteristics of the signal.
Additionally, the presence of coloured noise might hamper an unbiased reconstruction of the signal spectrum. Consider the case where the transfer function would just result in scaling the signal, i.e.

$$p_t = h\, x_t + n_t \ .$$

If the corresponding noise is not a white noise process (i.e $n_\omega^{FT} \neq const$), then the signal-to-noise ratio [S/N-ratio] (i.e. the signal variance divided by the noise variance) is a function of frequency. Both effects, the convolution of the signal with the response function and the contamination with coloured noise would require the optimal filter method (Press et al., 1999) to estimate the signal from the proxy. The consequence for the reconstruction problem is illustrated with an elementary example. Consider the case that a climate signal is reconstructed from two proxies. Let the climate signal[3] be simply a white noise process. One proxy is more sensitive to the high frequency climate signal than to the low-frequency fluctuations. This behaviour is known for isotopic concentrations ($\delta^{18}O$) in ice cores (Fisher et al., 1985). Let the second proxy have a higher signal-to-noise-ratio in the low-frequency range, which is observed in accumulation rates derived from ice cores (Fisher et al., 1985). In reconstructing the low-frequency part of the climate signal, one would put more weight on the second proxy than on the first one (see Fig. 3.1 for illustration). For the high-frequency signal reconstruction the first proxy should get the larger weight. This example underlines that the combination of several proxies may depend on the time scale of interest. For this reason, the concept of pre-filtering reconstructions is introduced in section 3.2.

### 3.1.2 Statistical Structure of the Noise

The response function has been introduced as a univariate time series concept. Because the general reconstruction problem deals with more than one proxy the statistical interdependence of the

[3]Note that a climate signal need not to be deterministic.

proxies determines the reconstruction quality. On the one hand the proxies carry the climate signal, which puts a statistical relationship into proxy set. On the other hand the noise components can be correlated between two proxies. Consider two tree-ring width chronologies from two sites. Both chronologies are sensitive to the same climate factor (for example temperature) during all seasons. Let the imprint of the climate signal be the result from summer and winter temperatures. If one reconstructs the winter-season signal from the width measurements, the summer signal is part of the noise component in both proxies. This example is the motivation for a clear distinction of two noise components:

$$n_{t,i} = c_{t,i} + e_{t,i}\,, \tag{3.4}$$

where the index $i = 1, 2, \cdots, P$ labels the individual proxies in a proxy data set. The noise is the sum of a *climate noise* $c_{t,i}$ and a *local noise* $e_{t,i}$. The climate noise is that part of variability in a proxy time series that is the result of the climate response but not considered in the reconstruction.[4] The local noise $e_{t,i}$ is an exclusive part of the variability in the i-th proxy. In statistical terms, the local noise $e_{t,i}$ is independent from the local noise $e_{t,j}$ of a different proxy $j$. The presence of climate noise is an intractable problem in the reconstruction due to its covariability among the proxies. Straightforward averages of a number of proxies can not efficiently reduce the covarying noise. Denoting the expectation operator with angle brackets, the effect of the climate noise is given below for idealised proxies $p_{t,i} = hx_t + c_{t,i} + e_{t,i} \quad (i = 1, 2, \cdots, P)$. Let the proxies have the statistical moments:

$$\begin{aligned}
\langle x_t \rangle = \langle c_{t,i} \rangle = \langle e_{t,i} \rangle = \langle p_{t,i} \rangle &= 0 \\
\langle x_t^2 \rangle &= \sigma_x^2 \\
\langle c_{t,i}^2 \rangle &= \sigma_c^2 \qquad i = 1, 2, \cdots, P \\
\langle e_{t,i}^2 \rangle &= \sigma_e^2 \qquad i = 1, 2, \cdots, P \\
\langle e_{t,i}\, e_{t,j} \rangle &= 0 \qquad i \neq j \\
\langle c_{t,i}\, c_{t,j} \rangle &= \gamma_c \qquad i \neq j
\end{aligned}$$

Taking the average of all proxies, $\overline{p_t} = P^{-1} \sum_{i=1}^{P} p_{t,i}$, leads to

$$\langle \overline{p_t}^2 \rangle = \underbrace{h^2 \sigma_x^2}_{\text{signal}} + \underbrace{\frac{1}{P}\sigma_e^2}_{\text{local noise}} + \underbrace{\frac{1}{P}\sigma_c^2 + \left(1 - \frac{1}{P}\right)\gamma_c}_{\text{climate noise}} \quad . \tag{3.5}$$

In the case of uncorrelated noise, the S/N-ratio is linearly increasing with the number of averaged proxies. Correlated climate noise limits the S/N-ratio:

$$\lim_{P \to \infty} \text{S/N} = \lim_{P \to \infty} \frac{h^2 \sigma_x^2}{\frac{1}{P}\left(\sigma_e^2 + \sigma_c^2\right) + \left(1 - \frac{1}{P}\right)\gamma_c} = \frac{h^2 \sigma_x^2}{\gamma_c} \quad . \tag{3.6}$$

Including more proxies does only reduce parts of the noise variance. The presence of correlated noise and its effects for the reconstruction depend on the proxy type and their spatial distribution. Annual averaged tree-ring width are prone to highly correlated climate noise when serving for wintertime NAO index reconstructions. Similar effects will restrict the reconstruction quality of the winter NAO index if annually averaged ice-core proxies are the source of information. Chapter 5.2.2 will show that the simplified theoretical example is in qualitative agreement with the observed results.

[4] Of, course other reasons could lead to covarying noise.

### 3.1.3 A Note on Nonstationary Proxy-Climate Relationships

A principal concern in the reconstruction problem is that several factors can disrupt the stationary proxy-climate relationship. State-of-the-art reconstruction techniques are based on the assumption that the observed relationships between proxies and climate signals were unchanged in the past ('uniformitarian principle'). Recently, a discussion has started about the possible biases in climate reconstructions caused by externally forced or anthropogenic climate variability (Rutherford et al., 2003; Zorita and González-Rouco, 2002; Cook et al., 2002). Bringing this discussion forward to the model of a linear relationship between proxies and climate (Eq. 3.1), a change in the response function or a modification of the noise would lead to a misinterpretation of the proxies. The response function would change over the years if the processes which determine the proxy sensitivity were different.

In the scope of large-scale climate pattern reconstruction represented by an index (like the NAO), shifts in the pattern could also modify the response function. The NAO, for example, has shown an increasing positive state during the last 30 years, coincident with a shift of the Icelandic Low to the northeast (Hilmer and Jung, 2000). This shift had a profound influence on the sea ice export through the Fram Strait (Hilmer and Jung, 2000) and a variety of climatic parameters in the North Atlantic region (Jung et al., 2003). Proxies from regions with significant changes in the relationship between the local climate parameters and the NAO would show an altered response to the NAO. Whether the recent shift is a unique phenomenon of the 20th century due to greenhouse gas forcing, as proposed by Ulbrich and Christoph (1999), is not answered yet.

Nonstationary noise is another problem that is likely included in proxies. Tree-ring width chronologies give a prominent example. Each chronology is an averaged value of some cores taken from several trees. Since the age of the trees generally differ, the earliest years of a chronology are less frequently sampled than the more recent years. A smaller sample size leads to larger errors in the ring-width chronology. Thus, tree-ring width proxies typically show a time-dependent S/N-ratio (see Sec. 5.2.2).

How can we cope with such nonstationary behaviour in reconstruction methods based on the uniformitarian principle? The identification of nonstationarities is a difficult task that requires large sample sizes, generally (Wunsch, 1999). As long as the climate signal is available the reconstruction can be compared with the observed signal[5]. The reconstruction procedure can be divided into a calibration step and a validation step (see also Sec. 3.2) . The validation uses that part of the time series that is withheld from the calibration of the reconstruction model. It serves as a test for the validity of the reconstruction outside the calibration period. An attempt will be presented that can help to identify changes in the reconstruction quality in times where the climate signal is unavailable. It makes use of a permutation method that allows for estimating the time-dependent spread of the reconstruction conditional upon the proxy ensemble (see Sec. 5.2). The risk of being confronted with nonstationary effects in the reconstructions can be further reduced when proxies from different regions and proxies of different kind are included.

[5] unfortunately, the observation can suffer from nonstationary errors, too.

## 3.2 Description of the Reconstruction Methods

The general framework for time series reconstructions is composed of four subjects:

- selecting suitable proxies
- calibrating a linear transfer model
- verifying (synonymous with validating) the transfer model
- the reconstruction itself (application of the transfer model)

The first step is a crucial factor in determining the overall skill in the following reconstruction steps. Proxies of poor reconstruction potential should be withheld from reconstructions, if *a priori* information is available. The second point is the central aspect of the reconstruction. The aim is to a find an approximation to the inverse response function $\mathcal{H}^{-1}(\mathbf{X})$. Simultaneously, the noise should be reduced efficiently. Having established the transfer model, it is a mandatory practice to check the reconstruction skill of the model, which is done in a verification step. The verification results allow for estimating the reconstruction error. Possible nonstationarities may also be detected. In practise, many different methods have been used for each of those subjects. Referring to the problem of reconstructing the NAO index, for example, the range of methods encompasses the univariate linear regression (Appenzeller et al., 1998b) or multiple linear regression (Glueck and Stockton, 2001). More elaborated methods combine the principal component analysis and the multiple linear regression (Cook et al., 1994, 2002; Luterbacher et al., 2002a). It is hard to decide which of the methods will give the best results. The ultimate goal, finding a universal method with optimal statistical properties (i.e., robust, unbiased estimates with least squares errors, or unbiased reconstructed signal variance) that works with all kinds of proxies is obviously a difficult task. Comparable problems are known to exist in related fields like global sea surface temperature reconstructions. The result and discussion of Schneider (2001) is an underpinning example that an optimum reconstruction is hard to achieve in practice. Three methods are tested in this study. The *principal component regression* (Sec. 3.2.1) was motivated by previous works Cook et al. (1994, 2002) and Luterbacher et al. (2002a). The *best linear unbiased estimate* (Sec. 3.2.2) was applied to paleoclimatic reconstructions by Evans et al. (2002). The *weighted average regression* (3.2.3) is rather based on heuristic considerations. The theoretical background of the three methods is described next. A comparison of their reconstruction results is presented in Sec. 4.2.

The main goal of this study is the reconstruction of the low-frequency variability of the NAO index. Recent reconstructions focused, more or less, on the full spectrum of the variability. Here, the decadal and interdecadal time scales are of particular interest. Therefore and for the reasons given in Sec. 3.1.1 it is the intention of 'revitalising' the filter strategy of Guiot (1985). The three reconstruction methods are used in two different ways. The first technique is called *post-filtering* In this configuration, the method reconstructs the full spectrum of the climate signal. Any filter operation is applied afterwards.[6] The term *pre-filtering* is attributed to the technique where the time series (proxies and signals) are filtered before the reconstruction. The differences between both techniques is part of the discussion later on. The flow chart in Fig. 3.2 shows the principal stages of the reconstruction techniques.

[6] Exceptions are the filtering operations that remove linear or secular trends prior to the reconstruction process.

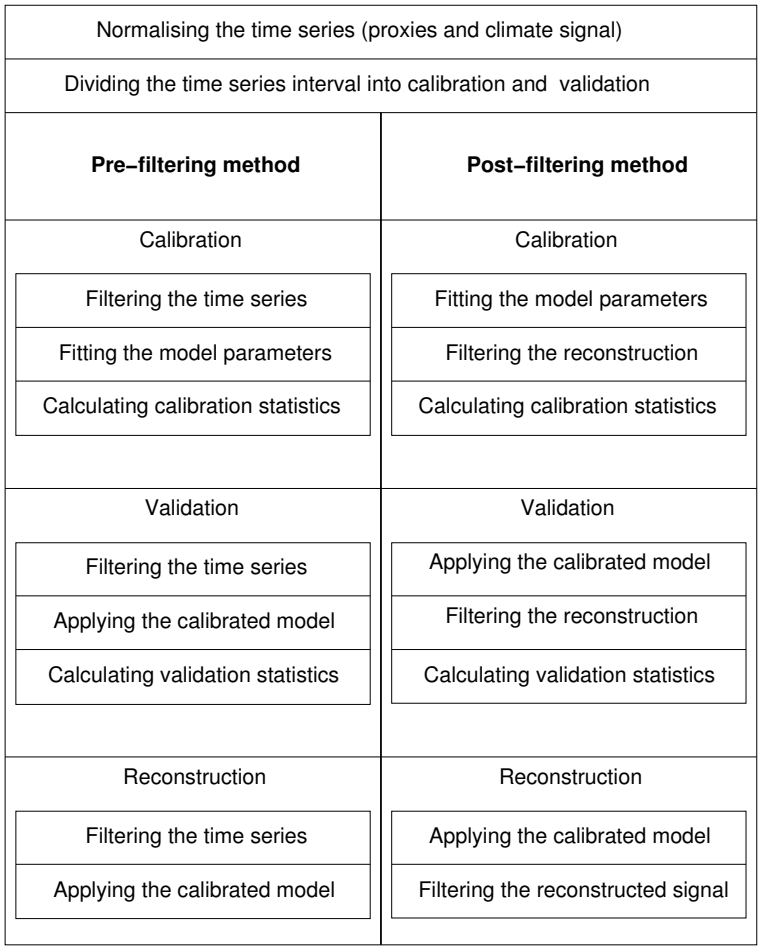


Figure 3.2: *Flow chart of the pre- and post-filtering reconstruction methods.*

### 3.2.1 Principal Component Regression

The general multiple linear regression (MLR) problem is to find a linear combination of $P$ predictors $\mathbf{P}_i$, so that the predictand $\mathbf{X}$ is approximated. In the reconstruction problem the proxies are the predictors and the NAO index is the predictand. The approximation of the MLR has the property of minimum least square errors. Given the predictors and the predictand vectors, which are time series of length $N$, the MLR solution is

$$\widehat{\mathbf{X}} = \mathbf{P}\widehat{\mathbf{B}} = \mathbf{P}\left(\mathbf{P}^T\mathbf{P}\right)^{-1}\mathbf{P}^T\mathbf{X} \quad . \tag{3.7}$$

The estimated partial regression coefficients in $\widehat{\mathbf{B}}$ account for the covariance between each predictor and the predictand and the covariance structure within the predictor set. A common problem encounters the MLR procedure if the number of predictors is too large. The accuracy of the linear regression model (measured in terms of the multiple correlation) is positively biased. A perfect regression is possible when the number of predictors exceeds the time series sampling ($P > N$). Moreover, the chance of *multicollinearity* (i.e., linear dependence among the predictors) increases with the number of predictors.

A possible way to deal with a large data set of predictors is the principal component analysis (PCA)[7]. The PCA transforms the $(N \times P)$-matrix $\mathbf{P}$, which contains the time series of the $i$-th predictor in the $i$-th column, into an orthogonal basis frame:

$$\mathbf{P} = \mathbf{A}\mathbf{F}^T = \mathbf{A}'\mathbf{L}^{1/2}\,\mathbf{F}^T \qquad \text{with } \mathbf{A} = \mathbf{A}'\mathbf{L}^{1/2}\,. \tag{3.8}$$

The $(N \times P)$ matrix $\mathbf{A}$ consists of the amplitude vectors (i.e. principal components [PC]). Note that the matrix $\mathbf{A}'$ contains the normalised PCs. $\mathbf{L}$ is a diagonal $(P \times P)$-matrix containing the eigenvalues of the predictors' covariance matrix, and the columns of the $(P \times P)$-matrix $\mathbf{F}$ are the eigenvectors. The relationship between the predictors' covariance matrix and the eigenvectors are given by the expression

$$\mathbf{P}^T\mathbf{P} = \mathbf{F}\mathbf{L}\mathbf{F}^T \quad . \tag{3.9}$$

The PCA provides an orthogonal basis for the representation of the total variance of the predictors. The first mode (the largest eigenvalue and its corresponding principal component and eigenvector) represents the largest amount of the total variance; the second mode captures the largest fraction of the remaining (unexplained by the first mode) variance etc. Depending on the covariance matrix, the PCA can be very efficient in representing the total variance in a few principal modes. Replacing the predictors with the principal components, the solution in Eq. 3.7 becomes

$$\widehat{\mathbf{X}} = \mathbf{A}\widehat{\mathbf{B}}_O = \mathbf{A}\mathbf{L}^{-1}\mathbf{A}^T\mathbf{X} \quad . \tag{3.10}$$

The partial correlation coefficients $\widehat{\mathbf{B}}_O$ in Eq. 3.10 are related to $\widehat{\mathbf{B}}$ in Eq. 3.7 by the transformation $\widehat{\mathbf{B}}_O = \mathbf{F}^T\widehat{\mathbf{B}}$. This demonstrates that the MLR is invariant under this orthogonal transformation. The *principal component regression* (PCR) has the advantage to reduce the number of predictors. Several truncation rules have been suggested (see Preisendorfer, 1988; von Storch and Zwiers, 1999), but none of these rules accounts for optimising the MLR skill. In this study, the key problem with PCR is to decide how many PCs enter the regression model.

The description of the noise structure in section 3.1.2 demonstrates that the covariance matrix is expected to be the sum of two components: the signal and the climatic noise form the off-diagonal elements of the covariance matrix. The results of the PCA could fail in representing the signal in the high-ranked modes, if the noise covariability is of the same (or larger) magnitude as the signal covariance. Truncation rules which identify the high-ranked modes to be important would filter out parts of the signal information and the PCR could not give best results.

Thus, an alternative way of choosing predictors from the PCs has to be employed. The high-ranked PCs are included as long as they are highly correlated with the climate signal. PCs which explain large amounts of variance but are almost uncorrelated with the signal will be excluded. They can be replaced with appropriate lower ranked PCs. The applied selection rule is the result of trial and error. First, 'North's Rule-of-Thumb' (North et al., 1982; von Storch and Zwiers, 1999) indicates which eigenvalues are statistically distinct from their following lower-ranked eigenvalues. This rule seems to provide helpful information even for the lower ranks. Second, the magnitude of the correlation between the PCs and the signal is compared. If both criteria are considered to be passed the PCs enter the PCR.[8] If the PCR is used in the reconstruction, the calibration step involves the PCA procedure (i.e. determining the PCs, Eq. 3.8, 3.9), and estimating the regression coefficients (Eq. 3.10) of the selected PCs.

[7] synonymous with empirical orthogonal function (EOF) analysis

[8] Fixed thresholds based on statistical theory have not been used. Rather, the stability of the results were compared with respect to changes in the PCs.

The primary concern about the PCR is that the MLR mismatches the physical relationship between the proxies and the signal. The predictors in MLR are assumed to be the variables that have an influence on the predictand. One would expect the NAO to influence the proxies and not the proxies the NAO. The ordinary MLR with proxies as predictors and a climate signal as a predictand is a contradictory model. Each predictor has the role of contributing independent information to the estimate of the predictand. If one reconstructs the NAO index, it is questionable how much independent information is represented in the proxies. The use of PCs in the MLR obscures this drawback. The information about the climate signal is concentrated in a few orthogonal modes. Eq. 3.7 and 3.10 both form a weighted average of the proxies. The difference is that - in case of truncation - the PCA 'rewards' those proxies that have large covariances by decreasing the weights of the other proxies.

### 3.2.2 Best Linear Unbiased Estimate

The previous reconstruction method still has some disadvantages, which call for another solution to the reconstruction problem. The *best linear unbiased estimate* (BLUE) accounts for these major drawbacks. Nonetheless, paleoclimatic reconstructions based on the BLUE theory are rare. Recently, Evans et al. (2002) made use of this theory to reconstruct the leading modes of SST variability from proxy data.
The concept of the response function is similar to the Gauss-Markov observational scheme. Given $P$ observational variables $p_{t,i}$ in the $(N \times P)$-matrix $\mathbf{P}$ (i.e. the proxy time series arranged in columns) and the unobserved state matrix $\mathbf{X}$ [i.e. a $(N \times M)$-matrix with $M$ climate signal time series in its columns] the basic linear model can be written as

$$\mathbf{P} = \mathbf{X}\mathbf{H}^T + \mathbf{N} \tag{3.11}$$

The $(P \times M)$-matrix $\mathbf{H}$ represents the linear responses of the proxies to the climate signals and $\mathbf{N}$ contains the errors. Note that the $M$ climate signals may be interpreted in different ways. For example, in the case of a univariate climate variable like the NAO index the row vector $\mathbf{X}_t$ can represent a temporal sequence of the climate variable centred at time $t$. Thus, the stationary response function in Eq. 3.1 is a special case of the state space. Denoting the signal and error covariance matrices with $\mathbf{S}_{xx}$ and $\mathbf{S}_{nn}$, the best linear unbiased estimate of the unobserved system state is given by

$$\widehat{\mathbf{X}}^T = \mathbf{K}\mathbf{P}^T = \mathbf{S}_{xx}\mathbf{H}^T(\mathbf{H}\mathbf{S}_{xx}\mathbf{H}^T + \mathbf{S}_{nn})^{-1}\mathbf{P}^T \quad . \tag{3.12}$$

The $(M \times P)$ matrix $\mathbf{K}$ is called the weight matrix. It is seen that the BLUE is a weighted average of noisy observations which accounts for the error covariance $\mathbf{S}_{nn}$. The corresponding analysis error covariance is

$$\mathbf{S}_{aa} = (\mathbf{I} - \mathbf{K}\mathbf{H})S_{xx} \quad , \tag{3.13}$$

where $\mathbf{I}$ is the $(M \times M)$ identity matrix. The BLUE reconstruction performs the scaling and noise reduction in one step, thereby including all information about the noise from the proxies. The theoretical advantages of the BLUE can be of limited practical importance. The reconstruction of a climate signal by means of proxy observations needs a lot of *a priori* information. The response function, the signal variance and the error covariance must be available to yield the best approximation. In real cases, neither the response function nor the error covariance is known *a priori*. Instead, they have to be estimated from the proxies and the climate signal in this study.

The response function is estimated by means of linear regression techniques. In this study the response function is a simple instantaneous linear response in order to reduce the number of regression parameters. This constraint can be circumvented to some extend when the data are prefiltered (see Sec. 3.1.1). The $P$ centred (i.e. zero mean) proxies are regressed on the centred climate signal ($M = 1$).

$$\mathbf{P} = \mathbf{X}\widehat{\mathbf{H}}^T + \widehat{\mathbf{N}} \quad . \tag{3.14}$$

The vector $\widehat{\mathbf{H}}^T$ holds the estimated[9] linear regression coefficients, and $\mathbf{X}$ is the observed time series of the signal. The residuals are the estimates of the errors ($\widehat{\mathbf{N}}$) which yields an estimate of the error covariance matrix $\widehat{\mathbf{S}}_{nn}$. Finally, the signal variance has to be estimated ($\widehat{s}_{xx}$). This is the calibration step of the reconstruction procedure. The estimated weight matrix in Eq. 3.12 reduces to a vector and becomes

$$\widehat{\mathbf{K}}^T = \widehat{s}_{xx}\widehat{\mathbf{H}}^T(\widehat{s}_{xx}\widehat{\mathbf{H}}\widehat{\mathbf{H}}^T + \widehat{\mathbf{S}}_{nn})^{-1} \quad . \tag{3.15}$$

Since the linear response function and the noise components are estimated by means of linear regression they are related to each other. The noise covariance matrix is estimated from the residuals of the linear regression and is thus related to the proxy covariance by

$$\mathbf{P}^T\mathbf{P} = (\mathbf{X}\widehat{\mathbf{H}}^T + \widehat{\mathbf{N}})^T(\mathbf{X}\widehat{\mathbf{H}}^T + \widehat{\mathbf{N}}) = \widehat{s}_{xx}\widehat{\mathbf{H}}\widehat{\mathbf{H}}^T + \widehat{\mathbf{S}}_{nn} \quad . \tag{3.16}$$

It follows with the linear regression estimate $\widehat{\mathbf{H}}^T = \widehat{s}_{xx}^{-1}\mathbf{X}^T\mathbf{P}$ and Eq. 3.15, 3.16 that

$$\widehat{\mathbf{K}}^T = \mathbf{X}^T\mathbf{P}(\mathbf{P}^T\mathbf{P})^{-1} \quad . \tag{3.17}$$

The BLUE estimate is equivalent with the MLR when the response function and the noise is estimated by means of linear regressions. The initial idea of the BLUE theory, the concept of the climate signal influencing the proxies, loses its advantage over the MLR. The solution of the BLUE is directed to the MLR through the linear regression estimates of the model parameters. However, it must be kept in mind that other ways of estimating the parameters can break up the equivalence.

### 3.2.3 Weighted Average Regression

The idea behind the *weighted average regression* (WAVER) is rather simple and follows the considerations in Sec. 3.1. Assuming that a noisy climate signal is present in $P$ proxies $\mathbf{P}_i$, it should be possible to reduce the noise by means of averaging the proxies. The success of this method depends on the noise structure (see Eq. 3.6). The simple weighted averaging does only reduce the local noise variance. The covariance of the climate noise is not considered. In order to simplify the averaging process the proxies (and the signal) can be normalised. The transformation of the proxies to a unique scale is necessary for the weighted average

$$\overline{\mathbf{P}} = \mathbf{P}\mathbf{K} \quad . \tag{3.18}$$

The vector $\mathbf{K}$ contains the weights for the $P > 1$ proxies, which are arranged in the columns of the matrix $\mathbf{P}$. The weight for the i-th proxy depends on its correlation $r_i$ with the signal. The squared correlation is the fraction of signal variance that is explained by the proxy. Intuitively, one can use the explained variance for defining the proxy weights:

$$k_i = sgn(r_i)r_i^2\left(\sum_{m=1}^{P} r_m^2\right)^{-1} \quad . \tag{3.19}$$

[9] Note that they are estimated in $P$ individual univariate regressions.

Since the correlation could be negative the sign of the correlation has to be taken into account. The explained variance is divided by the sum of all individual explained variances because the sum of the weights should be one.
Defining the proxy weights in that way does not guarantee optimal statistical properties (for example, least square errors are not minimised). This can be easily seen in the case of two proxies. If one proxy was a perfect copy of the signal ($r_1 = 1$) and the second had a correlation of $0 < r_2^2 < 1$ the weight of the first proxy is not one. Instead, the weighted average would include the second proxy, thereby adding unnecessary noise. In this example, the weights clearly miss the optimal solution to the problem. In case of the NAO index reconstruction, proxies are never perfect. Therefore, the problem will never be so drastic. Instead, it might be useful that the weights reduce the influence of a highly correlated proxy. It will be shown later (see Sec. 5.2.3) that the estimated correlations can suffer from large uncertainties. The weighted average is able to reduce the effect of a single overestimated correlation.
In a second step, the weighted average proxy time series $\overline{\mathbf{P}}$ has to be rescaled to the signal. The averaged time series is regressed on the signal. The regression parameters transform the weighted averages yielding the reconstructed signal:

$$\widehat{\mathbf{X}} = \widehat{b}\,\overline{\mathbf{P}} + \widehat{a}\,\mathbf{1} \quad , \tag{3.20}$$

where $\mathbf{1}$ is a vector consisting of elements with value one.[10] Application of the WAVER in reconstructions requires the determination of the proxy weights (Eq. 3.19) and the estimation of the regression parameters (Eq. 3.20). This will be achieved in the calibration step.
The close resemblance between Eq. 3.18 and Eq. 3.12 stresses the fact that the weighted averaging reconstruction method is a simplification of the BLUE method. Compared with the PCR, the weighted average replaces the eigenvector analysis and the truncation of the predictors.

## 3.3 Applied Filter Technique

Univariate time series filtering and spectral analysis methods are almost always a constituent part of time series reconstructions. Previous reconstruction studies often applied filters to the reconstructed time series. A few studies have incorporated the filter concept into the reconstruction method. Guiot (1985) and Osborn and Briffa (2000) decomposed the temporal variability of tree-ring chronologies into different frequency ranges before reconstructing climatic signals. The preceeding considerations of Sec. 3.1.1 have shown that the reconstruction should take frequency-dependent relationships into account. A comfortable, mathematically well-funded way to decompose the variance of a time series into several frequency bands is the *maximum overlap discrete wavelet transform* [MODWT]. The basic concepts and the important properties of this filter method are introduced. A comprehensive mathematical background about the MODWT can found in the book of Percival and Walden (2000).
Let $\mathbf{X}$ be a $N$-dimensional vector whose elements are given by a time series $x_t$ where $t \in \{0, 1, \ldots, N-1\}$. The j-th level MODWT wavelet coefficients $\mathbf{W}_j$ are the filter results of

$$w_{t,j} = \sum_{u=0}^{N-1} h^{\circ}_{j,mod(t-u,N)} x_u \quad . \tag{3.21}$$

[10] Although normalised time series are used in this section, the constant of the regression model is included. Non-centred data can be appropriately shifted to the signal.

Here $h^{\circ}_{j,mod(t-u,N)}$ is the j-th level MODWT wavelet filter periodised to length N. The index $mod(t-u,N)$ is $t-u$ where $t-u \geq 0$ and $N+(t-u)$ elsewhere. This results in a circular shift of the filter coefficients. The filtering operation can be thought of a linear transformation which band-pass filters $x_t$ in a temporally localised range centred at $t$. The resulting wavelet coefficients are associated with changes in the time series $x_t$ of scale $2^{j-1}$. Eq. 3.21 can be conveniently expressed in matrix notation as

$$\mathbf{W}_j = \mathbf{W}_j \mathbf{X} \tag{3.22}$$

with $\mathbf{W}_j$ a $(N \times N)$-matrix containing the circularly shifted filter coefficients $h^{\circ}_{j,mod(t-u,N)}$ in its rows. Similarly, one can define the MODWT scaling coefficients by application of the corresponding scaling filters

$$v_{t,j} = \sum_{u=0}^{N-1} g^{\circ}_{j,mod(t-u,N)} x_u \tag{3.23}$$

or equivalently in matrix form

$$\mathbf{V}_j = \mathbf{V}_j \mathbf{X} \quad . \tag{3.24}$$

The j-th level scaling coefficients are now associated with averages of length $2^j$ and longer. The scaling filter $g^{\circ}_{j,mod(t-u,N)}$ is equivalent to a temporally localised low-pass filter. In this study the 'coiflet' scaling and wavelet filters of width $L = 6$ (CO6) and the 'least asymmetric' filters of width $L = 8$ (LA8) are used. Computations are done with the 'pyramid' algorithm.
In applications one has to limit the scale j. Larger integer numbers j are associated with larger filter widths $L_j = (2^j - 1)(L-1) + 1$ and consequently an upper bound should be specified. Here, the largest scale $j$ to be analysed is given by the condition $J_0 < \log_2[N(L-1)^{-1} + 1]$, which ensures that at least one wavelet coefficient is not affected by the circularity condition. The periodised filters have the same elements as their corresponding MODWT filters.
One important characteristic of the MODWT is the energy decomposition

$$\|\mathbf{X}\|^2 = \sum_{j=1}^{J_0} \|\mathbf{W}_j\|^2 + \|\mathbf{V}_{J_0}\|^2 \tag{3.25}$$

where the squared norm of the vector $\|\mathbf{X}\|^2$ is the energy of the time series given by $\sum_{t=0}^{N-1} x_t^2$. Note that for centred time series the energy is a measure of its variance. The original time series can be recovered from the wavelet and scaling coefficients by use of the composition formula

$$\mathbf{X} = \sum_{j=1}^{J_0} \mathbf{W}_j^T \mathbf{W}_j + \mathbf{V}_{J_0}^T \mathbf{V}_{J_0} \tag{3.26}$$

where $\mathbf{W}_j^T (\mathbf{V}_{J_0}^T)$ is the matrix transpose of $\mathbf{W}_j (\mathbf{V}_{J_0})$. The transformation of the j-th level wavelet coefficients yield the so-called details of scale j of the analysed time series $\mathbf{X}$. The j-th level details are the band-pass filtered versions of the original time series with the frequency characteristics prescribed by the j-th level wavelet filter. Too short filter widths are prone to leakage effects. The CO6 filter suffers from leakage effects that disturb its band-pass filter character. On the other hand, the coiflet filter has good phase properties. Features in the time series of the wavelet coefficients are almost in phase with the features in the time series of the corresponding details. The leakage effects can be reduced when the LA8 filter is used instead of the CO6 filter, but the zero-phase quality slightly decreases.

# Chapter 4

# NAO-Signature in Greenland Ice Cores

This chapter guides through the physical processes linking ice-core proxies with the NAO and the application of the reconstruction methods to ice-core proxies. Previous studies explored the influence of the NAO on Greenland ice-core proxies. They identified ice cores as potential sources for the reconstruction of the NAO (Barlow et al., 1993, 1997; White et al., 1997; Rogers et al., 1998; Appenzeller et al., 1998a). However, the quantitative assessment of the influence of the NAO was restricted to the local temperatures and accumulation rates (precipitation). A detailed analysis of the atmospheric transport mechanisms, which are important for the isotopic concentrations in precipitation, has not been presented yet. The impact of the NAO on the local climate and the concurrent changes in the transport mechanisms are analysed in section 4.1. The results provide insight into the reconstruction potential of Greenland ice-core proxies. In section 4.2 ice-core proxies are used to test the reconstruction methods.

## 4.1 The Imprint of the NAO on the Climate

The physical connection between ice core proxies and climate factors has been described in chapter 2. This section presents the impact of the NAO on those climate factors which are important for proxies in the Greenland area. The intention behind is to provide a rational physical basis for the following NAO reconstructions. The results help to estimate the potential reconstruction skills of Greenland's proxies. Attention is directed to the climate variables temperature and precipitable water. Cyclone movements and atmospheric moisture transports as well as isentropic trajectories are analysed in order to shed some light on the moisture transports which are responsible for Greenland's precipitation.

### 4.1.1 Temperature and Precipitable Water

Observational records of temperature and precipitation are rare on Greenland. A few coastal stations exist where continuous instrumental observations have been recorded. In the 1980s and 90s automatic weather stations have been installed, which are the only ground-based observations from the central Greenland's ice shield (Stearns et al., 1997). Therefore, the monthly mean NCEP/NCAR reanalysis data (Kalnay et al., 1996; Kistler et al., 2001) from 1948 to 1998 are chosen as the primary data source for the following regression analyses.
The isotopic composition of snow is influenced by the ambient air temperature during the formation of precipitation. Due to the strong correlation of $\delta^{18}$O with the near-ground temperature

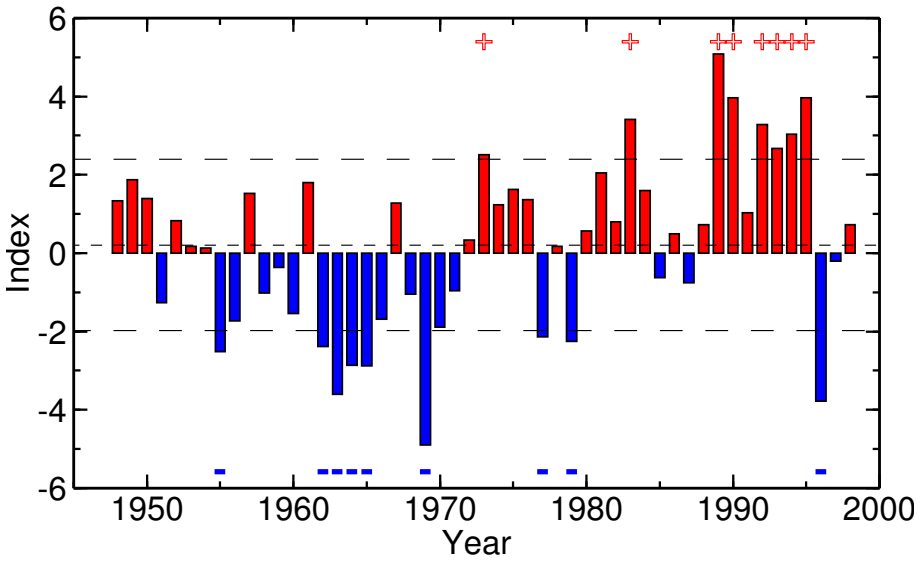


Figure 4.1: *Time series of the winter-season (DJFM) NAO index from Hurrell (1995). Years exceeding (falling below) one standard deviation are marked with red crosses (blue minus signs). The 1948–1998 mean and standard deviation are represented by the dashed and long-dashed lines, respectively.*

(Werner and Heimann, 2002), the air temperature of the lowest sigma-level in the NCEP/NCAR reanalysis is regressed on the winter (DJFM) NAO index from Hurrell (1995) (Fig. 4.1). The associated regression and correlation patterns are depicted in Fig. 4.2. Temperature changes induced by variations of the NAO exhibit large magnitudes (see Fig. 4.2b) over the Labrador Sea and Greenland Sea, but of opposite signs. Strong NAO phases [i.e. a high NAO index of +1 standard deviation (STDDEV)] are accompanied by negative temperature anomalies over the Labrador Sea and West Greenland that exceed -2 K. East from Greenland, positive anomalies of +2 K are induced by +1 STDDEV in the NAO index. The correlation pattern (Fig. 4.2a) clearly shows a decreasing influence of the NAO from southwest to northeast over Greenland. Both aspects, a large amplitude and a strong correlation, favour the western and southern part of Greenland as a potential archive of the NAO history.

The possible effect of the NAO on the precipitation over Greenland is indirectly shown through the effect on precipitable water. The reason for using this variable instead of the precipitation itself is that precipitation from the NCEP/NCAR reanalysis is completely model-dependent [‘class C’ variables, Kalnay et al. (1996)] and has some deficits (Cullather and Bromwich, 2000) in Arctic regions. Precipitable water is a ‘class B’ variable and probably more realistic. It is important to realise that precipitable water is not in a firm relation with precipitation. An estimate of the precipitation amount from the precipitable water must be derived from calculating the moisture balance. However, the associated regression and correlation patterns are interesting since significant changes in the precipitable water change the expected range of precipitation. The regression pattern (Fig. 4.3b) indicates that the largest changes are located over the ocean regions west and southwest of Greenland. It must be noted that the orographic effects and surface boundary conditions shape the amplitude of the regression pattern: first, the higher the surface topography the smaller the vertical air column and the smaller the vertically integrated water content of the air

column. Second, and more important, low level air masses contain more water vapour over the relatively warm ocean than over cold land surfaces. Clearly, the correlation pattern (Fig. 4.3a) is less influenced by surface boundary conditions than the regression pattern. It shows that at high NAO phases the precipitable water is reduced in nearly all parts of Greenland. The highest linear relationship is found, again, over the western and southern parts of Greenland. In this region, precipitation is expected to be closely linked with the NAO variability. Previous results of Appenzeller et al. (1998a), who analysed the NAO-precipitation correlation using 15 years of monthly ECMWF reanalysis data, agree with the results above. Further, correlations with precipitation records from coastal Greenland stations (Hurrell, 1995) and modelling studies of Bromwich et al. (1999) support the idea of a pronounced influence of the NAO in western and southern areas of Greenland.

The presented regression analyses were calculated with time series of winter (DJFM) means. Only a few paleoclimatic reconstructions are available with subannual resolution so far. Proxies of sufficient dating accuracy and fine resolution are rare.[1] Most data of the published ice core proxies have an annual resolution. Reasoned on the basis of these proxies, a reconstruction of the annual mean NAO index is preferable but its usefulness for climatic analyses is small. Hurrell and van Loon (1997) demonstrated that the correlation between the sea level pressure in Stykkisholmur (Iceland) and Lisbon (Portugal) is strong during winter months and considerably weakened during summer months. One reason that contributes to the lowered correlation is the migration of the dominant pressure systems during the year (Mächel et al., 1998; Portis et al., 2001). Thus, traditional station-based NAO indices of annual means cannot represent the spatial pattern of the NAO. Therefore, a reconstruction of the winter NAO index might be more useful.

The reconstruction of winter information from proxies that represent the integrated climate effects of one year ultimately contain more climate noise than in the ideal case of wintertime proxies. This effect is illustrated in Fig. 4.4. The composites of annual temperature cycles over western Greenland (67.5–80°N/45–60°W) and central Greenland (70–75°N/30–45°W) stress the fact that the temperature differences between the high and low NAO years are restricted to winter seasons. Since the selection of high (low) NAO years (see Fig. 4.1) is based on the threshold of +1 (-1) STDDEV in the winter NAO index, the largest differences occur during the winter month. The rest of the year the annual cycles do not differ in accordance with the short decorrelation time of continental atmospheric temperatures and the negligible month-to-month autocorrelation of the NAO index (Jung, 2000). This implies that an annual mean temperature value contains a signal from the winter NAO and a considerable amount of noise from rest of the year. Comparing the monthly standard deviations with the differences of the composite, it is found that the annual cycle of the variance mitigates the disturbing effect to some extent. The low variance in the summer months reduces the noise component in the annual means. (see Fig. 4.4 lower lines in the graphs).

Summarising the important facts, the investigation of the relationship between temperature, precipitable water and the NAO identifies the highest reconstruction potential for NAO index reconstructions in the area of western Greenland. The region where most of the ice core drilling projects are located, central Greenland, provides a reasonable reconstruction potential for ice core proxies. Seasonally resolved proxies should be used in winter NAO index reconstructions.

[1] Recently Vinther et al. (2003) have shown that the explicit use of winter-season information of the ice cores ($\delta^{18}$O) can improve the reconstruction.

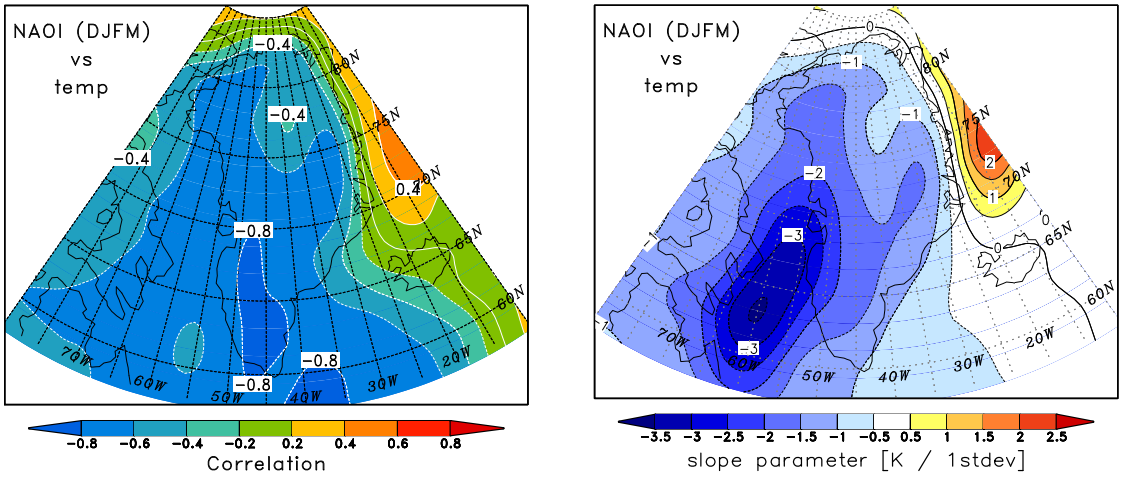


Figure 4.2: *Associated correlation pattern (a) and regression pattern (b) of the NCEP/NCAR temperature on the lowest sigma-level (0.995). The NAO index (DJFM) from Hurrell (1995) was used in the regression analysis over the interval 1948–1998.*

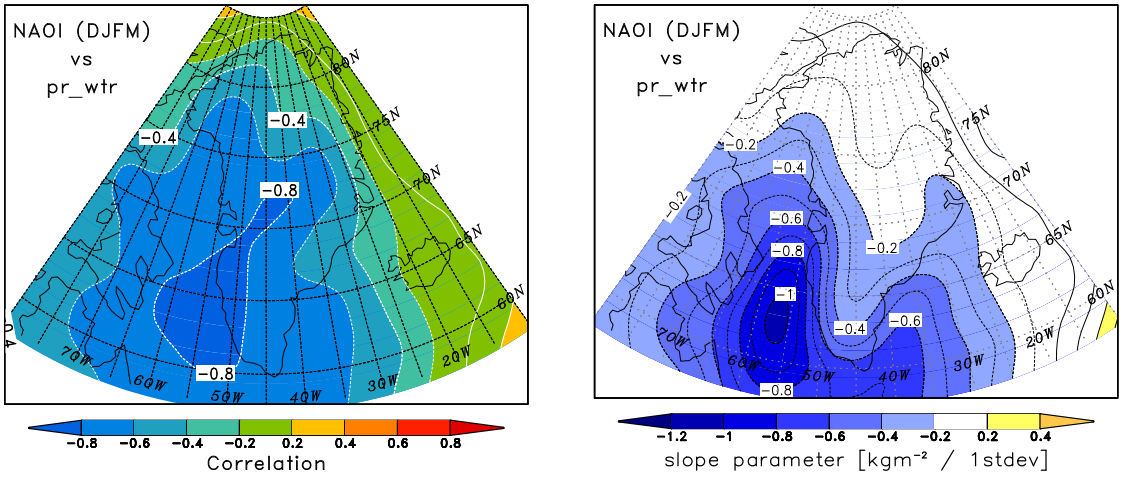


Figure 4.3: *The same as in Fig. 4.2 but for precipitable water from the NCEP/NCAR reanalysis.*

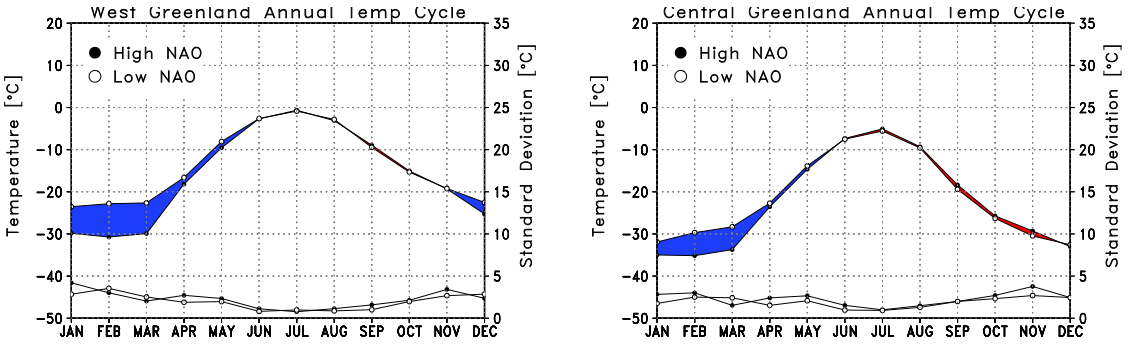


(a) (b)

Figure 4.4: *Composites of the annual temperature cycles in (a) western Greenland (67.5–80°N/45–60°W) and (b) central Greenland (70–75°N/30–45°W). High (low) year composites are marked with filled (open) circles. Positive (negative) high-low differences are coloured in red (blue). The lower lines in each plot are the standard deviations in the composites. Note the different scales. Standard deviations (right axis) are scaled by a factor two compared with the annual mean temperature scale.*

### 4.1.2 Water Vapour Transport Mechanisms

The interpretation of $\delta^{18}$O as a local temperature signal is a simplification of the intricate processes (described in section 2.1) forming the $\delta^{18}$O-signal in precipitation. Regarding the reconstruction of the NAO, it would be important to understand what is the integral effect of the NAO on the isotopic concentration. Obviously, the large-scale atmospheric changes over the North Atlantic that accompany the NAO variability have an impact on the moisture transport towards Greenland and the origin of the precipitating waters. Hurrell (1995), Schröder (2001) and Ruprecht et al. (2002) have shown that the vertically integrated moisture fluxes are drastically changing during high and low NAO index years. In this section the fluxes are re-investigated in the Greenland area since detailed inspections have barely been available, which focused on the variability related to the NAO (e.g. Bromwich et al., 1999).

The moisture transport that is under investigation was calculated from the NCEP/NCAR reanalysis data on pressure levels. Here the vertically integrated transports are analysed. The total transport is separated into a mean and an eddy component. The mean transport is the contribution of the seasonally averaged wind and specific humidity. The eddy transport is the net result of the high-frequency (i.e. time scales shorter than a season) deviations from the seasonal means. Details of the calculations can be found in Schröder (2001). Composites are calculated for high and low NAO phases according to the years marked in Fig. 4.1. The comparison indicates the major mean flux southeast of Greenland over the North Atlantic (Fig. 4.5). The magnitude of the mean flux is strongly increased and more zonal during high NAO phases in that region. Over the western part of Greenland the mean transport is directed to the north and northwest. This transport is considerably reduced during high NAO phases. The eddy flux is less important for the total transport over the North Atlantic southeast of Greenland, and it is mostly unaffected by the NAO variability. To the west, the contribution of the eddy transport to the total moisture fluxes increases. The main transport is directed from south (southeast) to the north. The direction is almost con-

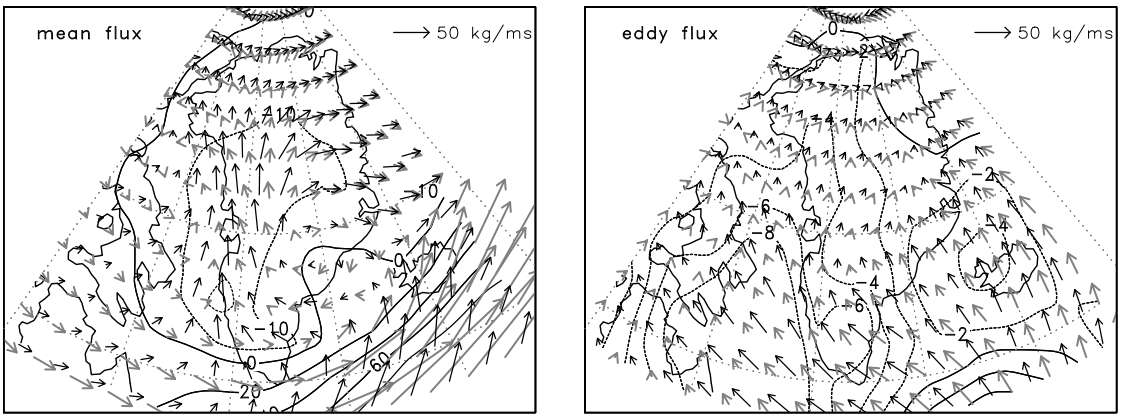


(a) (b)

Figure 4.5: *Vertically integrated moisture transport of (a) the mean atmospheric circulation and (b) the eddy transport. Averaged transport vectors of the high (low) NAO index years are drawn in grey (black). Contour lines represent the difference between the magnitudes of the vectors. Negative values indicates smaller transport magnitudes in the high NAO index phase.*

stant over Greenland (with exceptions in northern Greenland) with respect to the variability of the NAO. The eddy flux magnitude is reduced over southern and western Greenland during high NAO years. Apparently, the moisture transport towards central Greenland is channelled into two inflow streams, one from the southeast and another from the southwest. This reinforces the earlier results of Ohmura and Reeh (1991), Calanca (1994), Barlow et al. (1997) and Bromwich et al. (1998). The divergence in the fluxes gives a fair estimate of the precipitation amounts. Schröder (2001) has investigated the influence of the NAO on the divergence in moisture fluxes. The largest and probably most robust differences are found over western Greenland. The reduced convergence in the eddy component could decrease the precipitation during high NAO years. However, errors in the moisture advection scheme of NCEP/NCAR (Cullather and Bromwich, 2000) and topographic effects (Calanca, 1994) prohibit a detailed investigation over Greenland. A quantitative assessment of the NAO-precipitation relationship seems not admissible. Qualitatively, it could be concluded that precipitation is linked to the synoptic activity in southern and western Greenland, and the activity is covarying with the NAO. This is supported by the outcomes of earlier studies (Robasky and Bromwich, 1994; Serreze et al., 1995; Chen et al., 1997; Serreze et al., 1997; Bromwich et al., 1999).

If the eddy transport was accomplished by the synoptic activity [2] and correlated with the NAO, one would expect systematic differences in the cyclone activity over the Labrador Sea, the Baffin Bay and the southeast of Greenland. Several works on cyclone statistics investigated the intimate connection between the cyclone frequency in the climatological region of the Islandic low and the NAO (Rogers, 1997; Serreze et al., 1997; Sickmöller et al., 2000; Ubl, 2001; Geng and Sugi, 2001; Gulev et al., 2001; Löptien, 2003). A high NAO index is mainly the result of a greater number of cyclones in the Islandic region. Over the Labrador Sea and the Baffin Bay, the frequency of cyclones does not depend on the phase of the NAO in a regular manner. Thus, the question is how can the precipitation be lowered during high NAO phases? Ubl (2001) has shown that the

[2] Note that the eddy fluxes also contain covariability on time scales larger than 8 days (Calanca, 1994)

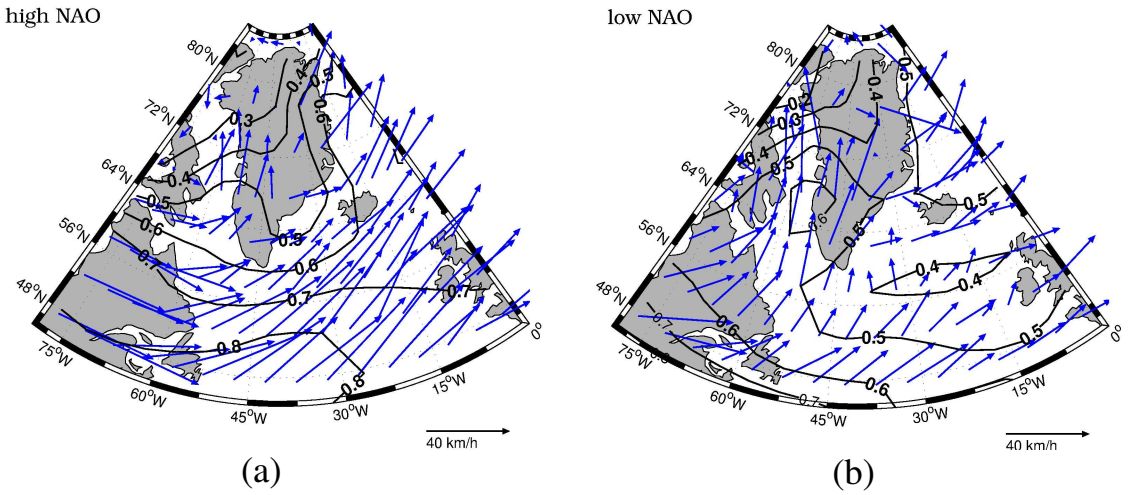


Figure 4.6: *Averaged cyclone centre motion for (a) the high and (b) low NAO index winters (JFM). Blue arrows indicate the average speed and direction of all cyclone centres that moved through the* $\approx 5^\circ \times 5^\circ$ *grid box during the selected composite years. The constancy (i.e. the mean vector magnitude divided by the mean scalar speed) of the vectors is given by the contours.*

mean cyclone motion systematically changes between high and low NAO index years. Fig. 4.6 depicts the average velocity vectors of the cyclone centres. During high NAO phases the cyclones move more zonal and faster from Labrador over the Atlantic towards the east. Cyclones over the Labrador Sea and the Baffin Bay enter this region from the high latitudes in the west. In contrast, during low NAO phases cyclones can enter the Baffin Bay from the southwest. Reminding that the number of cyclones is nearly the same in high and low NAO phases, it seems that the cyclones from warmer southern regions can carry more precipitation towards Greenland in low NAO index years. This implies that the transport history of the precipitated waters is different for high and low NAO phases.

Another way to illustrate the spatial changes in transport characteristics is the calculation of individual virtual air parcel trajectories. Ideally, one would like to follow air parcels which are responsible for precipitation on Greenland. Different trajectory methods have been developed and applied for various purposes (e.g. Danielsen, 1961; Petersen and Uccellini, 1979; Merrill et al., 1986; Fuelberg et al., 1996). Some workers analysed trajectories for a better understanding of the variability of chemical species and aerosols in arctic regions (Kahl et al., 1989; Davidson et al., 1993; Kahl et al., 1997). In the following section, the isentropic back trajectories are analysed in order to highlight their relation to the NAO. The basic idea behind isentropic back trajectories is that quasistatic, frictionless motions are approximately adiabatic. For such atmospheric conditions the potential temperature of an air parcel is constant along its trajectory as long as diabatic heating is negligible (Danielsen, 1961; Merrill, 1994; Fuelberg et al., 1996). Adiabatic motions are fully horizontal in isentropic coordinates. The vertical velocity is implicitly given by following the height of the isentropic layer. The back trajectories are calculated for the winter season NDJFM[3]. The potential temperature $\theta = 296$ K is chosen as the isentropic height level. This level corresponds to a mean pressure level of $p = 500$ hPa on the 70°N latitude belt during winter. The destination points (i.e. the backwards trajectory calculation starts at those points) are located

[3]November to March is used in order to obtain larger samples of trajectories for each winter.

| Low NAO years | High NAO years |
|---|---|
| 1955 | 1989 |
| 1963 | 1990 |
| 1969 | 1994 |
| | 1995 |

Table 4.1: *Selected high and low NAO years based on a 1 STDDEV threshold for the NAO index values. Four (three) years with a NAO index above +1 (below -1) STDDEV have been chosen as high (low) NAO years. Note that the NAO index of Jones et al. (1997) was used and the standardisation was based on the winter season (NDJFM) index 1948–1998.*

west off Greenland. Kinematic trajectories[4] are followed 5 days back in time. Details about the calculations are given in Danielsen (1961); Merrill et al. (1986); Leckebusch (1999). The original program code was written by Bleck (1967) and updated at the 'Institut für Geophysik und Meteorologie der Universität zu Köln' (Melzer et al., 1998).
The difference between high and low NAO index years is analysed by means of the composite technique. Tab. 4.1 lists the high and low NAO index years. The two-dimensional density distribution of the trajectory points is a convenient measure of the spatial characteristics. Smoothed kernel-estimated (Silverman, 1986) density fields are shown in Fig. 4.7. The kernel density estimation is combined with a nonparametric cluster-analysis algorithm (Comaniciu and Meer, 1999) in order to detect local maxima in the density field. It must be admitted that the cluster analysis is not an optimal tool for statistical inferences but it suffices for highlighting the features in the spatial distribution of the trajectories. The spatial distributions show the locations of the air parcels three days (Fig. 4.7a,b) and four days (Fig. 4.7c,d) before they reach the destination sites. The density fields reveal a maximum over the north of Canada during the high NAO phases. Similarly, during the low NAO index years a maximum is centred over northwest Canada. The most striking difference is a second maximum further southeastwards over Labrador and the Great Lakes. Another important difference can be seen over the North Atlantic southeast of Greenland. In the case of low NAO, air parcels that originate from the central and east North Atlantic can frequently reach West-Greenland. But this is not the case in high NAO situations. The results strongly support the idea that air masses follow two distinct paths towards Greenland. As a consequence, it is conceivable that both source regions and trajectories of precipitating air masses are similarly affected by the NAO. Finally, it should be emphasised that more efforts would be required to follow the precipitation back to its source region. Isentropic trajectories can not be used to follow precipitating air parcels back to their source regions due to diabatic effects and boundary-layer mixing processes. Parametrisation of these effects and the proper selection of the precipitation events at the destination points are necessary (Dirmeyer and Brubaker, 1999; Leckebusch, 1999).
The overall conclusion is that the NAO signal in $\delta^{18}$O-proxies from Greenland is not a local temperature signal. The effect of changes in the source regions and transport pathes of the precipitating air masses might either amplify or damp the local temperature signal. A detailed quantification will require modelling studies similar to those of Armengaud et al. (1998), Werner (2000), and Hoffmann et al. (2001).

[4] derived from the horizontal wind fields of 4-times daily NCEP/NCAR reanalysis data.

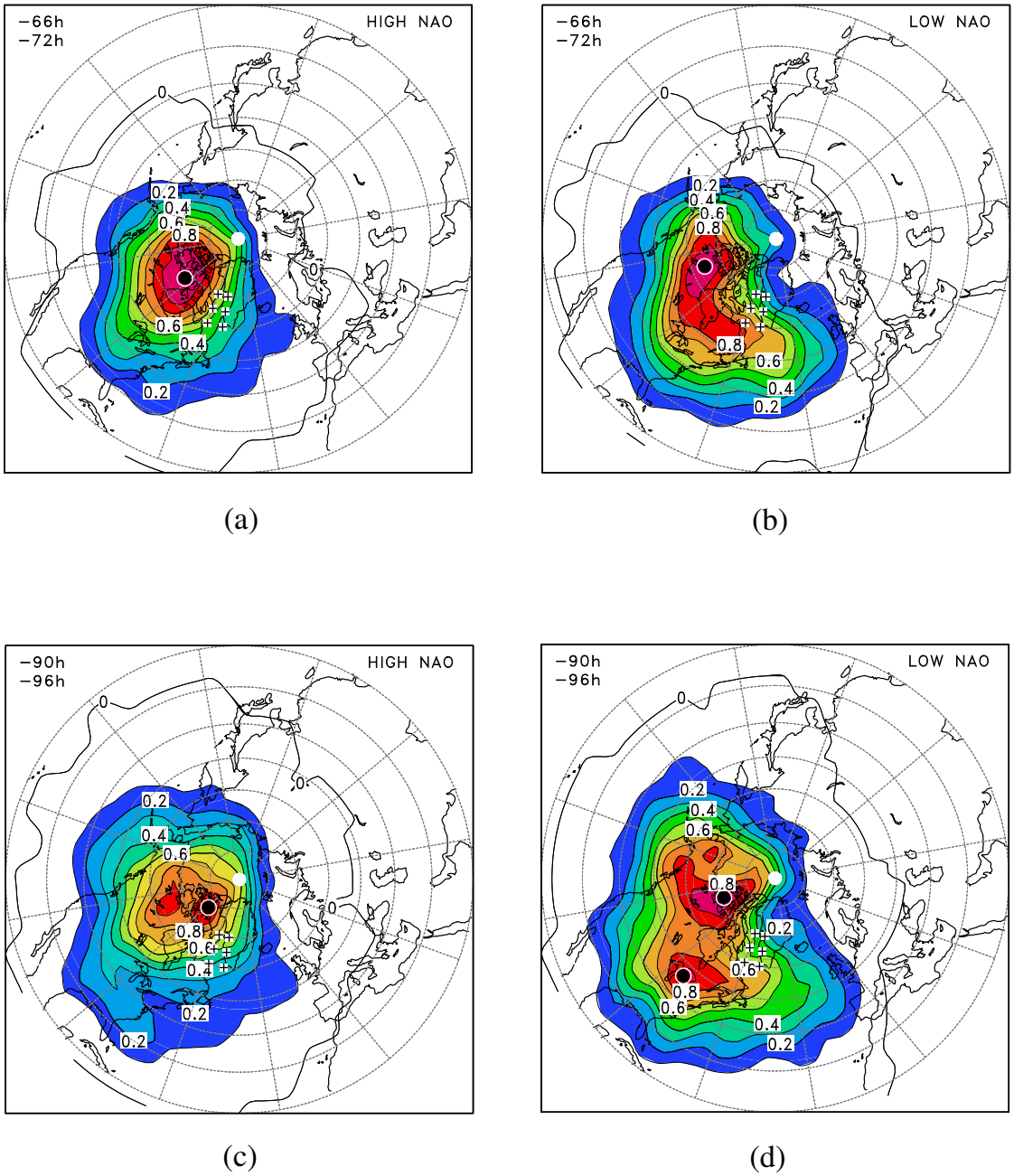


Figure 4.7: *Kernel-estimated density fields of wintertime (NDJFM) 296K-isentropic back trajectory points: on the left (a, c) the high NAO index years, on the right (b, d) the low index years. The density fields of the trajectory points are shown for two successive travel times: (a, b) three days, (c, d) four days before passing one of the sites west of Greenland (marked with crosses). Note that each density field is scaled with respect to its maximum value. Cluster centres are marked with black filled circles.*

## 4.2 Testing the Reconstruction Methods with Ice-Core Proxies

Reconstructions of climatic signals from proxies are difficult for several reasons. The difficulties arise from the intricate relationship between the proxies and the climate signal. Practical limitations of the reconstruction methods are mainly caused by (relatively) small sample sizes, i.e. too short calibration intervals. In this section the skill of the reconstruction methods (PCR, WAVER, BLUE) is tested. Note that the special configuration of the BLUE method is equivalent to the MLR. The MLR is included in the comparison to demonstrate the 'worst-case' disagreement between the calibration and validation statistics. A composite of 16 ice-core proxies with annual resolution (10 $\delta^{18}$O, 6 accumulation proxies, see App. A.1 for details) is the basis of the reconstruction. This proxy set covers the temporal interval 1777–1978. The climate signal is represented by the wintertime (DJFM) NAO index of Jones et al. (1997) during the years 1825–1978. All time series are normalised to zero mean and unit standard deviation over their complete time interval.[5] The discussion of the results gives insight into the key problems pertinent to both the proxies and the reconstruction methods.

Before the PCR is calculated the covariance structure of the proxies is analysed. The leading eigenvectors of the proxy covariability are important because they determine the weights of the proxies in the reconstruction (see Sec. 3.2.1). The PCA of the proxies is calculated for the period 1902–1978. The first mode explains 45% of the total variance. The second mode is well separated (statistically significant) from the first mode because the explained variance of the second mode only amounts to 11% of the total variability. The eigenvector structure is depicted in Fig. 4.8a. All proxies have the same sign. This monopole structure in the eigenvector is associated with a PC time series that is a weighted average of the proxies, where the $\delta^{18}$O-proxies have a larger weight than the accumulation proxies. It is a remarkable fact that almost half of the variance is represented in one eigenmode. Clearly, a common signal must be present in the proxies, but the NAO is not the dominating contributor to this signal. When the proxies are linear regressed on the NAO index and the eigenvectors of the residuals are determined, the first eigenvector of the PCA is similar to the previous one (Fig. 4.8b). The fraction of explained variance is only reduced to 42%. Comparing the structure of the regression pattern (Fig. 4.8c) with the eigenvectors, it is evident that some proxies have large weights in the eigenvector even though they are poorly correlated with the NAO index. The statistical behaviour is in qualitative agreement with the estimated reconstruction potential of central Greenland ice-core proxies (see Sec. 4.1). In conclusion, the NAO has a moderate impact on the climatic conditions in central Greenland, and signals unrelated to the NAO dominate the covariance of Greenland's proxies.

It is interesting to compare the behaviour found in the proxies with the PCA of the sea level pressure (SLP) over the North Atlantic. The NAO is often represented by the first mode of the PCA (Hurrell et al., 2003b). The PCA of the SLP data 1902–1978 (data from Trenberth and Paolino, 1980) is performed in the same manner as before. First, the complete SLP variability is analysed. Second, the residuals of the SLP variability regressed on the NAO index is examined. The residuals contain that part of the variance that is not represented in the regression pattern in Fig. 4.9a. The leading mode of the SLP field explains 40% of the SLP variability. The second and third modes are not well separated. They explain 17% and 15% of the variability, respectively. The associated eigenvector of the leading mode is depicted in Fig. 4.9b. The striking resemblance to the regression pattern reinforces the fact that the NAO variability is included in one single mode. Consequently, the two leading PCA modes of the residuals are identical with the second and third

[5] Under the assumption that the time series are weakly stationary processes, the choice of the interval is arbitrary.

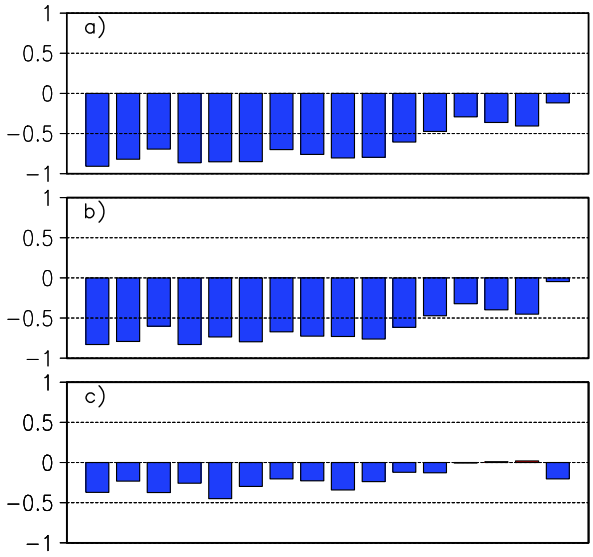


Figure 4.8: *Comparison between the first eigenvector of the Greenland ice-core proxies (a) and the first eigenvector of the proxy covariance when the variance explained by the NAO is subtracted from each proxy (b). The regression pattern is depicted in (c). Calculation include data from 1902–1978. Scales are unitless. Note that (counting from left to right) the first 10 positions are associated with the $\delta^{18}$O-proxies; the last 6 are accumulation proxies.*

modes of the SLP field. They explain 27% and 25% of the variance in the residuals. The ranks of the eigenvectors are interchanged (a result of the lacking separability) compared with their previous ranks in the PCA of the full SLP variability. The third eigenvector of the SLP covariance is depicted in Fig. 4.9c. The resemblance to the first eigenvector of the residuals (Fig. 4.9d) illustrates that the PCA is able to extract the NAO signal.

The possibility of concentrating the NAO signal in a single PCA mode is not guaranteed for proxies. The choice of the PCs that serve as predictors in the PCR must be under careful consideration. The primary goal of the selection is to find a basis for the reconstruction that provides a maximum S/N-ratio. Starting with unfiltered ('raw') reconstruction tests, the PC of the first mode of the PCA and the signal have a correlation of $r = 0.33$ ($r = 0.35$) over the period 1825–1901 (1902–1978) (see Tab. 4.2). Thus, the correlation in the time interval 1825–1901 is the same as in 1902–1978. The robustness of correlation is not given in the case of the second PC. The calibration in the period 1902–1978 fails to be verified in the validation period 1825–1901 and vice versa. The third PC is a better predictor than the previous one. Its correlation with the NAO index is robust with respect to the chosen temporal period. The combination of the first and third PC as predictors increases the correlation without inducing any biases (the correlations of the calibration and validation are at the same level [Tab. 4.2]). If the second PC is added to the predictors, the correlation between the calibrated reconstruction and the signal is increased. But the validation is now worse than before (when the second PC did not join the predictors). Nonetheless, the corresponding reconstructed time series is still close to the other reconstructions (see Fig. 4.10). The conclusion is that as long as the number of predictors is kept small the PCR is a robust reconstruction method. The optimum choice of the PCs can hardly be achieved without verifying the reconstruction against the signal in an independent validation interval. An alternative way is to extend the calibration interval at the expense of the validation interval. For example, if the calibration is extended to 1825–1978,

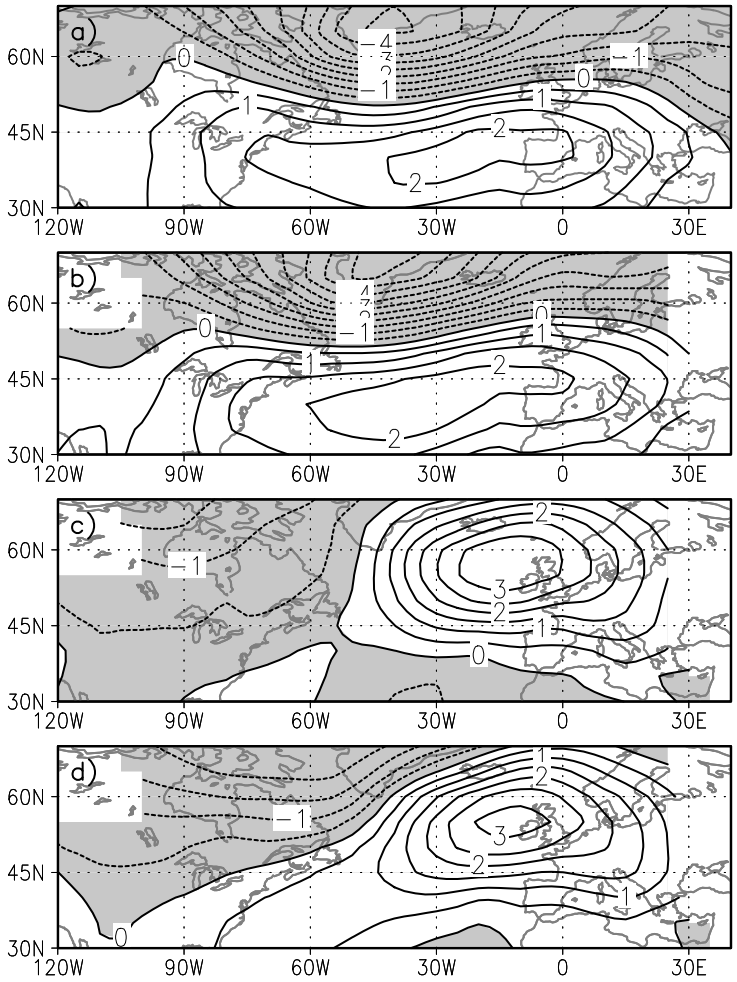


Figure 4.9: *Comparison between the regression pattern of the SLP regressed on the NAO index (a) and the first eigenvector of the SLP variability (b). The third eigenvector of the SLP (c) and the first one of the residual SLP field (d) are shown for reasons outlined in the text. The calculations includes data from 1902–1978. Contour interval is 0.5 hPa. Negative values are shaded.*

the correlation of the second PC will be close to zero and the PC will be rejected. It should be noted that statistical 'screening' techniques exist that could replace the trial and error procedure. However, validating the reconstruction would still be important (von Storch and Zwiers, 1999).

The validation step is a prerequisite for the WAVER method. The reconstruction with the WAVER method is prone to overfitting the model. The overfit results in an increased correlation coefficient in the calibration interval compared with the validation. However, the overfit of the WAVER reconstruction is considerable less than the overfit of MLR reconstruction. The large disparity in the calibration and validation statistics of the MLR (see Tab. 4.2) exceeds by far the results of the WAVER and the PCR, whereas the overfit in the WAVER and PCR methods are of comparable magnitude. Thus, the reconstruction skill of the WAVER is almost as good as the skill of the PCR, and the differences between both reconstructions (Fig. 4.10) are negligible compared with their deviations from the signal.

| | | 1825–1901 | | 1902–1978 | |
|---|---|---|---|---|---|
| Scale | Method | Calibration | Validation | Calibration | Validation |
| raw | PCR(1) | 0.35 | 0.35 | 0.33 | 0.33 |
| | PCR(1,3) | 0.37 | 0.36 | 0.39 | 0.38 |
| | PCR(1,2,3) | 0.38 | 0.30 | 0.43 | 0.35 |
| | WAVER | 0.41 | 0.31 | 0.41 | 0.35 |
| | MLR | 0.52 | 0.20 | 0.55 | 0.18 |
| W3 | PCR(1,3) | 0.45 | 0.42 | 0.43 | 0.40 |
| | WAVER | 0.59 | 0.43 | 0.54 | 0.40 |
| | MLR | 0.84 | 0.49 | 0.87 | 0.25 |

Table 4.2: *Correlation statistics of the reconstructions with Greenland ice-core proxies. The winter (DJFM) NAO index was used as the climate signal. The reconstructions were performed with three different methods (PCR, WAVER, MLR). The PCR was applied to different combinations of PCs (predictors). The predicting PCs are listed in parentheses. The first column ('Scale') indicates either the unfiltered (raw) or the filtered (W3) input data.*

The robustness of the reconstruction methods is controlled by the accuracy of the model parameters. A shortening of the calibration interval increases the error of the estimated parameters. Pre-filtering the time series causes a similar effect, especially low-pass filtering. The wavelet coefficients of scale 3 (the wavelet scale 3 will be referred to as 'W3'), which describe the decadal scale variability, give a good example. The W3 coefficients of the NAO index are reconstructed from the W3 coefficients of the proxies. This is the pre-filtering reconstruction technique outlined in Sec. 3.2. Notice that in the pre-filtering reconstruction the PCR estimates the eigenmodes from the W3 coefficients of the proxies. The correlation between the PCR reconstruction and the signal is again on the same level in the calibration and validation interval. The WAVER reconstruction has the tendency to increase the overfit (compared with the raw reconstruction). The overfit does not affect the validation results in a negative way. The correlations of the validation reach the level of the PCR results. The reconstructed time series of the W3 coefficients are virtually the same in both cases (Fig. 4.10c). In contrast, the reconstruction of the MLR method results in a large discrepancy between the correlations of the calibration and the validation interval (Tab. 4.2). The resulting reconstruction reproduces most of the signal's variance in the calibration but not in the validation period (Fig. 4.10c).

It is worth to take a closer look at the residuals of the reconstructions. The quality of the linear reconstruction method is not just measured by the correlation with the signal. In addition, the possibility of nonlinear response functions between the ice cores and the NAO should be considered. If nonlinear dependencies controlled the response functions, the residuals of any linear reconstruction method should reveal the neglected nonlinearities. The diagnosis of the residuals indicates that the linear approach, which used the PCR with the PCs of mode one and three, is a satisfactory model. The scatter of the standardised errors (i.e. divided by their standard deviation) plotted against the corresponding reconstructed values (Fig. 4.11) does not reveal any systematic dependencies. At least it can be concluded that the noise in the ice-core proxies hides any nonlinearities from being detected.

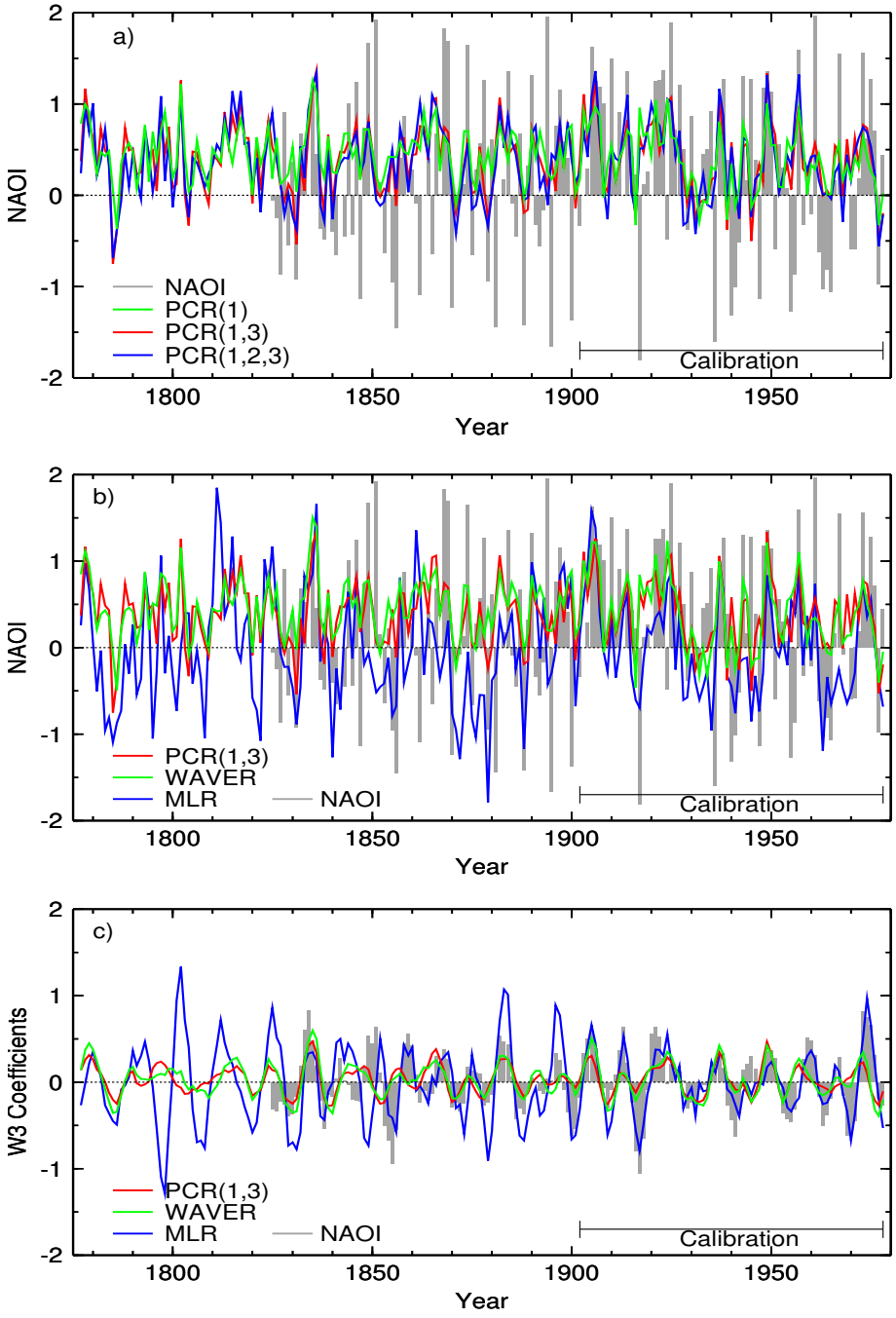


Figure 4.10: *NAO index reconstructions from the Greenland ice-core proxies: (a) the raw reconstructions of the PCR using the PC of mode 1 (green), the PCs of mode 1 and 3 (red), and the PCs of mode 1–3 (blue); (b) the raw reconstructions of the PCR with PCs 1 and 3 (red), the WAVER (green), and the MLR reconstruction (blue); (c) the corresponding W3 reconstructions. The calibration interval is 1902–1978. The winter (DJFM) NAO index (grey bars) is used as the climate signal.*

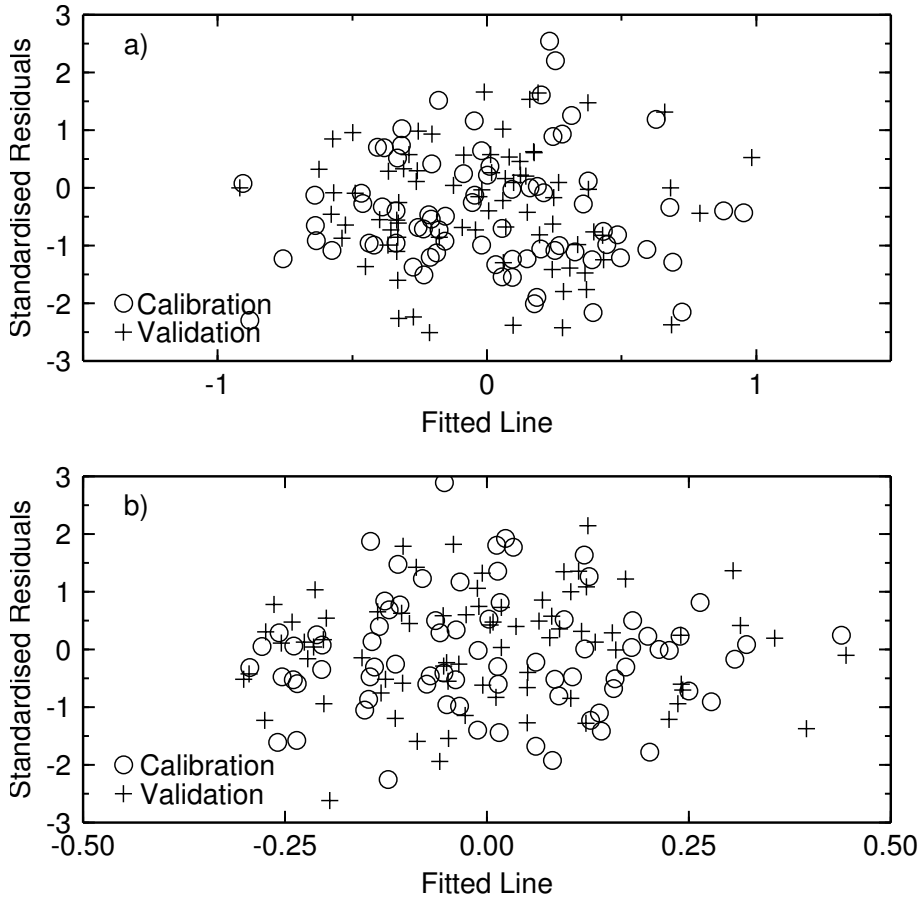


Figure 4.11: *Scatter plot of the PCR(1,3) reconstruction residuals. The residuals are plotted against the corresponding reconstructed values: (a) the raw reconstruction PCR(1,3), and (b) the W3 coefficients of the PCR(1,3) reconstruction. The residuals are normalised with respect to their standard deviations in the calibration and validation interval.*

# Chapter 5

# Multiproxy Reconstructions

The main reconstruction results are presented in this chapter. First, the decadal scale variability (8–16 years) of the wintertime (DJFM) NAO index is extended back to 1700. Second, it is attempted to reconstruct the interdecadal variability of the NAO index back into the 17th century. Each section contains a description of the used multiproxy data sets with emphasis on the proxy-NAO relationship. A central issue is to assess the statistical uncertainties of the reconstructed NAO indices. The comparison with independent estimates of the NAO's history follows. A climatic interpretation of the important features is given.

## 5.1 Decadal Variability

The quasi-decadal variability of the NAO has often been documented to contain oscillatory modes (White et al., 1996; Cook et al., 2002; da Costa and de Verdiere, 2002). Jung (2000) raised doubts about the significance of such spectral peaks. Feldstein (2002) concluded that the NAO index is broadly consistent with an AR(1)-process. Sutton and Allen (1997) described a dynamical ocean-atmosphere feedback loop that could enhance the decadal variability of the NAO. Grötzner and Latif (1998) identified a coupled mode in the North Atlantic with a time scale in the quasi-decadal range. The climate model comparison of Stephenson and Pavan (2003) did not support the existence of an oscillatory decadal mode. The discussion about the decadal variability partly results from the insufficient knowledge about the temporal evolution of the NAO index. Hurrell and van Loon (1997) found some evidence for nonstationary behaviour in the time series of the observed NAO index. However, a clear distinction between random fluctuations and nonstationarity is not possible (Wunsch, 1999). The early reconstruction results supported the idea that the decadal variability showed a modulated amplitude (Appenzeller et al., 1998b; Cook et al., 1998). The reliability of these reconstructions was later disputed by Schmutz et al. (2000) [see also Luterbacher et al. (2002a) and Cook (2003)]. It takes more effort to reach a consensus on the nature of decadal NAO variability. This section presents reconstruction results that shed some further light on the decadal time scales of the NAO index.

Ice-core proxies of Greenland reconstruct the NAO signal with some uncertainties. The presence of covarying noise prohibits the efficient exploitation of the reconstruction potential. The remedy for covarying noise is the incorporation of proxies from remote regions. European tree rings provide a valuable supplement to the ice-core archive. Their widespread abundance in Europe is appealing for the reconstruction purpose. An increased number of proxies from different regions promise to improve the reconstruction. The multiple proxy network that is used in this

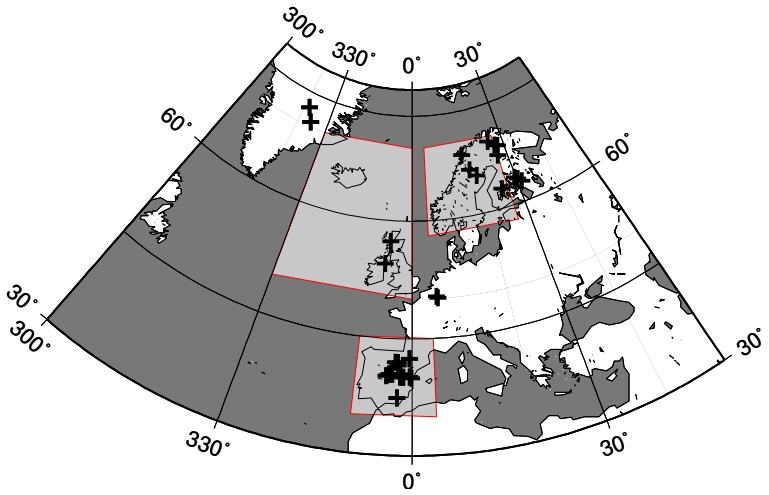


Figure 5.1: *Locations of proxies used for the decadal scale reconstruction (marked with crosses). Note that some crosses in Greenland and Spain represent more than one proxy. The highlighted areas mark the regions used for the probability density function (PDF) estimates shown in Fig. 5.2.*

chapter consists of several ice core proxies from Greenland (annual accumulation rates and annual isotopic concentrations of $\delta^{18}$O) and tree-ring width chronologies from Europe.[1] In order to compromise between the statistical constraint of an appropriate proxy number and the desire for a long extension of the NAO index, the analysis is restricted to the reconstruction period 1700–1978. Five proxies from Greenland and 38 from Europe have been available for the reconstruction (see Fig. 5.1 for their locations). The strategy of the reconstruction is to divide the trees into regional groups. For each region, an independent reconstruction is produced. From the regional reconstructions, a mean reconstruction is formed. The comparison of the regional reconstructions is important for the interpretation of the mean reconstruction. This section starts with an analysis of the NAO's influence on the winter climate in Europe. The decision which regional proxy groups are formed is based on the former analysis. The regional and mean reconstructions are described in Sec. 5.1.2. In the discussion (Sec. 5.1.3), the reconstruction is compared with the reconstructions of Luterbacher et al. (2002a) and Cook et al. (2002). The primary aspect is the climatic interpretation of the deviations among the reconstructions. This section ends with a short summary and conclusion.

### 5.1.1 Spatial Differences in the Proxy-NAO Relationships

The benefits of multiproxy data have been demonstrated by Mann et al. (1998) for temperature reconstructions. Recently, Mann (2002) recommended the use of multiproxy data for the reconstruction of spatial and temporal details. In this study, the spatial details of the NAO are not explicitly reconstructed, but it is still necessary to have a multiproxy data set in order to incorporate as much of the spatial information as possible (see section 5.1.3 for a further discussion of

[1]The data are kindly provided by several contributors of the WDC ice core data archive and contributors of the International Tree-Ring Data Bank, IGBP PAGES/World Data Center for Paleoclimatology, NOAA/NGDC Paleoclimatology Program, Boulder, Colorado, USA. Data are available at *http://www.ngdc.noaa.gov/paleo/paleo.html*.

this issue). However, the choice of proxies may be a prerequisite for the quality of the final reconstruction since the NAO is well known for its regional climatic characteristics (Hurrell and van Loon, 1997). In order to find climatic criteria for preselecting and grouping the European trees, the relationship between the NAO and European climate using monthly NCEP/NCAR reanalysis data 1948–2000 (Kalnay et al., 1996; Kistler et al., 2001) has been analysed. The monthly means (winter month DJFM only) of sea level pressure, temperature, specific humidity and precipitation were decomposed into their principal components by the PCA in order to find nearly homogeneous climate regions. The resulting regions are depicted in Fig. 5.1. For each area the probability density functions (PDF) of monthly temperatures and precipitation rates were estimated (Kleppek, 2001). A composite analysis was performed relative to the NAO index: Months with NAO index values exceeding plus (minus) one standard deviation were assigned to the high (low) NAO data subsets. The PDFs are estimated for both subsets using a Gaussian kernel (Silverman, 1986). Note that all points of the $2.5^\circ \times 2.5^\circ$ grid lying inside the rectangles were used rather than the areally averaged data. Figure 5.2 depicts the results for the regions of Scandinavia, the Iberian peninsula, and the East Atlantic sector around Iceland and the British Isles.

Scandinavia is characterised by shifts in the temperature PDFs from lower values during weak NAO month to higher values during times of strong NAO (Fig. 5.2a). The bimodality in the PDF is due to the climatic differences between the north and south of this region. The precipitation PDFs suggest that high precipitation rates are more frequent and more extreme during high NAO phases (Fig. 5.2d). The influence of the NAO on the climate of the Iberian peninsula is stronger on precipitation than on temperatures (Fig. 5.2 b+e). High precipitation rates occur more frequently in the weak NAO phase than in the strong NAO phase. Temperature PDFs just show small differences. During high NAO winters higher temperatures prevail but there is less evidence for changes in the extremes. The third region of interest is the eastern North Atlantic sector inclusive the British Isles. The temperature changes are similar to those observed in the PDFs of southwestern Europe with preferred values above the mean during strong NAO winters (Fig. 5.2 c). On the other hand, precipitation characteristics are comparable to the differences in Scandinavia (Fig. 5.2f). The results are in agreement with the outcomes of Hurrell (1995), who investigated the influence of the NAO on European temperatures and precipitation using ECMWF data from 1979–93. The NCEP/NCAR reanalysis data, however, are available for more than 50 years now and allow an even closer assessment of the statistical properties. The precipitation reanalysis data may be of lower standard than the temperature data, but they should be of sufficient quality for the purpose of the presented composite analysis, unless any systematic errors in the precipitation depend on the strength of the NAO.

It is expected that proxies from the above regions are exposed to different climatic variations connected to the NAO. Thus, it seems reasonable to group the proxies in accordance with the climatic evidence. Each group records the NAO signal from a different ‘perspective’. Comparing the resulting regional reconstructions with each other can help to attribute some of the observed discrepancies in the published NAO reconstructions (see section 5.1.2). However, it must be remembered that the identification of the regions is probably biased towards an unprecedented anthropogenically forced climate state. In preindustrial times, the selected regions may have shown different climatic responses to the NAO. Other regions could have shown a larger impact to the NAO. The proxy selection and regional grouping itself could be biased by those factors (Cook et al., 2002; Cook, 2003). Moreover, the criterion of selecting the regional groups only follows the climatic evidence. Dendroclimatic aspects are neglected (cf. Sec. 2.2, Fig. 2.3). Since the used tree-ring width chronologies stem from different tree species, each species might respond in a different way to the NAO-related climate forcing. The biological diversity of the tree’s sensitivity can result in

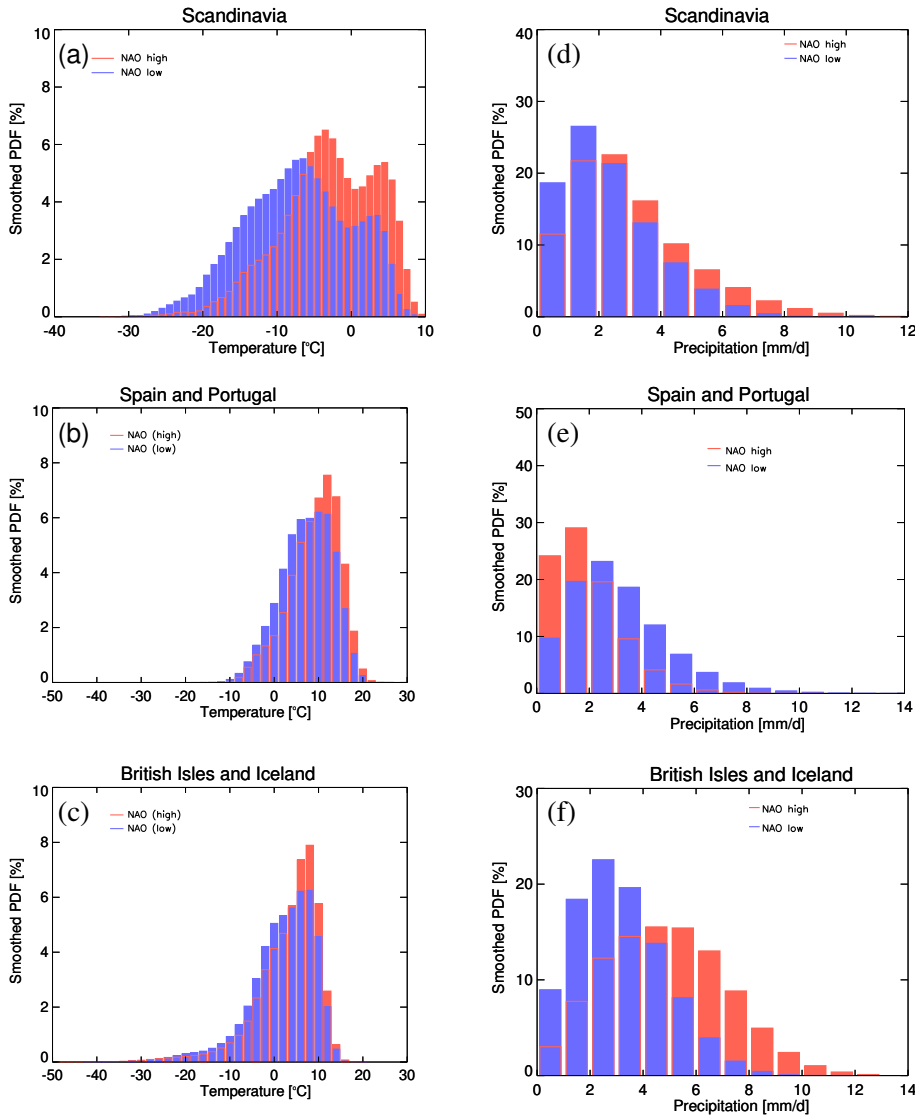


Figure 5.2: *PDFs of temperature and precipitation rates in different geographical regions (see Fig. 5.1) and for high and low NAO index winters. Figures (a), (b), (c) display temperature PDFs calculated from monthly mean values inside of each region; (d), (e) and (f) the same but for precipitation. Red bars show the PDFs for the high NAO index and blue bars represent the results for the low NAO index. Note the different scales on the axes.*

an indefinite signal representation within each group.

### 5.1.2 Reconstruction Results

The signal to be reconstructed is an index of decadal NAO variability. The updated[2] wintertime (DJF) NAO index of the years 1825–1978 defined by Jones et al. (1997) represents the climate signal of the NAO. The MODWT is applied to extract the decadal scale variability from the NAO

[2] available at *http://www.cru.uea.ac.uk/~timo/projpages/nao_update.htm*

| | 1825–1901 | | 1902–1978 | |
|---|---|---|---|---|
| | Calibration | Validation | Calibration | Validation |
| GR | 0.59** | 0.45 | 0.59** | 0.54* |
| SC | 0.58** | 0.39 | 0.67** | 0.53* |
| BB | 0.34 | 0.18 | 0.35 | 0.18 |
| SP | 0.60** | 0.30 | 0.65** | 0.59** |
| R1a/b | 0.76** | 0.57** | 0.87** | 0.77** |
| R2a/b | 0.71** | 0.46 | 0.82** | 0.69** |
| COOK | 0.80** | | 0.75** | |
| LUT | 0.69** | | 0.88** | |

Table 5.1: *Correlation statistics for different NAO-Index reconstructions on wavelet scale 3 (8–16yr bandpass). Reference index is the winter (DJFM) NAO index after Jones et al. (1997). GR, SC, BB, SP refer to the pre-filtered reconstructions from Greenland, Scandinavia, British Isles and Belgium, and Spain. R1a (R1b) is the mean of the regional reconstructions based on the 1902–78 (1825–1901) calibration period. R2a and R2b are the mean reconstructions derived from the post-filtered regional reconstructions. COOK and LUT are the reconstructions from Cook et al. (2002) and Luterbacher et al. (2002a). Significant correlations (estimated from the Monte Carlo simulations described in the text) are marked with * (5%) and ** (2.5%).*

index and the proxies. The pre-filtering technique is preferred to the post-filtering (see Sec. 3.1.1 and the following discussion). The winter season is used since the NAO is pronounced during the northern hemisphere cold season (Hurrell and van Loon, 1997). Although the annual resolution of the proxies might favour the reconstruction of an annually averaged NAO index the winter season is preferred. An extensive number of dynamical, observational and modelling studies have put their emphasis on the winter season. Therefore, a reconstruction of the winter season is more important than annual means.

According to the regional differences, the proxy ensemble is divided into four regional groups: Greenland (5 ice-core proxies, hereafter labelled GR), Scandinavia (11 tree-ring chronologies, SC), British Isles and Belgium (4 tree-ring chronologies, BB) and Spain (23 tree-ring chronologies, SP). Detailed information about the proxies are summarised in the appendix (A.2). Note that the assemblage of the BB trees is still a trade-off between the climatic and statistical obligations. Two tree-ring chronologies from Scotland have been available over the period 1700–1978. Two chronologies from Belgium are added to this group because Belgium is a location with an analogous climatic impact of the NAO. The WAVER method is used to reconstruct the NAO index separately for each region. The four resultant time series are finally averaged. The simple average from the four reconstructions is calculated and rescaled to the variance of the W3 coefficients of the NAO index (denoted *mean reconstruction*). A weighted average according to Eq. 3.18–3.20 was also tested, but minor differences in the reconstructions were found. The years 1902–78 are chosen as the calibration period and the years 1825–1901 are reserved for the model validation and vice versa. Interchanging both periods permits assessing (at least to some extend) the robustness of the calibration procedure. It may also help to uncover problems arising from the nonstationary 20th century climate change (Cook et al., 2002; Rutherford et al., 2003).

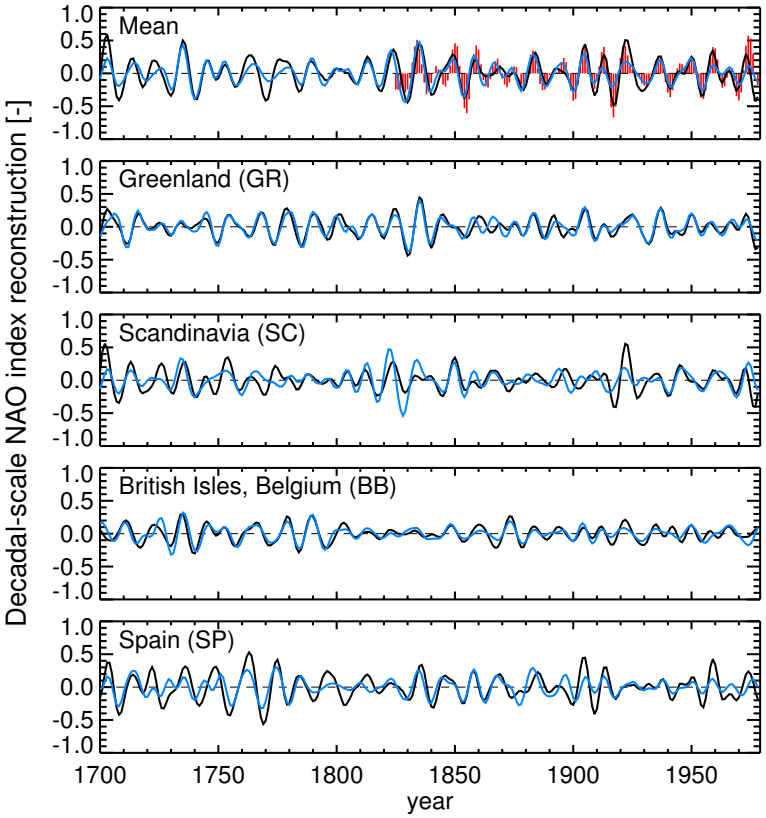


Figure 5.3: *Time series of the reconstructed winter (DJFM) NAO index for the decadal scale variability (W3 coefficients): the mean reconstruction, rescaled to the NAO index from Jones et al. (1997) (red vertical bars), reconstructions from Greenland ice cores (GR), Scandinavian trees (SC), British and Belgian trees (BB) , Spanish trees (SP). The black (blue) curves are reconstructions with respect to the calibration period 1902–78 (1825–1901).*

The mean reconstruction based on the calibration years 1902–78 (denoted as R1a) approximates the W3 coefficients of the NAO quite well. The correlation is $r = 0.87$ for the calibration period (Tab. 5.1). The validation process reveals that the model performance decreases outside the calibration period. The correlation coefficient for the validation period is 0.57. This is above the 2.5% significance level estimated by Monte Carlo simulations (see appendix B for more information). But it clearly demonstrates that the noise component in the reconstruction is still large.

Using the 19th century years for the calibration and 1902–78 for the validation instead, (this reconstruction will be denoted as R1b), the difference between the correlations in both periods is considerably reduced (see Tab. 5.1) and more than 57% of the signal variance is reproduced by the reconstruction. The corresponding reconstructed decadal scale time series are depicted in Fig. 5.3. Note that the wavelet coefficients have been transformed into the details of scale $j = 3$ according to Eq. 3.26 (Sec. 3.3).

The regional time series reconstruction provide some further insight into the reconstruction process. Obviously, the GR reconstruction is the most robust one concerning the interchange of the calibration period. The tree-ring reconstructions from Scandinavia and Spain are rather sensitive. Surprisingly, the reconstruction based on the four BB ring width series shows a rather good agree-

ment between both calibrations, albeit having the smallest correlations to the NAO signal. The observed sensitivity could be an expression of the changed NAO-proxy relationships during the 20th century. A result that is supported by the previous ideas of Cook et al. (2002), Zorita and González-Rouco (2002), and Rutherford et al. (2003).
An encouraging result is that the mean reconstructed index is able to reproduce the phase and amplitude of the large anomalies. There are a few features of this time series to be mentioned. The 18th century decadal fluctuations are of the same amplitude as those of the 19th and 20th century. One of the strongest positive anomalies occurred in the 1730s and is comparable with the peaks around 1835 and 1922 (the positive phase in the 1920s was the second strongest observed event of the 20th century after the late 1980/90s event). However, the regional reconstructions unmask the puzzling characteristics of such events. Whereas the positive peak at 1920 is present in all reconstructions except for Spain, the positive phase of the 1830s is not reproduced by the British and Belgian proxies, and the early event around 1735 is due to the large amplitudes of the tree-ring reconstructions. Thus, there is no unique signal contribution from spatially separated proxies to the mean reconstruction. The consequences of this incoherent temporal representation of the NAO signal is discussed in the next section, where this index is compared with recently published reconstructions. Finally, it will be shown that the pre-filtered reconstruction method is advantageous to the procedure that utilises unfiltered data, at least on the decadal time scale.

### 5.1.3 Discussion

Two aspects of the reconstruction have to be discussed. First, the performance of the new reconstruction method (i.e. using pre-filtered time series instead of unfiltered time series in the calibration) is analysed. Second, how well does the reconstruction match existing NAO index reconstructions? For this purpose, two recently published time series from Luterbacher et al. (2002a) and Cook et al. (2002) serve as reference values. Since the reconstruction is limited to the decadal variability, the comparison is restricted to the 8-16yr band-pass filtered time series (i.e. the W3 coefficients) of these NAO index reconstructions.
The advantages of the pre-filtering over the post-filtering technique is quantified with Monte Carlo simulations for the decadal scale variability (W3). Artificial proxies are created following the example of Chap. 3.1.2 and the improvement of the reconstruction due to the pre-filtering procedure is assessed. A white noise process is selected as a climate signal and some artificial proxy ensembles are created with varying member size $M$. The proxies consist of the signal and either red or blue noise (cf. Fig. 3.1 for further illustration). Half of the proxies are contaminated with an AR(1) process, whose lag-1 autocorrelation is $r = 0.7$. The remaining proxies are the sum of the signal and AR(1) processes with autocorrelation $r = -0.7$. The S/N-ratio integrated over all frequencies amounts to S/N=0.1 . The noise in each artificial proxy is assumed to be independent. Thus, the simulation accounts for the local noise component but neglects the climate noise (compare Chap. 3.1.2). The simulated time series are of the same length as the used NAO index (154 years). The artificial proxies are then processed in exactly the same way as the true data. The simulations are repeated 1000 times. The first and second order statistics are calculated from the resulting correlations between the signal and the reconstructions. The results demonstrate that the pre-filtering technique is superior to the post-filtering method. Although the difference is rather moderate the spread of the estimated correlation is considerably narrowed. One obtains more accurate estimates with a smaller range of sample variance (Tab. 5.2).
The design of the artificial proxies is a simplified approximation to the real proxies since covarying noise components are neglected in the simulations. The improvement reached by pre-filtering the

| $M$ | Statistic | Mean | STDDEV | $p_5$ | $p_{95}$ |
|---|---|---|---|---|---|
| 2 | $r_{cal}$ | 0.58 (0.43) | 0.13 (0.18) | 0.33 (0.10) | 0.77 (0.70) |
| | $r_{val}$ | 0.50 (0.41) | 0.19 (0.21) | 0.14 (-0.01) | 0.73 (0.71) |
| | RE | 0.21 (0.12) | 0.24 (0.24) | -0.23 (-0.26) | 0.50 (0.40) |
| 10 | $r_{cal}$ | 0.85 (0.73) | 0.06 (0.10) | 0.75 (0.53) | 0.93 (0.87) |
| | $r_{val}$ | 0.75 (0.66) | 0.11 (0.15) | 0.52 (0.39) | 0.89 (0.86) |
| | RE | 0.54 (0.41) | 0.18 (0.23) | 0.20 (-0.03) | 0.77 (0.68) |
| 20 | $r_{cal}$ | 0.91 (0.83) | 0.03 (0.07) | 0.85 (0.69) | 0.96 (0.92) |
| | $r_{val}$ | 0.85 (0.77) | 0.07 (0.11) | 0.71 (0.57) | 0.94 (0.90) |
| | RE | 0.69 (0.57) | 0.12 (0.17) | 0.48 (0.26) | 0.84 (0.79) |

Table 5.2: *W3 reconstruction statistics of Monte Carlo simulations using the pre-filtering (post-filtering) technique. The numbers in parentheses are the post-filtering results. Artificial proxies were generated with prescribed global S/N-ratio 0.1. The proxies contained noise generated by an AR(1) process with lag-1 correlation $\pm 0.7$ ($M/2$ each). The results are shown for different proxy member sizes $M$: $r_{cal}$ ($r_{val}$) the correlation statistic of the calibration (validation); RE the reduction of error (Cook et al., 1994). Columns contain the mean, the standard deviation (STDDEV) and the 5% (95%) percentiles $p_5$ ($p_{95}$).*

real proxies may be less pronounced than indicated by the simulation results. In order to assess the influence of the pre-filtering in the case of the NAO signal, the reconstruction is repeated with unfiltered data for both calibration intervals. The decadal-scale filter is applied afterwards. The mean reconstructions, labelled with R2a (R2b) for the calibration interval 1902–1978 (1825–1901), show reduced correlations in the verification periods compared with the pre-filtering results (Tab. 5.1). The improvement is within the expected range.

Next, the reconstruction is compared with those of Cook et al. (2002) and Luterbacher et al. (2002a) (hereafter denoted as COOK and LUT). It should be mentioned that the LUT reconstruction was based on a similar calibration interval (1901–95). The COOK index instead used the period 1826–1974 for the calibration. The wavelet coefficients of these two reconstructions are shown in Fig. 5.4 together with R1a and R1b. At first glance there is a good agreement during the 20th century but some discrepancies can be found during the 19th and 18th century, culminating in the period 1740–60 where the largest differences occur in both the phase and the amplitude. Temporal variations in the linear relationships between two time series can be illustrated when the correlation is estimated from data in different temporal intervals. A data window of 77 years is shifted in 1yr-steps along the time axis (*running correlation analysis*). The correlation between the wavelet coefficients of two time series is estimated for each data segment and assigned to the first year of the interval (i.e. the correlation 1700–1776 is assigned to 1700). The window width is set to 77 years because smaller sample sizes are barely suitable for confident correlation estimates. A test with larger window widths indicated that the results are robust against moderate (width 85, 90 yrs) changes of the window width.

The correlation between LUT, COOK and R1a/b is characterised by three main features worth to be mentioned. First, there is a decrease in the LUT-R1a correlation when the data window leaves the calibration period 1902–78 (see top of Fig. 5.5 the drop during 1840–50). The use of nearly the same calibration intervals (i.e. starting at 1901/02) in both reconstructions might be responsible for this distinct shift. The calibration correlations with the NAO index are positively biased [see

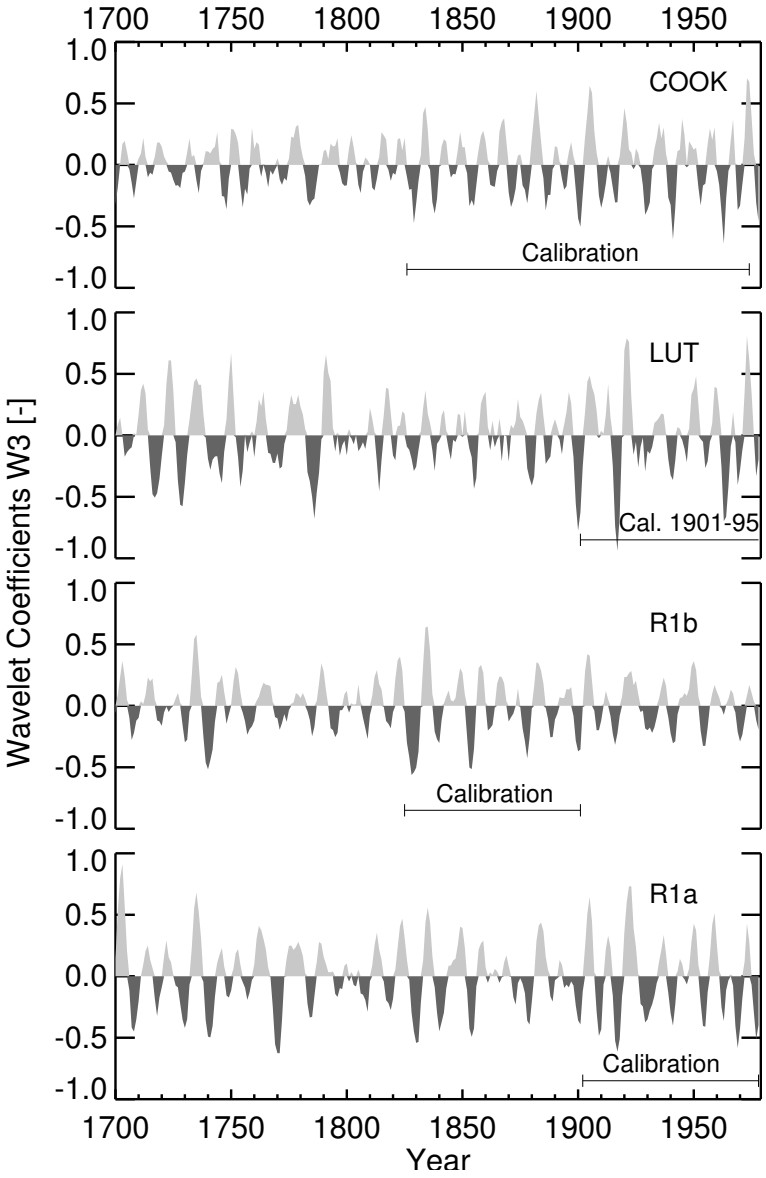


Figure 5.4: *Comparison of the reconstructed third level wavelet coefficients (W3) of the NAO index: this study (R1a, R1b) and those from Cook et al. (2002) and Luterbacher et al. (2002a). Note that R1a (R1b) are the mean reconstructions calibrated in the 1902–78 (1825–1901) period.*

Tab. 1 for R1a and Fig. 2a in Luterbacher et al. (2002a)]. Thus, including the calibration data raises the LUT-R1a correlation. Second, the correlation between R1a and COOK is above the 5% significance level (estimated with Monte Carlo simulations, App. B) back until 1750. The correlation with the COOK index is possibly positively biased because of the use of some identical proxies. The comparison with the LUT index is therefore more conservative. The correlation time series shows no significant correlation during the years before 1825 except for the years 1700–40 (LUT-R1a). The latter period is characterised by a re-strengthening in the correlation (above the significance level in case of R1a-LUT). Third, prior to 1740 a striking divergence in the correlation

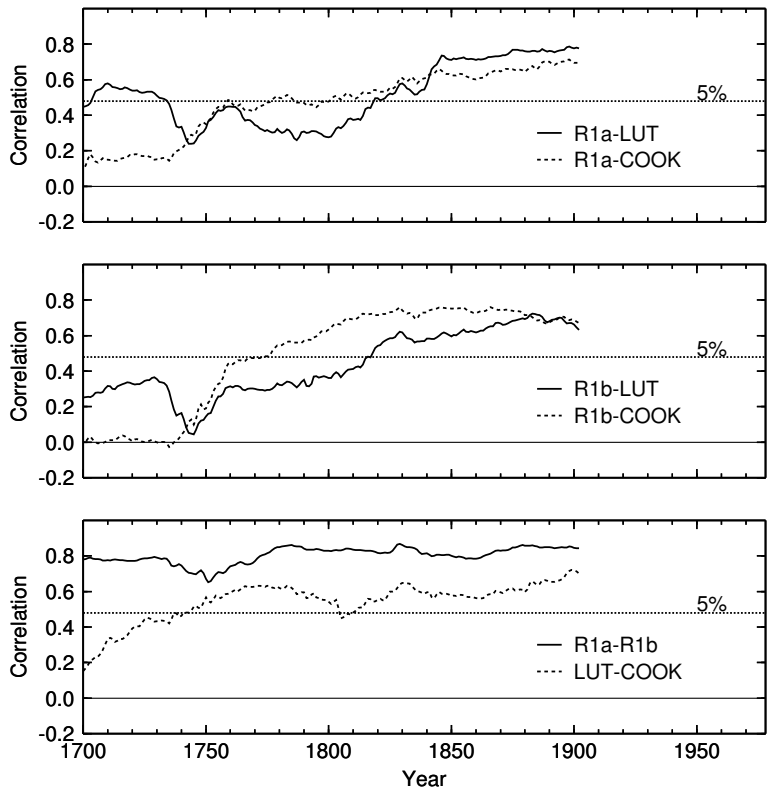


Figure 5.5: *77-year-window running correlations between the reconstructed W3 coefficients shown in Fig. 5.4. Correlations above* $0.48$ *are statistically significant at the 5%-level (dotted line). The significance level was estimated from Monte Carlo simulations of independent white noise processes passed through the same filter techniques as the reconstructions. Note that the correlation index is assigned to the first year of the moving data window (e.g. 1700 for the period 1700–76).*

occurs. The increase in LUT-R1a correlation prior to 1740 is not found in the correlation with COOK. In the latter case it breaks down from 0.5 to a level of 0.15 or even to zero in case of the 1825–1901 calibration (R1b). Comparing LUT and COOK we find a similar result with highly significant correlations except for the first decades of the 18th century. These important features are independent of the reconstruction method. The general features in the running correlation are also present in case of the unfiltered calibrations (Fig. 5.6).

What can be learned from the intercomparison of the reconstructions? The correlation statistics suggest that there is a time-dependent reconstruction skill on the decadal scale variability. Several potential sources might contribute to the fluctuations in the correlation. The stochastic nature of correlation estimates is a limiting factor for inferences from the running correlation analysis. The choice of the data window length determines the second moment statistics of the correlation coefficient. The difficulties of interpreting running correlations have been discussed by Gershunov et al. (2001). They emphasised that the variance of the correlation coefficient must carefully be tested against the random noise hypothesis. With that in mind, transient changes similar to the minimum around 1740 (Fig. 5.5 top) might occur just by chance.

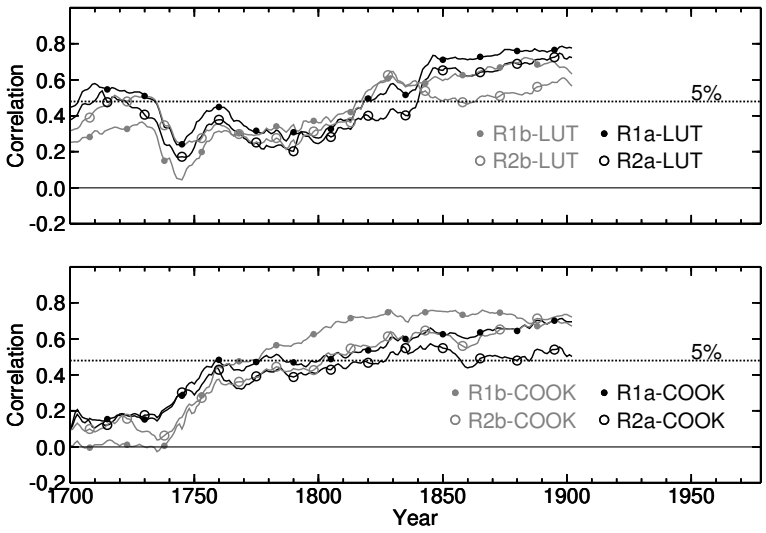


Figure 5.6: *Comparison of the pre-filtered and the post-filtered reconstruction results. Shown are the 77-yr-window running correlations with LUT (top) and COOK (bottom). R1a (filled black circles) is the reconstruction using the pre-filtering method and R2a (open black circles) used the unfiltered data in the calibration period 1902–78. The grey lines are the corresponding correlation results with respect to the calibration period 1825–1901 (R1b and R2b). Note that the correlation index is assigned to the first year of the moving data window (e.g. 1700 for the period 1700–76).*

The most interesting feature is the early period from 1700–40 where the correlation between LUT and R1a is again significant, whereas the correlation with COOK is fading away. One could argue that this is still in the range of random variations but the exact timing of the disparity makes it rather unusual. It is conceivable that the discrepancy highlights the systematic differences in the spatial distribution of the proxy networks. The majority of the proxies of LUT and R1a (R1b) are located in the European sector, whereas the COOK reconstruction made use of European and North American proxy information. Cook et al. (1998, 2002) and Cullen et al. (2000) argued that the quality and the associated spatial pattern of the reconstructed NAO depends on the spatial distribution of the proxy locations. In this context, it has to be mentioned that the number of predictors in the COOK reconstruction slightly changed during the 18th century. If this caused systematic changes in the spatial distribution of the predictors, a loss of agreement with R1a and LUT would be possible.[3]

Physical causes for time-dependent relationships have also been proposed by Schmutz et al. (2000), Cullen et al. (2000), and Luterbacher et al. (2002a). Ancient changes in the locations of the NAO centres, similar to the recent shift of the NAO in the 1970s (Hilmer and Jung, 2000), can disturb the stationarity assumption of the NAO-proxy relations. This could lead to misinterpretations of the proxy signal depending on the proxy site locations. Thus, the results hint at a possible change in the NAO-proxy relationship. Suppose the climatic impacts of the NAO change in the areas where the proxies are located. As a consequence, the covariability among proxies from different regions varies as well. Due to the underlying stationarity assumption the transfer models integrate these changes into the reconstructions. The correlation between the reconstructions and

[3]Unfortunately, no further details about the change in the predictors in the COOK reconstruction have been available in this study.

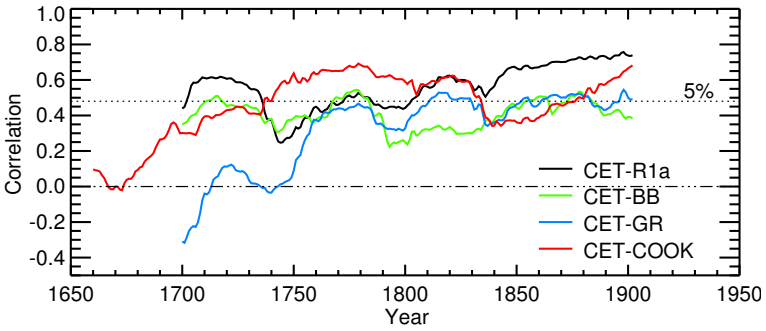


Figure 5.7: *77-yr-window running correlations between the winter (DJFM) Central England temperature (CET) and the COOK reconstruction over the years 1660–1978 (red) and between CET and the reconstructions of this study based on the calibration period 1902–78: mean reconstruction (black), Greenland region (blue), and British Isles and Belgium (green). Correlations above* $0.48$ *are statistically significant at the 5% significance level (Monte Carlo test). Note that the correlation index is assigned to the first year of the moving data window (e.g. 1700 for the period 1700–76).*

the wintertime Central England Temperature (CET) time series (Manley, 1974) is shown in Fig. 5.7. CET is highly correlated with the NAO index (Jones and Hulme, 1997). Taking the regional reconstructions, there is a remarkable stability for the BB time series but a marked decrease in the correlation between CET and the GR reconstruction. It was already noted in section 5.1.2 that the regional contributions to the mean reconstruction are time dependent. Here we find some evidence that climate variations decoupled from the NAO are still present in regional reconstructions. The COOK reconstruction and the CET time series allow an extension of the analysis back into the mid 17th century. The results of Fig. 5.7 support the idea that climatic variations are responsible for the disparities in the reconstructions, but uncertainties remain due to the data adaptive reconstruction methods of Luterbacher et al. (2002a) and Cook et al. (2002). The correlation between LUT and CET on the other hand is considerably strong in the 17th century indicating the importance of the CET series as a predictor in their reconstruction. The loss in correlation between COOK on the one side and LUT, R1a/b on the other side may reflect a change in the spatial character of the NAO. However, there are some uncertainties remaining. Cook et al. (2002) indicated that reconstructions based on 20th century calibration periods could be biased. If the calibration of a transfer model is purely derived from data that contain externally driven climate variability the model can fail to reproduce the internal variability of the NAO. Note that this is somewhat different to the conclusions of Rutherford et al. (2003). They found minor problems arising from calibrations in nonstationary time periods. However, they used temperature data to reconstruct temperature data. In the case of the NAO reconstruction, a transformation of the proxy data is needed because the proxies are only indirect indicators of the NAO variability. Thus, there are two factors attributing to the bias. First, if the internal climate modes were superimposed by externally driven climate variability, proxies might fail in reproducing the natural climate variability. Second, any change in the response of the proxies to the NAO could cause severe problems in the NAO reconstruction. The second point seems to be the determining factor.

During the 20th century, climate variations of the atmospheric circulation or changes in the probability distribution of circulation modes induced by anthropogenic effects are likely to project onto the natural mode of the NAO (Hsu and Zwiers, 2001). From this fact one could conclude that

calibrations with the 20th century data were less representative in preindustrial times. The calibration with the 19th century data, however, leads to even lower correlations in the early decades of in the 18th century (Fig. 5.5, R1b-COOK). The comparison with the CET index indicates the same correlation tendency towards lower values in early the 18th and late 17th century. Thus, it is hardly conceivable that a pure bias in the calibration step results in the observed differences in the reconstructions. The model results from Zorita and González-Rouco (2002) demonstrated that temperatures were more strongly influenced by external forcing factors (solar variability, greenhouse gas concentrations and volcanic activity) in the European sector than in North America. In their simulation with external forcing temperatures were less reliable than precipitation data for NAO reconstructions, especially when European temperatures were included. The spatial pattern of the externally forced temperature anomalies resembled that of NAO driven temperature variability. The anomalies preferably projected onto the NAO pattern in the European sector. Thus, temperature-sensitive proxies from this region could give a misleading estimate of the NAO state. This effect was most prominent on the longer (centennial) time scales in the model of Zorita and González-Rouco (2002). But even on decadal scales this effect should be present, since volcanic eruptions caused decadal temperature variations during that period (Crowley, 2000). The years around 1715 mark the end of the Late Maunder Minimum (1675–1715), where major changes in the solar and volcanic forcing occurred and Northern Hemisphere temperatures showed large variations (Lean et al., 1995; Mann et al., 1998; Crowley, 2000; Luterbacher et al., 2001; Shindell et al., 2001). This would further explain the closer resemblance between LUT and R1a because both mainly apply proxies from Europe. The reduced correlation with the COOK index at the beginning of the 18th (and late 17th) century could be attributed to the use of proxies from North America.

The aim of reconstructing the NAO index is to extend our knowledge of its natural variability. Climate change studies rely on the proper simulation of the background variability (Gillett et al., 2000, 2003). In particular, it is an unresolved problem whether the recent trend towards a high NAO state is in the range of natural variability. Gillett et al. (2003) pointed out that paleoclimatic reconstructions can provide a reference level for the detection problem. However, the uncertainties of the reconstructed NAO variability must be narrowed before the reconstructions can yield useful estimates of natural variability. The investigation of the decadal variability exemplifies the problems involved in estimating the magnitude of natural variability from reconstructions. It is demonstrated that the magnitude of the decadal variability strongly depends on the reconstruction methods.

Similar to the running correlation analysis, the running variance is calculated by means of a 77-year data window. The variance of the W3 coefficients is estimated within each time segment. The comparison of the temporal evolutions indicates a great sensitivity to both the reconstruction methods and the calibration interval (5.8a,b). Despite the apparent inconsistencies, the derived reconstructions hint at an increased decadal variability at the beginning of the 18th century (cf. Fig. 5.4). The wavelet variance of the reconstruction R1a equals the level of variability in the calibration interval 1902–1978 (Fig. 5.8a). Similar results are observed in the post-filtered reconstruction with the calibration interval 1825–1901 (R2b, Fig. 5.8b). On the contrary, the pre-filtered reconstruction (R1b) indicates a reduced wavelet variance compared to the 19th century. The increased variance in the 19th century may be interpreted as a calibration bias. Disregarding the years including the 19th century in the variance estimation it is seen that the 18th and 20th century are at the same level. The W3 coefficients of LUT show an intensified variability in the 18th

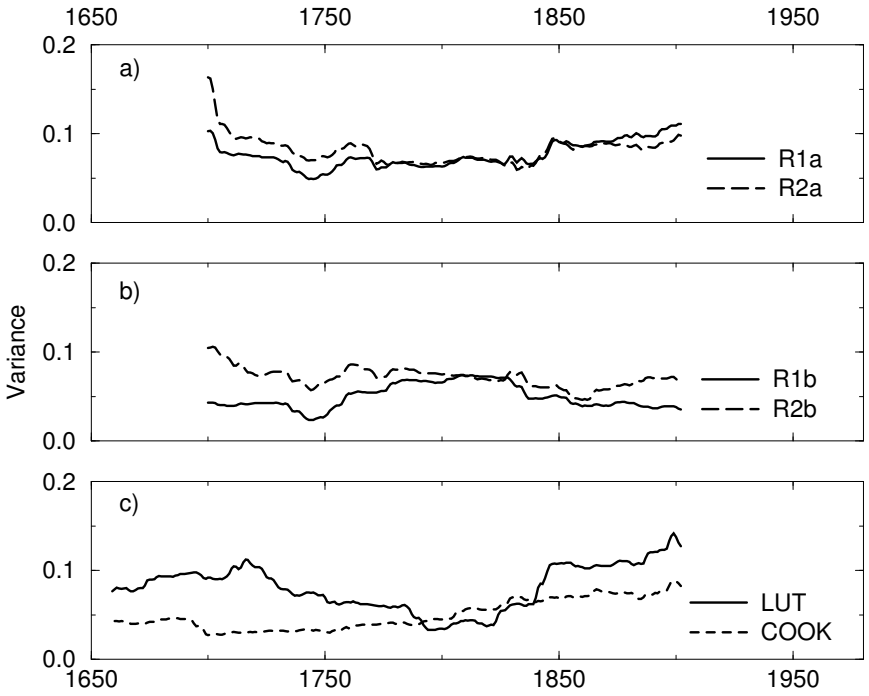


Figure 5.8: *77-yr-window running wavelet variance of the reconstructed W3 coefficients: a) the variance of the pre- and post-filtered reconstructions (R1a, R2a) using the calibration interval 1902-1978, b) the same as in a) but for the reconstructions R1b, R2b (i.e. the calibration 1825–1901), c) the wavelet variance of LUT and COOK. Values are assigned to the earliest year in the window range.*

century close to the magnitude of the 20th century[4]. The time series of the variance of the COOK reconstruction shows a peculiar trend. The largest variance is reconstructed in the 20th century. Going back in time, the reconstructed variance declines until 1700. This trend is rather unusual since it is not observed in the other reconstructions. Moreover, the trend is unlikely to be generated by a stationary process. The decline of the decadal scale variability is another expression of the reduced power in the low-frequency spectrum (Cook, 2003). The reason for this behaviour is not understood yet. Interestingly, the variance increases again prior to the year 1700. Although the level of variance is probably underestimated, the COOK reconstruction supports the result of an increased decadal variability at the end of the Maunder Minimum. The fact that the increased variability, compared to the 19th century, is present in all reconstructions (except for R1b) is a reinforcing indicator of the significant climatic changes during the Late Maunder Minimum.

The question remains whether the reconstructions can provide reliable information concerning the detection problem. At this stage, the reconstructions bring a small profit in the problem of detecting climate changes. The reconstructed indices do not provide a precise estimate of the preindustrial (natural) NAO variability. Differences in the methods imprint on the estimated vari-

[4]Note that the 20th century here does not include the years 1979–1999. Thus, the decades with the largest decadal variability are not part of the 20th century variance here.

ance levels. The calibration further determines the magnitude of the reconstructed variability. Low correlations in the calibration interval reduce the explainable variance in the reconstruction. Moreover, if data adaptive transfer models are employed, a distinction can hardly be recognised between the natural changes in the variability and those imposed by the data adaptive methods.

### 5.1.4 Summary and Conclusion

A pre-filtered reconstruction of the decadal NAO variability was presented extending the NAO index back to 1700. The verification of the reconstruction indicates a significant correlation with the station-based NAO index. Time-dependent reconstruction skills are found by comparison with reconstructions from Cook et al. (2002) and Luterbacher et al. (2002a). There are several possible explanations for this temporal dependency. First, some of the temporal fluctuations in the correlation could be explained by the stochastic variance in the correlation estimates. Second, data adaptive transfer models, in which the calibrated coefficients vary with time, contribute to changes in the correlation. A quantitative assessment of the effects induced by changes in the proxy ensemble could help to reduce the remaining uncertainties in the intercomparison of reconstructions. Despite these limiting factors, the most interesting aspects of the intercomparison are the diverging relationships in the first half of the 18th century. The likely explanation is that changes in the climatic conditions are responsible for this disagreement in the reconstructions. The changes could have been the result of solar or volcanic forcing that modified the NAO variability. Modelling studies of Zorita and González-Rouco (2002) support the idea of externally driven variability that projects onto the NAO pattern in the European sector.
It has to be kept in mind that the quality of some proxies might also vary with time due to biological effects, changing numbers of tree-ring measurements in a chronology (Bradley, 1999; Briffa and Osborn, 1999), or for example diffusion processes in ice cores (Meese et al., 1997). It remains to be seen whether the results are robust and can be reproduced with independent proxy information. The effect of the geographical distribution of the proxies on the reconstruction, as discussed by Cook et al. (2002) Mann and Rutherford (2002), and Zorita et al. (2003), should be under examination in future studies. An extension of the produced reconstruction into the 17th century could shed further light on the long-term stability and accuracy of the reconstruction. Moreover, an assessment of the various time scales of the NAO spectrum will be necessary to test the reliability of the results. The wavelet filter approach allows a comfortable multi-scale decomposition of the time series and is well suited for shorter time scales. On the longer scales, robust model fits require longer calibration intervals and thus the application is restricted to the decadal scales so far. However, in order to test the plausibility of the proposed ideas, a reconstruction of the interdecadal time scales is necessary. A careful verification and error estimation will be needed for the reconstruction of the long-term variations in the NAO. Paleoclimatic NAO reconstructions could then supplement the observations and model results concerning the role of the ocean-atmosphere interaction for long-term variations of the NAO.

## 5.2 Interdecadal Variability

In the extratropical northern hemisphere the atmosphere-ocean coupling is a matter of time scale. On time scales beyond decades (i.e. periods longer than 10 years) today's understanding of the governing processes in the coupled ocean-atmosphere system is grounded on modelling studies. The North Atlantic ocean is conceived to be an important actor for the generation of interdecadal variability (on time scales of 20–80 years). The strength of the meridional overturning circulation (MOC) in the North Atlantic is known to be linked to low-frequent fluctuations in the NAO (Jung, 2000; Eden and Jung, 2001; Visbeck et al., 2003). Since the THC (and thus the MOC) is closely related to the North Atlantic SST variability (Latif et al., 2003), the THC might exert an external forcing on the extratropical atmosphere. Mechanisms that could sustain an oscillation of the coupled system have not been conclusively demonstrated. From observations, periodic interdecadal variations of the NAO are hardly distinguished from a stochastic noise process. The lack of time series, long enough for trustworthy statistical inferences, may be circumvented by the use of paleoclimatic proxy information.
The objective of this study is to establish a reconstruction of the interdecadal variations of the NAO index that extends back into the 17th century. The transition from the 17th to the 18th century is of particular interest because of its marked changes in the external boundary conditions. Solar activity was significantly reduced during the 17th century (Maunder Minimum) (Eddy, 1976; Lean et al., 1995). Volcanic activity was relatively high and may have contributed to the cooling in the mature phase of the Little Ice Age (Crowley, 2000). Profound climatic changes occurred in the northern hemisphere (Wanner et al., 1995; Mann et al., 1998; Luterbacher et al., 2001; Briffa et al., 2001; Jacobeit et al., 2003; Soon and Baliunas, 2003). Changes in the winter circulation in the European sector were likely accompanied by alternated SLP pattern over the North Atlantic (Luterbacher et al., 2001).
In this section, the primary efforts go into the statistical evaluation of the reconstructions. A thorough examination of the North American tree-ring proxies reveals the chief obstacles in the reconstruction of the wintertime NAO index (Sec. 5.2.2). The reconstructions resulting from the multiproxy network are presented in Sec. 5.2.3. Thereby, problems are discussed that arise from the relative shortness of the station-based NAO index. The comparison with other NAO reconstructions is provided in Sec. 5.2.4 to complete the present view on the NAO's history of interdecadal variations.

### 5.2.1 Proxy Data

In Sec. 5.1 it has been shown that proxies from different regions are important for a precise reconstruction of the NAO index. Obviously, a widespread network of proxies contains more information about the NAO variability than locally restricted proxy data sets. Proxies from various regions, which are climatically influenced by the NAO but have different background errors, are the most promising data sets for successful reconstructions. Areas with potential proxy candidates are the North American continent, Greenland, Europe and the Mediterranean region.[5] In order to include the 17th century, the years 1623–1966 are chosen as the reconstruction interval. Note that the extension of the reconstruction (compared to the previous section 5.1) is at the expense of the overlap with the observational record of the NAO. Many ice-core proxies extending into the early 17th century do not include the years after 1966. Since the reconstruction method needs proxies that cover the entire time interval, the years 1623 and 1966 mark the lower and upper boundary.

[5] Other areas have been proved to provide valuable proxies too (Rimbu et al., 2001; Kuhnert et al., 2003).

The resulting proxy network comprises ice core proxies from Greenland (15 time series) and Canada (1), tree-ring chronologies from Europe (22), Morocco (7) and North America (29). Data were obtained from the IICC and ITRDB. The locations of the proxies are depicted in Fig. 5.9. The ice core proxies are annually averaged values of $\delta^{18}$O, accumulation rates and deuterium excess (see A.3 for details). Their reconstruction potential concerning the NAO are similar to the proxies of Sec. 4.2. The European tree-ring proxies form a subset of the proxies that were used for the decadal scale reconstruction in Sec. 5.1. The trees grew in areas where marked shifts in the PDFs of temperature and precipitation accompany the high and low NAO phases (Hurrell, 1995; Hurrell and van Loon, 1997; Kleppek, 2001, see also Fig. 5.1, 5.2). The tree-ring indices from Morocco are the proxies described in Glueck and Stockton (2001). The growth rate of these trees is under the influence of winter precipitation. Moroccan rainfall is closely related to the NAO during winter with below (above) normal precipitation during high (low) NAO phases (Lamb and Peppler, 1987; Hurrell, 1995; Glueck and Stockton, 2001). Therefore, the NAO variability can be reconstructed from Moroccan trees that are sensitive to the hydrological conditions at site.

The tree-ring chronologies from the North American continent are located in the east of the United States. In this region the NAO has some influence on the air temperature and precipitation. The impact of the NAO is less pronounced than in the eastern North Atlantic sector. Since the widths of tree-rings primarily represent the integral effects of growth-limiting factors (Fritts, 1976; Bradley, 1999), the wintertime signal of the NAO is expected to be weakly represented in the width indices. The inherent complexity of the signals in the North American tree-ring chronologies is discussed in the next section.

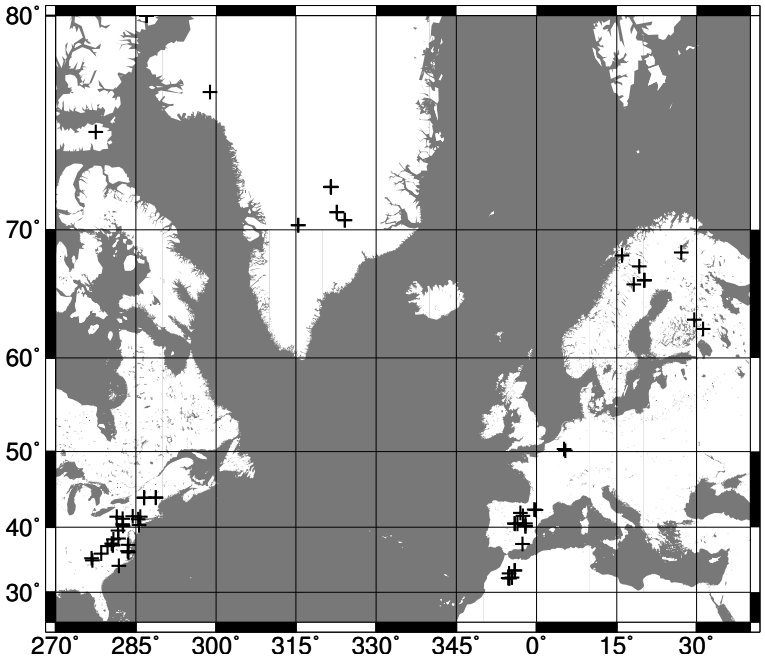


Figure 5.9: *Map of the geographical locations of the proxies used in this study. Black crosses mark the locations of the proxies.*

### 5.2.2 The NAO Signal in North American Trees

The tree-ring proxies from the eastern part of North America give an impressive example for the difficulties in disentangling winter climate signals from non-winter signals. As stated in Sec. 3.1.2 (Eq. 3.5–3.6), increasing the number of proxies should increase the S/N-ratio. Limits are imposed by the covariance structure of the noise. Here the wintertime NAO index is the climate signal. Any other climate signal contributes to the noise. The presence of non-winter signals is probably the most important source of covarying noise in the proxies. In the reconstruction process the S/N-ratio is expressed in terms of the correlation coefficient. The dependence of the correlation on the number of proxies is quantified by applying the WAVER method (see Sec. 3.2.3 for the methodology). A single realisation of the WAVER for a given number of proxies is not representative for the region. Therefore, a sufficient number of random realisations is produced. Given a subsampled set of $P_{sub}$ out of $P$ proxies there are $P![P_{sub}!\,(P-P_{sub})!]^{-1}$ possible combinations (without repetition), where '$P$!' is the factorial of $P$. The North American proxy set comprises $P = 29$ proxies from which one can create random subsamples of varying size. For example, if four proxies are picked out ($P_{sub} = 4$) there are 23751 combinations. Obviously, the full range of possible reconstructions is uncomfortable to calculate. It suffices to repeat the reconstructions for $R \approx 1000$ times to estimate the statistical properties described below.

The correlation statistics $r_{cal}$ and $r_{val}$ are estimated for each of the reconstructions. On the basis of these realisations one can estimate the mean, standard deviation and the 90% confidence ranges of the correlation. The spread of the correlations describes the uncertainty of the reconstruction due to the proxy choice. This kind of error in the estimate is not equivalent to the error of the reconstruction. The spread (hereafter called 'intraproxy' spread or error) of the correlation describes the sensitivity of the reconstruction quality due to the random selection of the proxies. If all proxies were of equal quality the spread of the correlation coefficients would be small. A mix of proxies having different reconstruction potentials would result in a large spread. The intraproxy spread has the power to estimate the time-dependent quality of the proxies. Conventional estimates of the reconstruction error extrapolate the verification error to times outside the verification interval, assuming stationary response functions. However, temporal changes in the quality of tree-ring proxies have been reported for example by Briffa et al. (1998) and Briffa and Osborn (1999). Some of these changes can be ascribed to sampling errors. The number of core samples that are averaged to define a tree-ring chronology is usually a function of time. The earliest (and latest) years in a tree-ring chronology are often derived from considerable small sample sizes. Assuming that the climate signal is common in all trees taken from a particular site, an increasing number of samples reduces the non-climatic noise in the tree-ring chronology.

To illustrate this effect, the time series of the sample sizes of all 29 tree-ring chronologies are averaged. The mean sample size of the North American tree-ring chronologies is fairly constant in the period 1750–1966 (Fig. 5.10a). Before 1750 the mean sample size linearly reduces to less than ten samples before 1623. The reconstruction error increases with a decreasing number of the mean sample size. The unfiltered reconstruction of the NAO index, using the calibration interval 1825–1902, is given as an example. The mean reconstruction and the intraproxy spread were calculated from 1000 randomly chosen subsamples ($P_{sub} = 15$). The smoothed (31 yr running mean) time series of the intraproxy spread (i.e. the standard deviation) is fairly constant during 1750–1966 (Fig. 5.10b). In the years before 1750 the standard deviation increases. The low-pass filtered (retaining periods $> 16$ yrs, see below) reconstructions are also accompanied by the growing intraproxy standard deviation in the 17th and 18th century (Fig. 5.10c). The subsampling reconstruction technique is thus a useful tool to detect nonstationary behaviour in

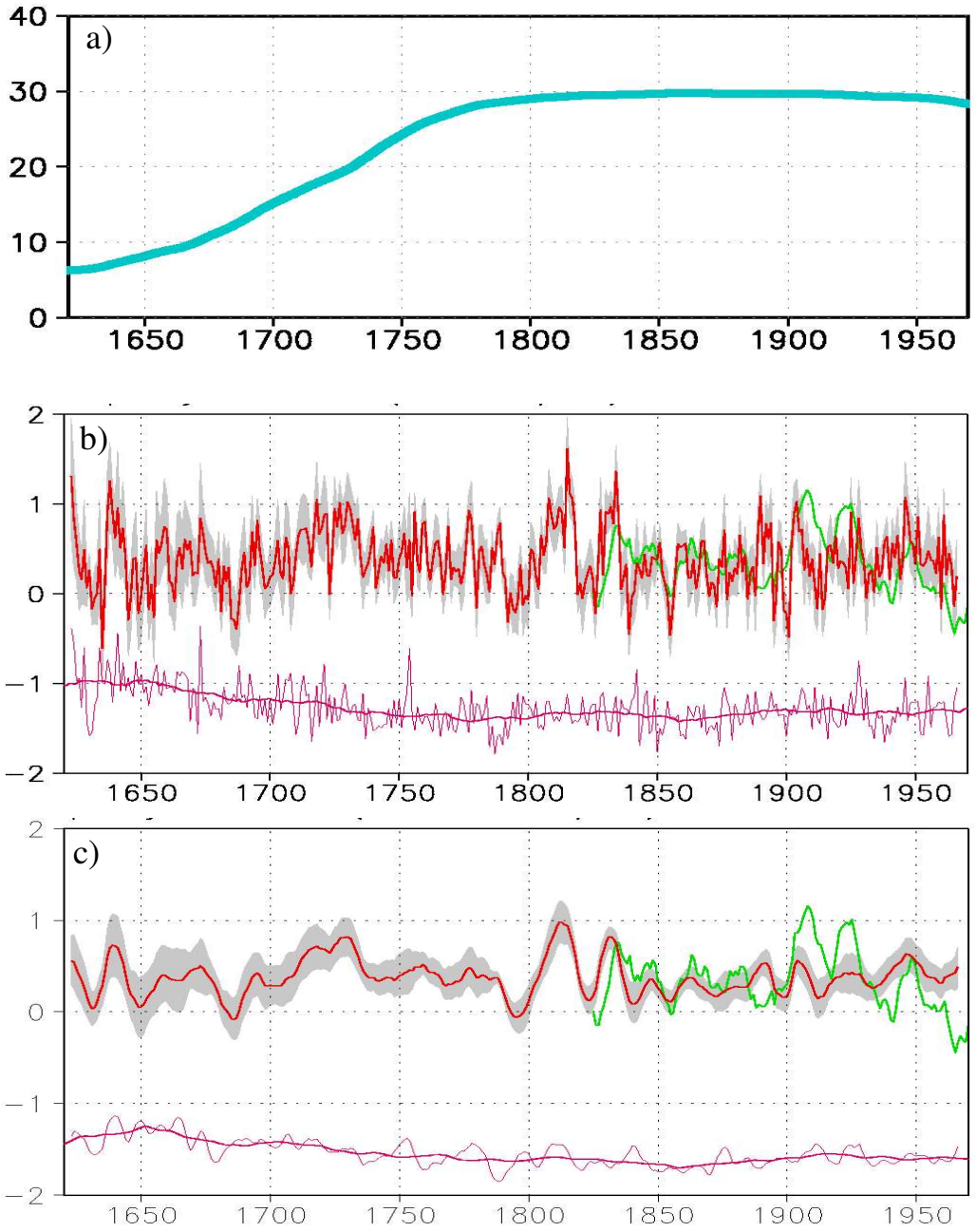


Figure 5.10: *Qualitative changes in tree-ring proxies and their effect on the NAO index reconstruction: (a) the number of tree-ring measurements used to create the individual tree-ring chronologies. The blue line is the average of the 29 tree-ring chronologies. (b) The mean of the 1000 subsampled reconstructions (red), the 90% confidence range of the intraproxy spread (grey shade), and the standard deviation (magenta). Note that the standard deviation has been vertically shifted and scaled for illustrative reasons. The thick magenta line marks the 31 yr running mean. (c) As in (b) but for the post-filtered reconstruction (scale coefficients S3).*

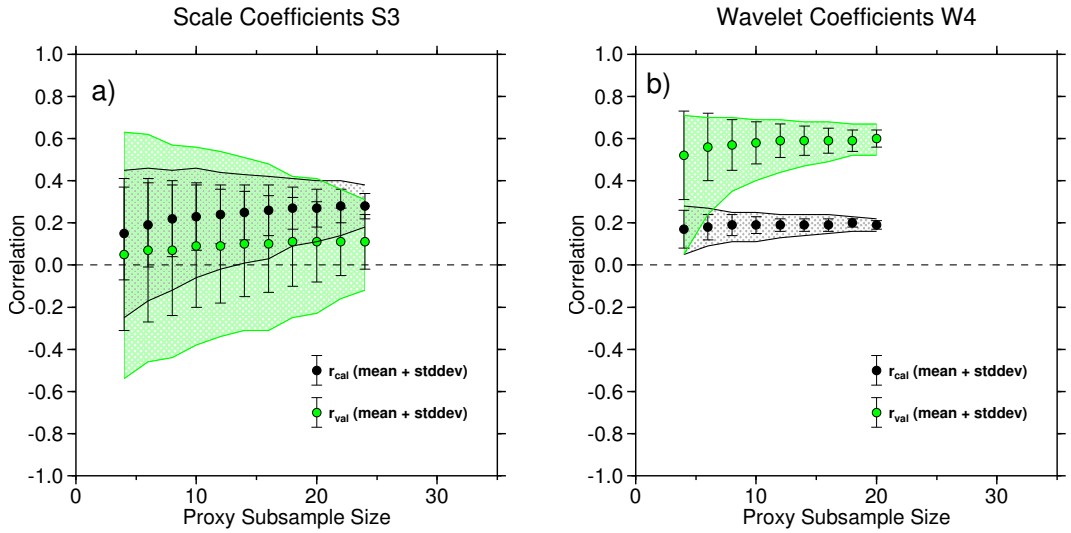


Figure 5.11: *Correlation statistics of the interdecadal NAO index reconstructions using subsampled North American tree-ring sets. 1000 random subsets of North American tree-ring chronologies were created for several subsample sizes $P_{sub}$, and the reconstructions of the wintertime NAO index were calculated. The mean of the correlations between the NAO index and the reconstructions (dots), the standard deviation (bars) and the 90% range of the intraproxy spread are depicted for the calibration (black) and validation (green): a) the S3 reconstruction, b) the W4 reconstruction. See text for details.*

the reconstruction. A few researchers accounted for this type of problem (e.g. Briffa et al., 1998; Esper et al., 2002), but it is not known by which factor the reconstruction error is increased.

The effect of the proxy sample size on the correlation between the NAO index and the reconstruction is investigated in the low-frequency range with periods greater than 16 years. The MODWT (Sec. 3.3) is used for the time series filtering (the LA8 filter is applied). Instead of analysing the wavelet coefficients the associated scale coefficients are subject to the reconstruction. Whereas a theoretical derivation of the wavelet correlation and its statistical properties were presented by Whitcher et al. (2000), the scale correlation has not been defined in that study. However, the scale coefficients of scale $j = 3$ (denoted as S3 ) may be interpreted as the sum of the wavelet coefficients of scales $j > 3$ (Whitcher et al., 2000). Therefore, the correlation between time series of the scale coefficients can be interpreted in a similar way. Since the scale coefficients contain trend-like variations which could disturb the results, the computation is repeated with the wavelet coefficients of scale $j = 4$ (W4 coefficients). The W4 coefficients represent the variability of the 16–32 year periods.

The reconstructions are performed with the post-filtering method for subsample sizes $P_{sub} = 4, 6, \cdots, 24$. The weighting factors of the proxies (see Eq. 3.18-3.20) are computed in the calibration interval 1825–1901. The validation is assessed in the interval 1902–1966. The S3 reconstruction is rather poor. Random selection of four proxies does produce a mean correlation $\overline{r}_{cal} < 0.2$ in the calibration interval (Fig. 5.11a). The validation results in zero mean correlations with extreme spread. Enlarging the subsample proxy size increases the calibration correlation slightly ($\overline{r}_{cal} \approx 0.3$) and reduces the intraproxy spread. The validation correlation is almost constant and close to zero. The most interesting aspect in Fig. 5.11a is the lack of a clear dependency of the

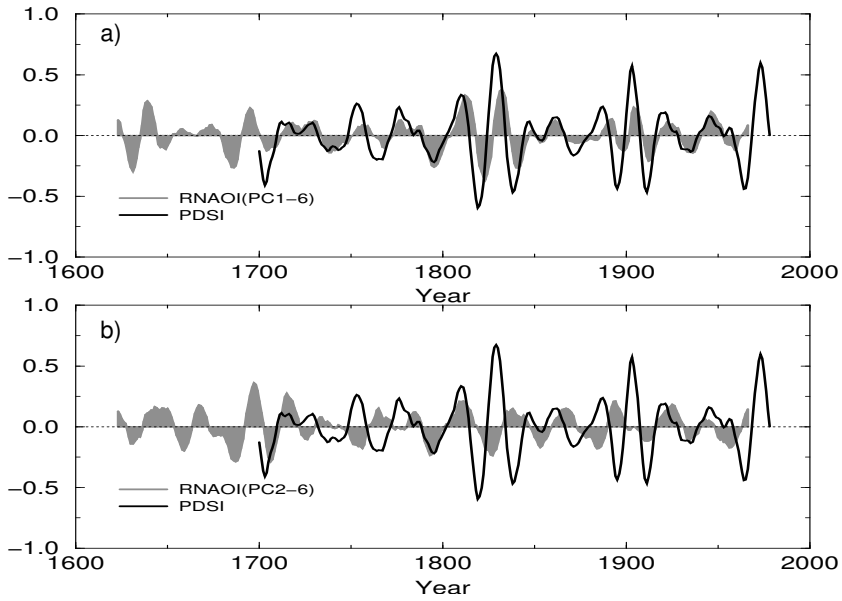


Figure 5.12: *Comparison of the W4 coefficients of the eastern North American PDSI (summer season) and the wintertime NAO reconstruction: a) the reconstruction based on the proxy variance truncated with the PCA using eigenmodes 1–6 (shaded curve), b) the reconstruction based on the proxy data truncated using eigenmodes 2–6. The PDSI is an areally average of the region (65°W–85°W/35°N–47.5°N). The gridded PDSI data are the reconstructions of Cook et al. (1999) available at http://www.ngdc.noaa.gov/paleo/usclient2.html.*

mean correlations on the subsample size $P_{sub}$. No significant improvement of the reconstruction is achieved by adding more proxies. In conclusion, the covarying noise component in the North American proxies precludes a reconstruction of the NAO's low-frequency variability. It should be noted that this conclusion is independent of the calibration interval.

The reconstructions are now repeated with the W4 coefficients in a slightly modified way. From the above results it is seen that the intraproxy spread of the correlations is very large but the reconstruction potential is low. One way to reduce the spread is to perform a PCA of the proxies. The PCA concentrates the variance in a few leading eigenmodes. The proxies can be approximated by a small number of leading eigenmodes. Thereby, the covariability among the proxies is increased. Thus, the intraproxy spread of the reconstructions is reduced. In the extreme case of retaining one single mode, there would be no spread at all (neglecting the case of zero weights for some proxies). The six leading modes of variability are retained for the approximation of the proxy variance. The calibration and validation interval are slightly modified to the years 1825–1899 and 1892–1966 due to computational constraints. As expected, the spread of the correlations is considerably narrowed (Fig. 5.11b). The improvement of the correlation with increasing proxy number is negligible. The most striking and surprising result is the low calibration skill and the high correlation in the validation period. Interchanging the calibration and validation interval inverts the difference between $r_{cal}$ and $r_{val}$ [not shown]. This curious outcome warns us not to draw premature conclusions about the true reconstruction skill.

How can this seemingly unconventional behaviour be understood? Usually, the greater number of trees contain climate signals imprinted during the non-winter season. Winter climates are of secondary importance for the tree growth (see Sec. 2.2 and references therein). Cook et al. (1999) showed that hydrological conditions during summer have a major effect on the trees in North America. They employed tree-ring proxies to reconstruct the summertime 'Palmer Drought Severity Index' (PDSI) (Palmer, 1965). Positive (negative) PDSI values indicate wet (dry) summers. While in Cook et al. (1999) the reconstructions are based on the tree's strong sensitivity to the hydrological conditions in summer, the reconstruction of the wintertime NAO index suffers from this climate signal. To demonstrate this, the post-filtering WAVER method is applied to the PCA-reduced proxy set (i.e. the proxies approximated by means of their six leading PCA). The calibration interval 1825–1966 is chosen. The W4 coefficients of the reconstruction are calculated with the MODWT. The comparison of the areally averaged (65°W–85°W/35°N–47.5°N) PDSI and the reconstruction of the NAO index shows a remarkable similarity (Fig. 5.12a). If the summer signal was separable from the NAO-induced variability, the reconstruction should deviate from the PDSI index. This is tested in a further PCA-truncation of the proxies where the first mode is excluded. The reconstructed time series is very different from the PDSI (Fig. 5.12b). The ubiquitous summer signal severely biases the reconstruction. Consequently, the correlation between the NAO index and the apparent reconstruction cannot be increased by additional proxies from within this region. Trees from remote regions and/or other types of proxies must be included to improve the reconstructions.
So far, the uncertainty of the intraproxy spread has been discussed. The statistical significance of the correlation between the NAO signal and the reconstruction has not been tested. The poor correlations in Fig 5.11 imply no significance. The problems of drawing statistical inferences from short time series are discussed in the the next section.

### 5.2.3 Reconstructing the NAO Index

The reconstruction of interdecadal variability is not a straightforward task. The problem is to find a trade-off between the chance of a bias and the variance of the estimated parameters of the reconstruction model (synonymous with transfer model). The statistical properties are discussed in this section.
Low-pass filtering inflates the autocorrelation of a time series. The filter process reduces the effective sample size (von Storch and Zwiers, 1999; Bretherton et al., 1999). Fitting transfer models with too short calibrations results in large uncertainties of the calibrated parameters. The consequences of filtering the time series are drastic for making statistical inferences about the reconstruction quality. Testing the significance of the correlation between the reconstruction and the signal will be impossible if the length of the validation interval becomes too short. The overlap between the proxies and the instrumental NAO index is 142 years long. In the previous section for example, the wavelet correlation on scale 4 was estimated from time series of length $N = 75$. As the W4 coefficients represent the period range of 16–32 years, the effective sample size is small [according to the formula of Whitcher et al. (2000) it is of the order 1]. Monte Carlo simulations were performed to estimate the confidence ranges of the wavelet correlation (see App. B). From generating 50000 pairs of independent white noise processes the confidence ranges of the W4 correlation were estimated. It was found that standard hypothesis tests are not possible. The significance levels (e.g. 5% or 10% levels) of rejecting the null hypothesis (i.e. the time series are uncorrelated) are close to $\pm 1$ (see Fig. B.2). Correlations estimated from time series shorter than 100 years are meaningless. If the time series length is doubled, statistical inference should

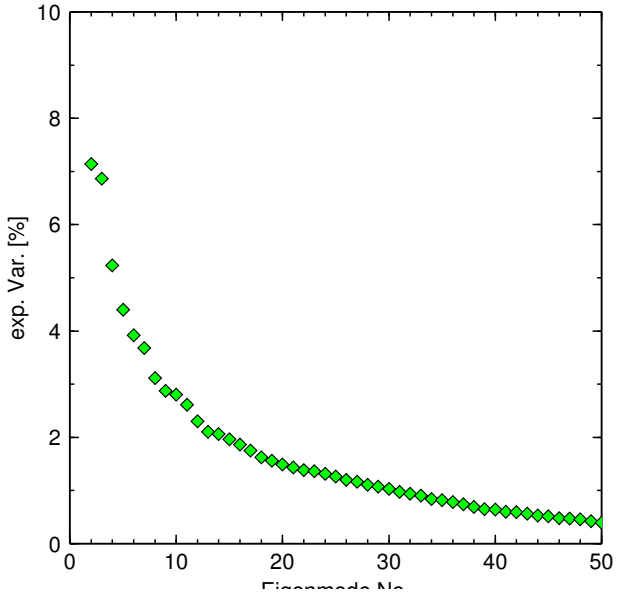


Figure 5.13: *Eigenvalue spectrum of the multiproxy data set. The PCA was applied to the unfiltered time series of the years 1623–1966. The explained variance of the eigenmodes 1–50 are marked with diamonds. Note that the explained variance is given by the eigenvalue divided by the sum of all eigenvalues.*

be possible. Given the length of the overlap in the NAO index and the proxies of about 140–160 years, traditional estimates of the reconstruction quality (i.e verifying the calibrated model) fails on the interdecadal time scales. The only way out is to compare the reconstruction with independent reconstructions (Sec. 5.2.4). One can avoid the inappropriateness of the effective sample size if the calibration includes information from variability in the high frequency range. On the other hand, using unfiltered time series may bias the estimates of the model parameters (see Sec.3.1.1). If *a priori* knowledge indicated the existence of frequency-dependent response functions, a correction of the calibrated model would be possible. Unfortunately, quantitative knowledge about the frequency character of the response functions for the given proxies is not available.

The reconstruction of the 16–32 year variability of the wintertime (DJFM) NAO index is produced with the same methods as described in Chap. 3. The proxy set consists of the PCA-truncated time series. The leading twelve eigenmodes of the unfiltered proxies are retained. About 55% of the total variance in the proxies is reproduced. The truncation at eigenmode twelve is justified by North's Rule-of-Thumb (North et al., 1982; von Storch and Zwiers, 1999). Although not all eigenvalues are separated from each other, the twelfth eigenvalue marks the transition from well separated to mixed eigenmodes. The marked transition is also notable in the eigenspectrum in Fig. 5.13. The WAVER method is applied to the truncated set of proxies. Either pre- or post-filtered time series are used. In order to highlight the sensitivity of the reconstruction to the length of the calibration interval the reconstructions are based on varying calibration intervals [stepwise enlarging the calibration interval 1825–1900 (1890–1966) by 15 years to 1825–1960 (1830–1966)]. The reconstructed W4 coefficients are depicted in Fig. 5.14. The pre-filtering method produces the reconstructions with smaller amplitudes than the post-filtering method. The

uncertainty in the reconstruction due to the chosen calibration interval seems to be time-dependent. Visually, large amplitudes in the reconstruction appear well defined. The reconstructions are less robust during the 18th century except for the early decades. The transition from the 17th to the 18th century is marked by a well-defined reversal from negative values to high positive values at 1700. The post-filtered reconstructions are characterised by a large quasi-periodic oscillation in the mid and late 1700s. The estimated amplitudes are sensitive to the calibration period. The earliest decades of the reconstruction are probably the most uncertain years in the reconstruction (the blurred shape in Fig. 5.14b).

Next, the influence of the pre-filtering on the reconstruction result is examined. The previous reconstructions of the low-frequency variability were either calibrated with the full variance spectrum (post-filtering approach) or with the band-limited variability in the 16–32yr period range. It is possible to perform the reconstruction at intermediate steps. The pre- and post-filtering methods can be combined to reduce the risk of a bias in the estimated transfer model. The pre-filtering is performed to reduce the high-frequency variance in the time series and the post-filtering cuts out the 16–32 yr periods. A variable setting of the cut-off frequency in the pre-filtering makes it possible to investigate the sensitivity of the reconstruction. The MODWT (with LA8 filter) is applied for both purposes and the W4 coefficients are reconstructed. Idealised low-pass filters (the scale filters of the MODWT) with cut-off periods at 4, 8, and 16 years are used for the pre-filtering. The reconstructed W4 coefficients are relatively unaffected by the pre-filtering procedure (Fig. 5.15). The major change is that the gradual inclusion of the high-frequency variance in the calibration process increases the amplitudes. The sign and the phase (i.e. the timing of the major excursions) do not depend on the pre-filtering process.

The subsampling of the proxy data set finally tests the sensitivity of the reconstruction to the given proxy set. The subsample size is set to $P_{sub} = 8$ and 1000 reconstructions are generated. The mean, standard deviation and 90% confidence range of the reconstructed NAO index are estimated and depicted in Fig. 5.16. Note that the subsample procedure was repeated with various subsample sizes. It was found that the possibility to detect nonstationary behaviour in the quality of the proxies is rather unaffected by the value of $P_{sub}$. The major effect of increasing (decreasing) the number of proxies in the subsamples is an increase (decrease) in the amplitude of the mean reconstruction and a smaller (larger) spread. The phase properties of the mean reconstruction do not change. The most important outcome of the subsampling procedure is the time-dependent standard deviation of the intraproxy spread (lower line in Fig. 5.16). The lowest standard deviation is observed in the calibration interval 1825–1966, except for the earliest years 1825–1850. The low spread in the calibration period is expected because each reconstruction tries to reproduce the same signal. The increase in the calibration years 1825–1850 is probably the result of the post-filtering process, which calculates a running weighted average from the unfiltered reconstruction. Therefore, the intraproxy spread of the post-filtered reconstruction is also a weighted average over several years. The years 1825–1850 of the calibration interval include some of the increased intraproxy spread from the earlier years. The greatest spread is associated with the earliest years in the 1620s and 1630s. The low variability in the mean reconstruction 1650–1675 coincides with a reduced intraproxy spread. After 1675, the mean reconstruction indicates pronounced oscillations. The quasi-periodic oscillations in the Late Maunder Minimum (1675–1715), however, are less robust. The 90% confidence range of the intraproxy spread indicates that even the sign of the reconstructed NAO index depends on the choice of the proxies. For example, some combinations of proxies hint at a negative phase of the NAO, although the mean reconstruction indicates a positive anomaly at 1700. The transition from the 17th to the 18th century will be discussed in detail in the next section.

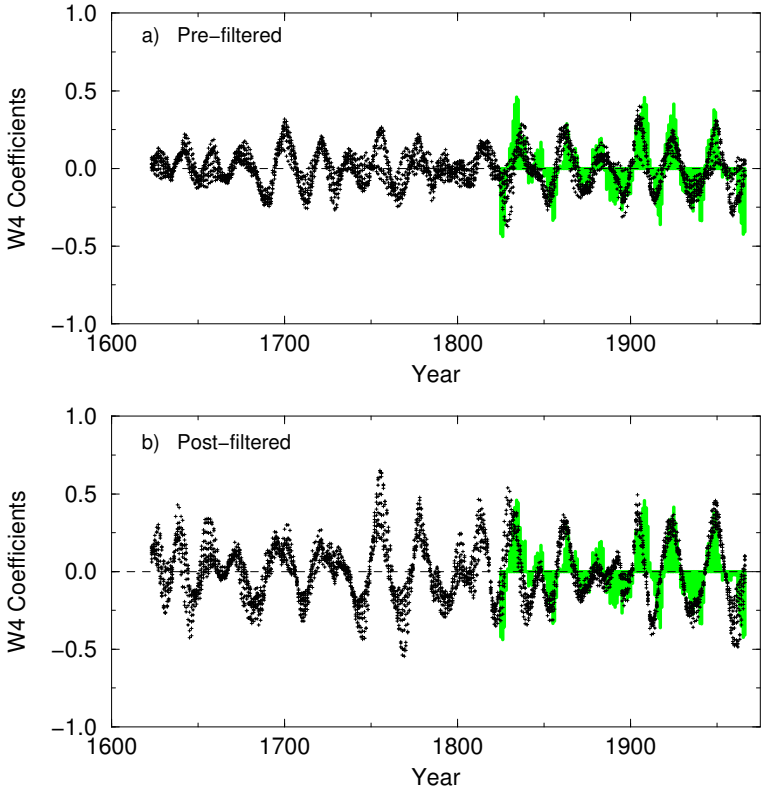


Figure 5.14: *Reconstruction of the W4 coefficients of the wintertime NAO index using various calibration intervals: a) results of the pre-filtering technique; b) as in a) but for the post-filtered reconstructions. The calibration interval was enlarged stepwise by 15 years from 1825–1900 to 1825–1960 and from 1890–1966 to 1830. Dots mark the W4 coefficients of the reconstructions. Shaded vertical bars mark the W4 coefficients of the observed NAO index.*

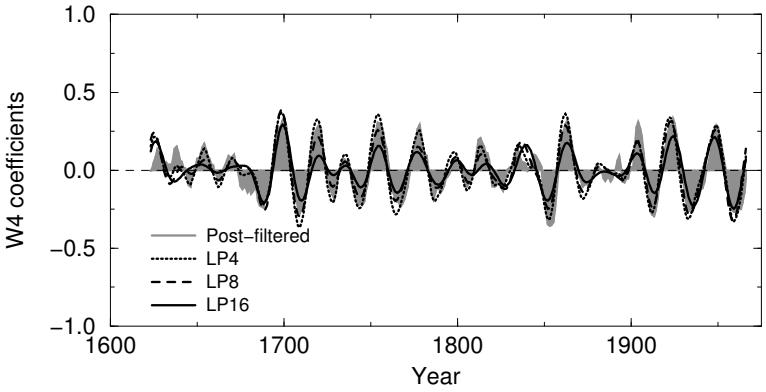


Figure 5.15: *Reconstruction of the W4 coefficients of the wintertime NAO index applying different low-pass filters in the pre-filtering step. The calibration interval was 1825–1966. The post-filtered reconstruction (grey shadings) was based on the unfiltered calibration, the time series LP4 (dotted line), LP8 (dashed line) and LP16 (solid line) used pre-filtered data for calibration. The number of the labels denote the nominal cut-off period of the MODWT scale filters.*

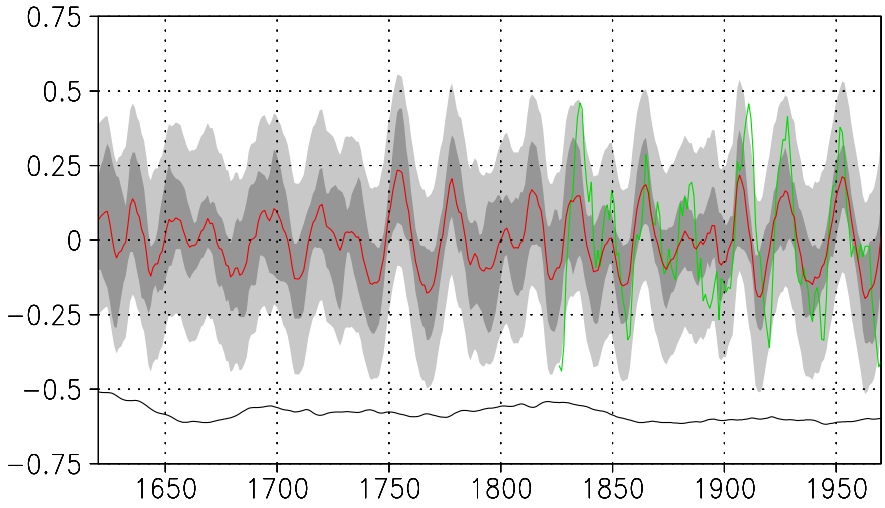


Figure 5.16: *Reconstruction of the W4 coefficients of the wintertime NAO index using the proxy subsampling procedure. The subsample size was $P_{sub} = 8$ and 1000 combinations were produced. Shown are: the mean of the 1000 reconstructions (red), the 90% confidence range of the intraproxy spread (dark grey), the standard deviation (offset by -0.75 and scaled by factor 2, black line). The W4 coefficients of the wintertime NAO index are marked with green. The reconstruction error (2×STDDEV of the residuals estimated from the calibration statistics) is denoted by light grey shading.*

Which reconstruction technique should be preferred to reconstruct the interdecadal variability of the NAO index? For the given proxy set and the given climate signal (the NAO index) differences between the pre- and post-filtered reconstructions are small. The results indicate that the post-filtering method is not strongly biased by the inclusion of high-frequency variability in the calibration process. On the other hand, the reduced effective sample size that is available to the pre-filtering calibration has a minor effect on the reconstruction results. Therefore, both methods can be used for this particular reconstruction problem. Note that the use of other proxies or other climate signals may point to different conclusions. In the next section results of the post-filtered reconstructions are compared with other reconstructions of the NAO's history.

### 5.2.4 Discussion

The reconstruction shown in the previous section is compared with those of Cook et al. (2002) (referred to as COOK) and Luterbacher et al. (2002a) (LUT). They are the most reliable estimates of the NAO's history in the pre-instrumental era. Although other reconstructions have been published in recent years (Appenzeller et al., 1998b; Proctor et al., 2000; Cullen et al., 2000; Rodrigo et al., 2001; Glueck and Stockton, 2001) they are less suitable for this discussion. Some of these reconstructions failed the verification tests of Cook (2003), and some do not extend back into the

17th century. The 17th century is the key period to be examined in this study. In this period, the low solar irradiance [Maunder Minimum 1645–1715 (Eddy, 1976)] is presumed to having caused large changes in the global climate, especially in the North Atlantic region (Lean et al., 1995; Wanner et al., 1995; Briffa et al., 2001; Luterbacher et al., 2001; Soon and Baliunas, 2003; Jacobeit et al., 2003; Mann and Jones, 2003). The reconstruction that is presented in this section is virtually the same as the multiproxy reconstruction of Sec. 5.2.3. The proxy set is the same as before but the regional proxies are transformed into uncorrelated PCs (by means of the PCA). The regions are North America (abbreviated to NA), Greenland inclusive Canada (GR), and Europe inclusive Morroco (EUR). For each of these regional proxy sets, the leading five PC time series are retained to provide the final predictor set. It is decided to include the sixth PC of the North American proxies since the first PC includes a climate signal from the summer (Sec. 5.2.2). These 16 time series are used as predictors for the wintertime NAO index. The post-filtering WAVER method is employed to reconstruct the NAO index. The calibration interval comprises the years 1825–1966. Since a verification of the reconstruction is impracticable on interdecadal time scales (Sec. 5.2.3), all the information is exploited in the calibration of the transfer model. After the calibration the NAO index is reconstructed in the interval 1623–1966. The post-filtered reconstruction will be referred to as 'PCSET' below. A noteworthy result is that the inclusion of the PC representing the NA summer signal is less troublesome in this reconstruction. The PCs of the GR and EUR region compensate for the bias.

The discussion is primarily focused on the wavelet coefficients of scales $j = 4$ (W4) and $j = 5$ (W5). The associated time scales are the periods between 16–32 and 32–64 years, respectively. On these time scales, variations are assumed to be associated with coupled ocean-atmosphere-ice mechanisms (Houghton et al., 2001; Kerr, 2000). Interdecadal variability at 65–80 yr periods may also be important (Schlesinger and Ramankutty, 1994; Delworth and Knutson, 2000) but is not considered here. The W4 coefficients are shown in Fig. 5.17a. It is obvious that the LUT reconstruction has a larger variance than COOK and PCSET. Note that the COOK and LUT reconstructions have been filtered in the same way as PCSET. The years 1900–1966 are visually best correlated among the time series because the 20th century has been used for the calibration in all reconstructions. The 19th century, the reconstructions are still in a fairly good agreement (probably due to the extended calibration interval of COOK and PCSET back to 1825). During the 17th and 18th century, the reconstructions are equivocal estimates of the state of the NAO. The phase relation pertaining to the years 1650–1750 is unstable. Especially the Late Maunder Minimum is defined by an ambiguous signal. The PCSET reconstruction displays a negative anomaly in the 1670/80s, whereas COOK and LUT indicate a positive anomaly. In the 1690s the PCSET shows a transition from negative to positive anomalies. The transition precedes those of LUT and COOK. The first two decades of the 18th century reveal huge swings from positive to negative and again positive values in PCSET. The opposite sign is reconstructed in LUT. It has been demonstrated in the previous section that the PCSET reconstruction is highly uncertain during the Late Maunder Minimum. Different proxy sets might be able to produce reconstructions close to LUT or COOK. It would be interesting to know how stable the reconstructions of COOK and LUT are with respect to the choice of proxies. The comparison with the reconstructions of Glueck and Stockton (2001) and Proctor et al. (2000), where the original data have been available, do not tally with one of the reconstructions depicted in Fig. 5.17a. A qualitative comparison with reconstructions of Appenzeller et al. (1998b) and Rodrigo et al. (2001) suffer from the different types of filter techniques. The timing of positive and negative excursions in the NAO index may depend on the period range passing the filter. Therefore, it is hardly possible to compare localised oscillations among the time series. The comparison between the W4 and W5 coefficients illustrates

the problem (Fig. 5.17). For example, the PCSET W4 reconstruction has a positive peak centred at the year 1700 and a negative peak about ten years later. The W5 coefficients indicate a positive anomaly lasting until 1720. Therefore, caution is advised if independent information is sought to support reconstructions. Historical data indicate that Europe experienced cold winters in the 1690s. Blocking events, leading to a reversal of the pressure gradient over the North Atlantic, were probably the typical pattern of the winter circulation (Wanner et al., 1995). Luterbacher et al. (2002b) concluded that different large-scale circulation patterns can produce extreme cold winters in Europe. However, their examples are both indicative for a weak or extreme negative NAO index. Thus, the documented climatic conditions are consistent with a negative NAO index during the last decade of the 17th century. Since the reconstruction of Luterbacher et al. (2002a) integrated the documentary data into their proxy network, the latter arguments do not give independent evidence for the validation of reconstructed indices. They just demonstrate that a negative NAO index during that time is more likely than a positive one.

The W5 reconstructions of COOK, LUT and PCSET show an omnipresent characteristic decrease in the variance during 1750–1850. In the 17th and early 18th century, the variability was comparable to that of the late 19th and early 20th century. However, the signs of the anomalies present contradictory information about the state of the NAO. The PCSET reconstruction, for example, indicates an intense negative phase of the NAO in the years $\approx$ 1670–1690. COOK and LUT indicate a positive anomaly. Generally, the reconstructions of Cook et al. (2002) and Luterbacher et al. (2002a) reproduce the same oscillatory behaviour in the Late Maunder Minimum. The PCSET reconstruction is almost inversely related to COOK and LUT.

A first attempt to quantify the relationship between the reconstructions is given by integrating the squared difference between two normalised reconstructions $z_{i,t}$, $z_{j,t}$, where t is the time index, and $i$, $j$ with $i \neq j$ denote the time series. The normalisation transforms the reconstructions into time series with zero mean and standard deviation one. The normalisation ensures that differences due to non-identical means[6] do not inflate the temporally integrated differences. Dissimilar variances in the time series are also neglected. Therefore, the time-dependent sum of the squared differences measures the correlation between two time series. The *sum of squared differences* (SSD) is given by

$$\mathrm{SSD}(T, T_0) = \sum_{t=T_0}^{T} (z_{i,t} - z_{j,t})^2 \ . \tag{5.1}$$

Note that the direction of the summation could be reversed and that the index $t$ represents integers. In the case of the reconstructions the integrations start at the (fixed) year $T_0 = 1966$ and end at the (variable) year $1623 \leq T \leq 1966$. Under stationary conditions, where the expected mean and variance of normalised time series equals 0 and 1 respectively, the expectation (denoted with angle brackets) of the SSD is related to the correlation coefficient $r_{i,j} =< x_{i,t}\, x_{j,t} >$ between the two time series by the equation

$$< \mathrm{SSD}(T, T_0) >= 2(1 - r_{i,j})|T - T_0 + 1| \quad , \tag{5.2}$$

The SSD is expected to increase linearly with T if $T_0$ is constant. Plotted against the time $T$, the slope of the line can be used to estimate the correlation between the time series. Using unitless time increments T, the slope becomes unitless too. Since $-1 \leq r_{ij} \leq 1$ the slope should lie in the range [0,4]. The SSD of uncorrelated time series should follow a line close to slope 2.

[6]Note that the expectation values of wavelet coefficients is zero, if some fundamental assumptions and sampling conditions hold. The calculated means of the reconstructed W4 and W5 coefficients are zero.

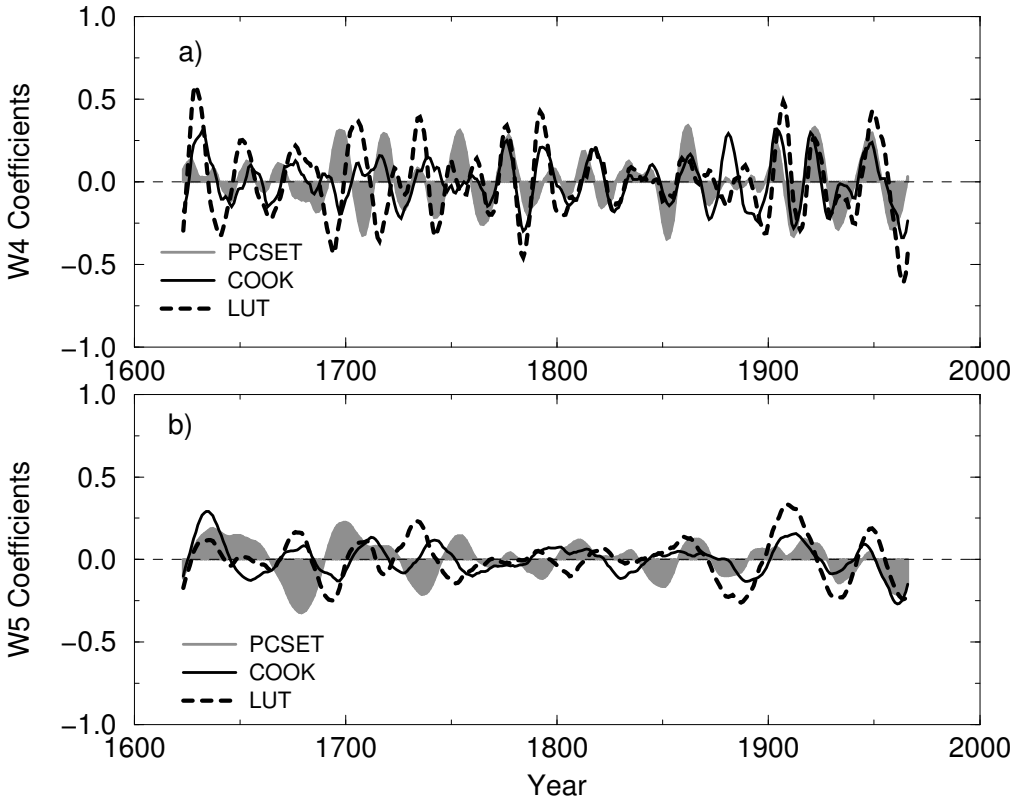


Figure 5.17: *Comparison of the reconstruction of this study with LUT and COOK on interdecadal scales: a) W4 coefficients (16–32 yr time scale), b) W5 coefficients (32–64 yr time scale). Grey shading marks the reconstruction of this study. The solid line represents the LUT reconstruction, the dashed line the COOK reconstruction. See text for details.*

In Fig. 5.18 the SSD of the three reconstructions are compared. The W4 coefficients of COOK and LUT are much closer related to each other than the PCSET either to COOK or LUT. The differences between LUT and PCSET are the largest of all three pairs. The question arises what can be learned from these results. Can evidence be found for significant correlations between two time series? To answer this question a set of 74 artificial proxies are generated as surrogate proxies. These artificial proxies are the sum of three components in accordance with Sec. 3.1.2. A unique realisation of a white noise process is the climate signal. Note that the white noise is an adequate approximation of the (weakly red) NAO index (Wunsch, 1999; Wanner et al., 2001; Hurrell et al., 2003b) on interannual time scales [see also Feldstein (2002) for a different point of view]. A second white noise time series takes on the role of the climate noise. Each proxy is then contaminated with a local (i.e. independent) noise component. In order to simulate the autocorrelation observed in the real proxies the local noise is generated by AR(1) processes with varying autocorrelations. The variance ratios of the three components are constraint to a proper range in the parameter space by trial and error. The lower and upper boundaries are found by comparing the covariance structure of the surrogates with the observed covariance of the true

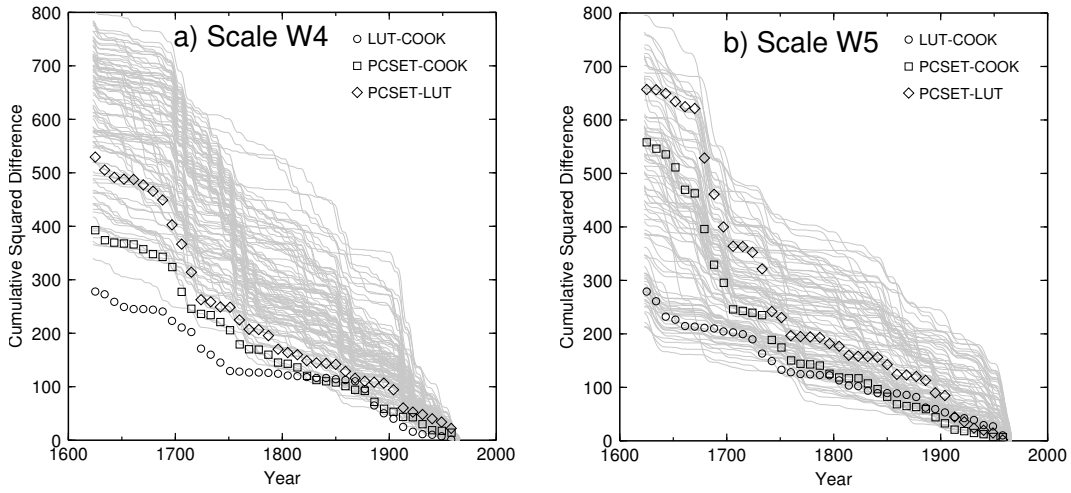


Figure 5.18: *Sum of squared differences (SSD) calculated from the reconstructions of this study, LUT and COOK. The SSD between the reconstructions LUT/COOK (circles), PCSET/LUT (squares), and PCSET/COOK (diamonds) are shown. The grey lines represent 100 SSDs estimated between PCSET and random noise processes. See text for details of the calculations.*

proxies. Additionally, the correlation between the artificial proxies and the artificial climate signal has to agree with the estimates of the correlation between the NAO signal and the real proxies. A final check is conducted with the PCA. The eigenspectrum of the surrogates is compared with the real proxies. The generated proxies are finally used for the reconstruction of the true NAO signal applying the same methods as in the case of PCSET. Recall that the artificial proxies are statistically independent from the NAO index. Since the PCSET reconstruction was based on 16 predictors, 100 random subsets of size $P_{sub} = 16$ are chosen from the 74 artificial proxies. For each reconstruction, the SSD is calculated with respect to the PCSET. They are marked with grey lines in Fig. 5.18. The large spread indicates that it is hard to distinguish between random noise and true reconstruction skills. The SSD between LUT and PCSET cannot be distinguished from random fluctuations. The SSD between COOK and PCSET likely equals the SSD of random noise. The only exception is the SSD between COOK and LUT. None of the generated artificial reconstructions falls below the corresponding line in the graph. Thus, the reconstructions of Cook et al. (2002) and Luterbacher et al. (2002a) are likely to have a true reconstruction skill in the 16–32 yr period range. Unfortunately, the new reconstruction PCSET fails this test, although the relation with COOK is marginally significant.

The SSD between the reconstructions in the period range of 32–64 yrs shows that the correlation between LUT and COOK are still marginally significant. The uncertainty range of the SSD concerning independent (uncorrelated) time series shows a larger spread than before (compare Fig. 5.18a with b). Thus, the problem of reduced effective sample sizes (due to filtering) constrains the inferences which can be drawn from the SSD. Using the SSD rather than the running correlation analysis (see Sec. 5.1.3) has some advantages because temporally localised features can be easily interpreted. Large slopes are indicators of large disparities. Small increases in the integrated differences indicate small deviations between the time series.

### 5.2.5 Summary and Conclusion

An attempt to reconstruct and verify the interdecadal variations of the NAO index during the Maunder Minimum has been presented. The multiproxy reconstruction dates back to 1623. The major drawbacks of using regional proxies have been demonstrated. The tree rings from the eastern part of North America mainly represent the summer climate. Thus, wintertime NAO index reconstructions can be significantly biased when proxies are used from regions where climate noise dominates the covariance of the proxies. The same holds for European trees, which have been successfully used in reconstructions of summer (or annual mean) temperatures (Briffa et al., 1992, 2001). Ice-core proxies with annual resolution may also be prone to climate noise from non-winter seasons. Ice-core proxies representing only the winter season may become important in future multiproxy reconstructions [see Vinther et al. (2003) for recent developments].
The presented reconstruction differs from LUT and COOK on interdecadal time scales, whereas COOK and LUT agree quite well. Clearly, a further comparison with independent NAO reconstructions is needed to raise the significance of the results on the 16–32 yr time scales. Careful investigations are necessary for the verification of the reconstructions. Ideally, time series analyses should be carried out with the same filter techniques when low-pass filtered reconstructions are compared among each other. The comparison of the three reconstructions does not support the proposed hypothesis that systematic changes in the spatial NAO pattern occurred, or externally driven variability projected onto the NAO pattern over Europe (Sec. 5.1.3). If climatic shifts [as proposed by Zorita and González-Rouco (2002)] were present in the reconstructions on decadal time scales, one would expect to observe the same behaviour on interdecadal time scales in the 17th century. There is no indication of climatic shifts in the 17th century. The reconstructions of Cook et al. (2002) and Luterbacher et al. (2002a) have a marked resemblance to each other. The reconstructed NAO index of this study is not congruent with LUT or COOK. Again, it has to be remembered that the significance of the results is questionable.
The results on the 32–64 yr time scale are particularly interesting for climate change studies. The increased interdecadal variability in the 17th and early 18th century is worth to be analysed in future, although the exact timing of transitions from preferred negative to positive states during the 17th century are not precisely reconstructed. The recent trend in the NAO index, which can not be attributed to anthropogenic forcing with confidence yet (Feldstein, 2002; Gillett et al., 2003; Cook, 2003), might be in the range of natural climate variations. Climate model simulations with realistic solar and volcanic forcing will be important for the confirmation of the reconstructions. If low-frequent changes of the NAO in the last decades of the 20th century were preceded by similar events in the Maunder Minimum, the recent warming in Europe and Siberia may be partly attributable to natural climate forcing. The symbiosis of climate modelling and paleoclimatic evidence will be a promising approach to this problem.

# Chapter 6

# Summary and Concluding Remarks

## 6.1 Summary

The study has been aiming at a better understanding of the natural climate variability of the North Atlantic Oscillation. A paleoclimatic approach was adopted to the problem of extending the NAO index back into the preindustrial era. The study focused on the decadal and interdecadal variability of the 17th and 18th century. The strategy of this study involved the exploitation of annually resolved natural climate proxies: ice-core indices from Greenland and Canada, and tree-ring chronologies from Europe, North Africa, and North America. The reconstruction problem was discussed in terms of stationary linear statistical response functions. It was found that two major obstacles must be overcome in paleoclimatic reconstructions: (1) the presence of covarying noise put a limit on the reconstruction potential in a multi-proxy data set, and (2) improper transfer functions may reconstruct climate signals with biased spectral characteristics.

A careful analysis was presented that describes the physical linkage between the proxies located in the Greenland area and the NAO. It was pointed out that the relationship between the isotope proxies and the NAO is rather complex. Systematic changes in the atmospheric circulation accompany the NAO variability. They change transport paths and source regions of precipitating air masses. This probably modifies the local temperature signal in the isotope proxies and influences the NAO signal in the proxies.

A reconstruction of the decadal variability of the wintertime NAO index was derived from a multi-proxy data set comprising ice core proxies from Greenland and tree-ring chronologies from Europe. The comparison with the reconstructions of Luterbacher et al. (2002a) (LUT) and Cook et al. (2002) (COOK) revealed a time-dependent correlation between the time series. In the early 18th century, European trees may have shown an anomalous response to the NAO. North American trees and Greenland ice cores were not (or less) affected by this alteration. It was concluded that either systematic differences in the spatial pattern of the NAO or externally (solar, volcanic forcing) driven variability, which projected onto the NAO pattern, occurred during the Late Maunder Minimum.

The reconstruction of the interdecadal variability of the wintertime NAO index demonstrated that a traditional verification of the reconstruction is not possible. However, the comparison among independent reconstructions allows for an assessment of the reconstruction quality. The outstanding feature of all three reconstructions (COOK, LUT, and this study) is the large 32–64 year variability during the 17th and the first half of the 18th century, followed by the quiescent interval between 1750 and 1850. Hence, the 20th century interdecadal variability is probably within the range of natural fluctuations.

## 6.2 Concluding Remarks

The reconstruction of the temporal NAO variability on decadal to interdecadal time scales is important for two reasons:

- The detection of anthropogenic climate signals requires a faithful knowledge of the natural variability.
- Instrumental records are too short for a representative view on the variability and the involved mechanisms on inter-/decadal time scales.

The presented results give new insight into the problem of estimating the natural variability associated with the NAO. The decadal variability of the 20th century is comparable with that of the early 18th century. Moreover, the reconstructed interdecadal time scales indicate that the 20–21th century variations are unlikely an unprecedented feature in the NAO index. Similar variability occurred in the 17th to early 18th century. However, the comparison with the reconstructions of Cook et al. (2002) and Luterbacher et al. (2002a) shows that it takes a lot more efforts to estimate the natural low-frequency variability with sufficient accuracy. Multiproxy data sets should be used, which combine a wide geographical distribution of proxies with a rich diversity of proxy types (Mann, 2002). These proxy data have the largest potential to reduce the risk of regional biases in the reconstructions (Cullen et al., 2000; Zorita and González-Rouco, 2002; Mann and Rutherford, 2002). Moreover, the problems arising from the insufficient temporal resolution (e.g. winter signals are reconstructed from annually averaged proxies) may be reduced by the variety of the proxies. Recent results of Jones et al. (2003a) pointed out that there is a pressing need to separate out the seasonal signals in proxies. Recent efforts of Luterbacher et al. (2002a) and Vinther et al. (2003) are encouraging examples of improving seasonal reconstructions.
Nonstationary shifts in the proxy-NAO response functions are likely accounting for the time-dependent discrepancies among the reconstructions. Although Cook et al. (2002) and Rutherford et al. (2003) note that extended calibration intervals can reduce the risk of nonstationary climate shifts biasing the reconstructions, Jones et al. (2003b) point out that reconstructions represent a combination of NAO variability and changes in the influence of the NAO on the proxies. In this study it was shown that a sufficient number of proxies allows for a detection of nonstationary NAO-proxy relations. Future developments of reconstruction methods should account for this fundamental problem. The use of models to generate and investigate 'pseudo-proxies', such as carried out recently by Zorita and González-Rouco (2002) and Mann and Jones (2003), will supplement the paleoclimatic research.
Whereas all previous NAO reconstructions were designed to provide 'best' estimates of the interannual NAO variability, this investigation emphasises the aspects of the low-frequency variability. The statistical analysis of the reconstructions revealed that traditional verification statistics are barely possible on interdecadal time scales. To overcome this problem, the incorporation of new independent paleoclimatic data like chemical tracers (Meeker and Mayewski, 2002), sediment cores (Black et al., 1999), and corals (Rimbu et al., 2001) will be important for a successful verification.
Recent results of (Kuhnert et al., 2003) have shown that North Atlantic corals provide a valuable archive of the NAO's history. New monthly resolved time series from Caribbean corals and sclerosponges are currently prepared for the purpose of climatological interpretation at the GEOMAR [M. Pfeiffer (2003), personal communication].

The marine proxy archives are of particular interest since they can provide important information about the variability of the North Atlantic Ocean. Therefore, they will be useful for testing simulations of coupled ocean-atmosphere (or ocean only) models. Moreover, by comparing and combining atmospheric NAO reconstructions with reconstructions of the North Atlantic Ocean SST anomalies, it might become possible to elucidate the influence of the North Atlantic Ocean dynamics and thermodynamics on the NAO.

# Appendix A

# Proxy Data

## A.1 Proxy Data Set Used for Testing the Reconstruction Methods

Table A.1: Ice-core proxies used for testing the reconstruction methods (Chap. 4.2). Data are provided by the WDC. The columns are (from left to right): position within the multiproxy set, file name (closely related to the names in the WDC archive), proxy name (from literature), location (latitude, logitude), top and bottom layer year (AD), proxy type [isotopic concentration ($\delta^{18}$O), accumulation ($\lambda$)], supplementary information about the annual average definition [win–win (sum–sum) annual layers defined as averages from winter to winter (summer to summer), if not available '?'].

| No. | File | Name | Lat | Lon | Time | Type | Average |
|---|---|---|---|---|---|---|---|
| 1 | ct84b-1y.txt | Site B | 70.65 | -37.48 | 1983 – 1716 | $\delta^{18}$O | ? |
| 2 | ct84d-1y.txt | Site D | 70.64 | -39.62 | 1983 – 1766 | $\delta^{18}$O | ? |
| 3 | ct85a-1y.txt | Site A | 70.63 | -35.82 | 1984 – 1622 | $\delta^{18}$O | ? |
| 4 | ct85g-1y.txt | Site G | 71.15 | -35.84 | 1983 – 1777 | $\delta^{18}$O | win–win |
| 5 | grip891.txt | GRIP891 | 72.56 | -37.6 | 1986 – 1772 | $\delta^{18}$O | ? |
| 6 | grip892.txt | GRIP892 | 72.56 | -37.6 | 1986 – 1772 | $\delta^{18}$O | ? |
| 7 | grip893.txt | GRIP893 | 72.56 | -37.6 | 1979 – 1772 | $\delta^{18}$O | ? |
| 8 | grip912.txt | GRIP912 | 72.56 | -37.6 | 1986 – 1772 | $\delta^{18}$O | ? |
| 9 | grip913.txt | GRIP913 | 72.56 | -37.6 | 1979 – 1772 | $\delta^{18}$O | ? |
| 10 | gisp2.txt | GISP2 | 72.58 | -38.47 | 1986 – 1772 | $\delta^{18}$O | ? |
| 11 | l84b.txt | Site B | 70.65 | -37.48 | 1983 – 1716 | $\lambda$ | win–win |
| 12 | l84d.txt | Site D | 70.64 | -39.62 | 1983 – 1766 | $\lambda$ | win–win |
| 13 | l85a.txt | Site A | 70.63 | -35.82 | 1984 – 1623 | $\lambda$ | win–win |
| 14 | l85e.txt | Site E | 71.76 | -35.85 | 1983 – 1722 | $\lambda$ | win–win |
| 15 | l85g.txt | Site G | 71.15 | -35.84 | 1984 – 1777 | $\lambda$ | win–win |
| 16 | accum.asc | GISP2 | 72.58 | -38.47 | 1987 – 1000 | $\lambda$ | sum–sum |

## A.2 Proxy Data Set Used for the Decadal Scale Reconstructions

Table A.2: Ice-core proxies used for the decadal scale reconstructions in Chap. 5.1. Data are provided by the WDC. The columns are (from left to right): position within the multi-proxy set, file names (closely related to the names in the WDC archive), proxy name (commonly used in literature), location in degrees (latitude, longitude), top and bottom layer year (AD), proxy type [isotopic concentration ($\delta^{18}$O), accumulation ($\lambda$)], supplementary information about the annual layer definition [win–win (sum–sum) annual layers defined as averages from winter to winter (summer to summer), if not available '?'].

| No. | File | Name | Lat | Lon | Time | Type | Average |
|---|---|---|---|---|---|---|---|
| 1 | ct85a-1y.txt | Site A | 70.63 | -35.82 | 1984 – 1622 | $\delta^{18}$O | ? |
| 2 | do18.bage.raw | GISP2 | 72.58 | -38.47 | 1986 – 1400 | $\delta^{18}$O | win |
| 3 | l85a.txt | Site A | 70.63 | -35.82 | 1984 – 1623 | $\lambda$ | win–win |
| 4 | accum.asc | GISP2 | 72.58 | -38.47 | 1987 – 1000 | $\lambda$ | sum–sum |
| 5 | greenacm1yr.txt[1] | Central West Gr. | — | — | 1983 – 1622 | $\lambda$ | sum–sum |

[1] this is a stacked record constructed from ice cores located in Central West Greenland (Fisher et al., 1996).

Table A.3: Tree-ring chronologies used for the decadal scale reconstructions in chapter 5.1. Data are provided by the ITRDB. All these tree ring indices cover the time period from AD 1700–1978. First column 'No.' indicates the position in the multi-proxy set. The column 'Filename' contains the original filename from the ITRDB. All other informations have been extracted from the listed files: The identification string for the site (Site ID), the identification string of the tree species (Species ID), the species name, the geographical position, and the height of the site (where available).

| No. | Filename | Site ID | Species ID | Species Name | Lat [Deg] | Lon [Deg] | Height [m] |
|---|---|---|---|---|---|---|---|
| 6 | brit026.crn | COUL | PISY | Scotch Pine | 57.53 | -5.35 | 250 |
| 7 | brit042.crn | SHANE | QUSP | Oak | 54.44 | -6.27 | 40 |
| 8 | belg001.crn | ARDEN2 | QUSP | Oak | 50.10 | 5.75 | 0 |
| 9 | belg003.crn | MEUSE2 | QUSP | Oak | 50.30 | 5.25 | 0 |
| 10 | finl001.crn | P01KRO | PISY | Scotch Pine | 62.98 | 31.30 | 192 |
| 11 | finl005.crn | P11KRO | PISY | Scotch Pine | 63.68 | 29.88 | 150 |
| 12 | finl008.crn | P25KRN | PISY | Scotch Pine | 63.10 | 30.63 | 165 |
| 13 | finl010.crn | PYHHAK | PISY | Scotch Pine | 62.85 | 25.48 | 185 |
| 14 | finl011.crn | LAAFOE | PISY | Scotch Pine | 67.00 | 27.12 | 320 |
| 15 | finl021.crn | KARHUN | PISY | Scots Pine | 68.83 | 27.25 | 200 |
| 16 | finl022.crn | UUSIJ | PISY | Scots Pine | 68.58 | 28.00 | 250 |
| 17 | norw001.crn | LOFOTN | PISY | Scotch Pine | 68.48 | 16.03 | 200 |
| 18 | norw007.crn | KARASJ | PISY | Scots Pine | 69.47 | 25.50 | 350 |
| 19 | swed011.crn | GLOMME | PCAB | Norway Spruce | 65.17 | 19.47 | 480 |
| 20 | swed017.crn | ARJEPL | PCAB | Norway Spruce | 66.07 | 17.98 | 600 |
| 21 | spai008.crn | SC4 | PINI | Black Pine | 40.87 | -2.13 | 1750 |
| 22 | spai009.crn | SC2 | PINI | Black Pine | 40.35 | -2.13 | 1250 |
| 23 | spai010.crn | TIE | PINI | Black Pine | 40.30 | -2.13 | 1350 |
| 24 | spai011.crn | TOR | PINI | Black Pine | 40.18 | -2.08 | 1500 |
| 25 | spai012.crn | GU3 | PISY | Scots Pine | 40.87 | -4.10 | 1950 |
| 26 | spai013.crn | NAF | PISY | Scots Pine | 40.02 | -0.12 | 1900 |
| 27 | spai016.crn | GR1 | PINI | Black Pine | 40.48 | -4.78 | 1450 |
| 28 | spai018.crn | GR4 | PINI | Black Pine | 40.43 | -4.93 | 1500 |
| 29 | spai019.crn | GU1 | PINI | Black Pine | 40.78 | -4.00 | 1600 |
| 30 | spai024.crn | PYR | PISY | Scots Pine | 42.83 | -0.78 | 1275 |
| 31 | spai026.crn | CAZ | PINI | Austrian Pine | 37.82 | -2.95 | 1800 |
| 32 | spai027.crn | CAZ | PINI | Austrian Pine | 37.83 | -2.93 | 1450 |
| 33 | spai037.crn | GUA | PISY | Scots Pine | 40.78 | -3.80 | 1950 |
| 34 | spai038.crn | GUA | PISY | Scots Pine | 40.80 | -3.95 | 1850 |
| 35 | spai039.crn | GUD | PINI | Austrian Pine | 40.30 | -0.73 | 1450 |

Table A.3: (continued)

| No. | Filename | Site ID | Species ID | Species Name | Lat [Deg] | Lon [Deg] | Height [m] |
|---|---|---|---|---|---|---|---|
| 36 | spai041.crn | GUD | PINI | Austrian Pine | 40.28 | -0.70 | 1475 |
| 37 | spai044.crn | HEC | PISP | two mix Pines | 42.48 | -0.42 | 1625 |
| 38 | spai045.crn | CUE | PINI | Austrian Pine | 40.25 | -1.93 | 1385 |
| 39 | spai046.crn | CUE | PINI | Austrian Pine | 40.27 | -1.93 | 1440 |
| 40 | spai047.crn | URB | PISY | Scots Pine | 41.98 | -2.87 | 1750 |
| 41 | spai048.crn | URB | PISY | Scots Pine | 42.02 | -2.90 | 1840 |
| 42 | spai049.crn | URB | PISY | Scots Pine | 42.03 | -3.03 | 1840 |
| 43 | spai050.crn | URB | PISY | Scots Pine | 42.00 | -2.85 | 1750 |

## A.3 Proxy Set Used for the Interdecadal Scale Reconstructions

Table A.3: Ice-core proxies used for the interdecadal scale reconstruction in Chap. 5.2. Data are provided by the WDC. The columns are (from left to right): position within the multi-proxy set, file names (closely related to the filenames in the WDCP), proxy name (commonly used in literature), location in degrees (latitude, longitude), top and bottom layer year (AD), proxy type [isotopic concentration ($\delta^{18}$O), accumulation ($\lambda$), deuterium excess (d)], supplementary information about the annual layer definition [win–win (sum–sum) annual layers defined as averages from winter to winter (summer to summer), if not available '?'].

| No. | File | Name | Lat [Deg] | Lon [Deg] | Time | Type | Average |
|---|---|---|---|---|---|---|---|
| 1 | cc-1ynew.txt | Camp Century | 77.18 | -61.11 | 1967 – 1242 | $\delta^{18}$O | ? |
| 2 | ct85a-1y.txt | Site A | 70.63 | -35.82 | 1984 – 1622 | $\delta^{18}$O | ? |
| 3 | d7273del_1yr.txt | Devon 72/73 | 75.41 | -82.5 | 1973 – 1512 | $\delta^{18}$O | ? |
| 4 | a77del18_1yr.txt | Agassiz 77 | 80 | 73 | 1977 – 1349 | $\delta^{18}$O | ? |
| 5 | a79del18_1yr.txt | Agassiz 79 | 80 | 73 | 1972 – 973 | $\delta^{18}$O | ? |
| 6 | a84del18_1yr.txt | Agassiz 84 | 80 | 73 | 1973 – 1217 | $\delta^{18}$O | ? |
| 7 | do18.bage.raw | GISP2 | 72.58 | -38.47 | 1986 – 1400 | $\delta^{18}$O | win |
| 8. | mc73.raw | MILCENT | 70.30 | -44.55 | 1966 – 1177 | $\delta^{18}$O | win |
| 9 | ct74.raw | CRETE74 | 71.12 | -37.32 | 1973 – 1280 | $\delta^{18}$O | win |
| 10 | grendel1-1yr.txt[1] | Central West Gr. | — | — | 1983 – 1622 | $\delta^{18}$O | ? |
| 11 | l74-12.txt | Crete 74 | 71.12 | -37.31 | 1973 – 553 | $\lambda$ | win–win |
| 12 | l85a.txt | Site A | 70.63 | -35.82 | 1984 – 1623 | $\lambda$ | win–win |
| 13 | accum.asc | GISP2 | 72.58 | -38.47 | 1987 – 1000 | $\lambda$ | sum–sum |
| 14 | l73mil.txt | Milcent 73 | 70.30 | -45.00 | 1966 – 1177 | $\lambda$ | ? |
| 15 | greenacm1yr.txt[1] | Central West Gr. | — | — | 1983 – 1622 | $\lambda$ | ? |
| 16 | dxs.new.ann2.txt | GISP2 | 72.58 | -38.47 | 1987 – 1400 | d | sum–sum |

[1] this is a stacked record constructed from ice cores located in Central West Greenland (Fisher et al., 1996).

Table A.4: Tree-ring chronologies used for the interdecadal scale reconstructions in chapter 5.2. Data are provided by the ITRDB. All these tree ring indices cover the time period from AD 1623–1966. First column 'No.' indicates the position in the multi-proxy set. The column 'Filename' contains the original filename from the ITRDB. All other informations are extracted from the listed files: The identification string for the site (Site ID), the identification string of the tree species (Species ID), the species name, the geographical position, and the height of the site (where available).

| No. | Filename | Site ID | Species ID | Species Name | Lat [Deg] | Lon [Deg] | Height [m] |
|---|---|---|---|---|---|---|---|
| 17 | finl001.crn | P01KRO | PISY | Scotch Pine | 63.63 | 31.50 | 192 |
| 18 | finl005.crn | P11KRO | PISY | Scotch Pine | 64.13 | 30.47 | 150 |
| 19 | finl021.crn | KARHUN | PISY | Scots Pine | 69.38 | 27.42 | 200 |
| 20 | norw001.crn | LOFOTN | PISY | Scotch Pine | 68.80 | 16.05 | 200 |
| 21 | swed002.crn | 328771 | PISY | Scotch Pine | 67.42 | 20.62 | 450 |
| 22 | swed004.crn | 253779 | PISY | Scotch Pine | 67.42 | 20.62 | 450 |
| 23 | swed005.crn | 252778 | PISY | Scotch Pine | 67.42 | 20.62 | 380 |
| 24 | swed007.crn | 662770 | PISY | Scotch Pine | 66.55 | 18.75 | 460 |
| 25 | swed009.crn | 251779 | PISY | Scotch Pine | 68.45 | 19.70 | 762 |
| 26 | belg001.crn | ARDEN2 | QUSP | Oak | 50.17 | 6.25 | 0 |
| 27 | belg003.crn | MEUSE2 | QUSP | Oak | 50.50 | 5.42 | 0 |
| 28 | spai001.crn | ORDES | PIMU | Pinus Mughus | 43.12 | -0.20 | 1870 |
| 29 | spai008.crn | SC4 | PINI | Black Pine | 41.45 | -2.22 | 1750 |
| 30 | spai010.crn | TIE | PINI | Black Pine | 40.50 | -2.22 | 1350 |
| 31 | spai011.crn | TOR | PINI | Black Pine | 40.30 | -2.13 | 1500 |
| 32 | spai012.crn | GU3 | PISY | Scots Pine | 41.45 | -4.17 | 1950 |
| 33 | spai019.crn | GU1 | PINI | Black Pine | 41.30 | -4.00 | 1600 |
| 34 | spai026.crn | CAZ | PINI | Austrian Pine | 38.37 | -3.58 | 1800 |
| 35 | spai038.crn | GUA | PISY | Scots Pine | 41.33 | -4.58 | 1850 |
| 36 | spai044.crn | HEC | PISP | two mix Pine | 43.33 | -0.70 | 1625 |
| 37 | spai047.crn | URB | PISY | Scots Pine | 42.63 | -3.45 | 1750 |
| 38 | spai049.crn | URB | PISY | Scots Pine | 42.05 | -3.05 | 1840 |
| 39 | morc001.crn | TOUSTD | CDAT | Atlantic Cedar | 32.70 | -5.42 | 2200 |
| 40 | morc004.crn | ESSSTD | CDAT | Atlantic Cedar | 33.08 | -5.30 | 2000 |
| 41 | morc005.crn | RMZSTD | CDAT | Atlantic Cedar | 34.30 | -4.33 | 2000 |
| 42 | morc006.crn | SNOSTD | CDAT | Atlantic Cedar | 34.25 | -4.12 | 2000 |
| 43 | morc007.crn | AFRSTD | CDAT | Atlantic Cedar | 32.55 | -5.00 | 2500 |
| 44 | morc008.crn | JAFSTD | CDAT | Atlantic Cedar | 32.92 | -5.50 | 2200 |
| 45 | morc009.crn | AMISTD | CDAT | Atlantic Cedar | 32.80 | -5.80 | 2150 |
| 46 | me016.crn | STNDRD | PCRU | Red Spruce | 46.53 | -69.50 | 0 |

Table A.4: (continued)

| No. | Filename | Site ID | Species ID | Species Name | Lat [Deg] | Lon [Deg] | Height [m] |
|---|---|---|---|---|---|---|---|
| 47 | nc001.crn | STNDRD | PCRU | Red Spruce | 36.22 | -82.55 | 0 |
| 48 | nc002.crn | STNDRD | PCRU | Red Spruce | 36.00 | -83.72 | 0 |
| 49 | nc003.crn | STNDRD | PCRU | Red Spruce | 36.12 | -82.37 | 0 |
| 50 | nc005.crn | STNDRD | TSCA | Eastern Hemloc | 35.13 | -83.30 | 0 |
| 51 | nc008.crn | BLKSTD | TADI | Baldcypress | 34.53 | -78.37 | 2 |
| 52 | nc009.crn | LASSTD | TADI | Baldcypress | 36.75 | -77.03 | 2 |
| 53 | nh002.crn | STNDRD | TSCA | Eastern Hemloc | 44.37 | -71.67 | 0 |
| 54 | nh003.crn | STNDRD | PCRU | Red Spruce | 44.17 | -71.63 | 0 |
| 55 | nj001.crn | STNDRD | QUAL | White Oak | 40.83 | -74.95 | 0 |
| 56 | ny001.crn | STNDRD | TSCA | Eastern Hemloc | 44.22 | -74.30 | 0 |
| 57 | ny009.crn | STNDRD | PCRU | Red Spruce | 44.22 | -74.25 | 0 |
| 58 | ny010.crn | STNDRD | TSCA | Eastern Hemloc | 44.22 | -74.25 | 0 |
| 59 | ny012.crn | STNDRD | TSCA | Eastern Hemloc | 42.28 | -74.30 | 0 |
| 60 | pa001.crn | STNDRD | TSCA | Eastern Hemloc | 41.12 | -78.17 | 0 |
| 61 | pa003.crn | STNDRD | TSCA | Eastern Hemloc | 41.37 | -75.53 | 0 |
| 62 | pa004.crn | STNDRD | TSCA | Eastern Hemloc | 41.55 | -78.20 | 0 |
| 63 | pa007.crn | STNDRD | TSCA | Eastern Hemloc | 40.38 | -78.08 | 0 |
| 64 | pa011.crn | STNDRD | TSCA | Eastern Hemloc | 42.45 | -76.47 | 0 |
| 65 | pa012.crn | STNDRD | TSCA | Eastern Hemloc | 40.38 | -78.87 | 0 |
| 66 | pa013.crn | STNDRD | TSCA | Eastern Hemloc | 42.25 | -79.62 | 0 |
| 67 | va009.crn | STNDRD | QUPR | Chestnut Oak | 37.92 | -79.75 | 0 |
| 68 | va010.crn | STNDRD | TSCA | Eastern Hemloc | 37.83 | -79.87 | 0 |
| 69 | va011.crn | STNDRD | QUAL | White Oak | 37.63 | -80.83 | 0 |
| 70 | va014.crn | STNDRD | QUAL | White Oak | 38.83 | -78.58 | 0 |
| 71 | va015.crn | STNDRD | TSCA | Eastern Hemloc | 38.55 | -79.55 | 0 |
| 72 | va017.crn | STNDRD | QUAL | White Oak | 38.53 | -80.33 | 0 |
| 73 | va021.crn | BWRSTD | TADI | Baldcypress | 36.78 | -77.47 | 9.00 |
| 74 | va023.crn | DRASTD | TADI | Baldcypress | 37.62 | -77.12 | 6.00 |

# Appendix B

# Wavelet Correlation: Monte Carlo Confidence Levels

Whitcher et al. (2000) developed approximate confidence levels for the correlation between the j-th level wavelet scale coefficients of two time series (denoted as *wavelet correlation*). For large wavelet scales and too short time series, the effective sample size is considerably reduced, and the large sample theory may result in erroneous confidence levels. The significance of the wavelet correlation can be tested by means of Monte Carlo simulations. 50000 random realisations of a bivariate (gaussian) white noise process were generated. The cross covariance of the bivariate noise process was zero. The probability density function (PDF) of the wavelet correlation between the two independent white noise processes was estimated from the generated random realisations. The PDF of the correlation coefficient $r(N, j, \mathcal{F})$ depends on the sample size (i.e. the time series length) $N$, the wavelet scale $j$ and the applied wavelet filter $\mathcal{F}$. The cumulative PDF is estimated by sorting the calculated correlations in ascending order. The value of the correlation for a specific cumulative probability (for example 95%) is given by the value of the corresponding list rank (47 500 in this example). The results for the coiflet filter of length $L = 6$ (CO6) and the least asymmetric filter of length $L = 8$ (LA8) [see (Percival and Walden, 2000) for further details about the filter properties] are depicted in Fig. B.1, B.2. The lines mark the correlations associated with a fixed confidence level. As the length of the time series increases the confidence levels becomes smaller, as expected. The larger the scale $j$, the smaller becomes the effective sample size. Smaller effective sample sizes leads to an expansion of the confidence ranges. When the characteristic time scale of periods associated with the band-passes equals or exceeds the time series length, the PDF of the correlation was not calculated. The choice of the mother wavelet filter has some implications for the the confidence ranges. The LA8 filter has a sharper band-pass characteristic than the CO6 filter. Therefore, the effective sample size is smaller, when the LA8 filter is used instead of the CO6 filter.

It must be noted that the confidence levels are depending on the nature of the stochastic process which is used for the Monte Carlo simulations. If the white noise process is replaced with red noise (often a more adequate basis for significance tests), the confidence levels change. The effect was tested for the W3 coefficients (CO6 filter) for AR(1) processes with lag-1 autocorrelations between -0.8 and 0.8. Interestingly, the effect of the autocorrelation is small (Fig. B.3). The band-pass character of the wavelet filter adjusts the spectral power characteristics of the red and white noise processes. It is expected that the influence is also small on different wavelet scales.

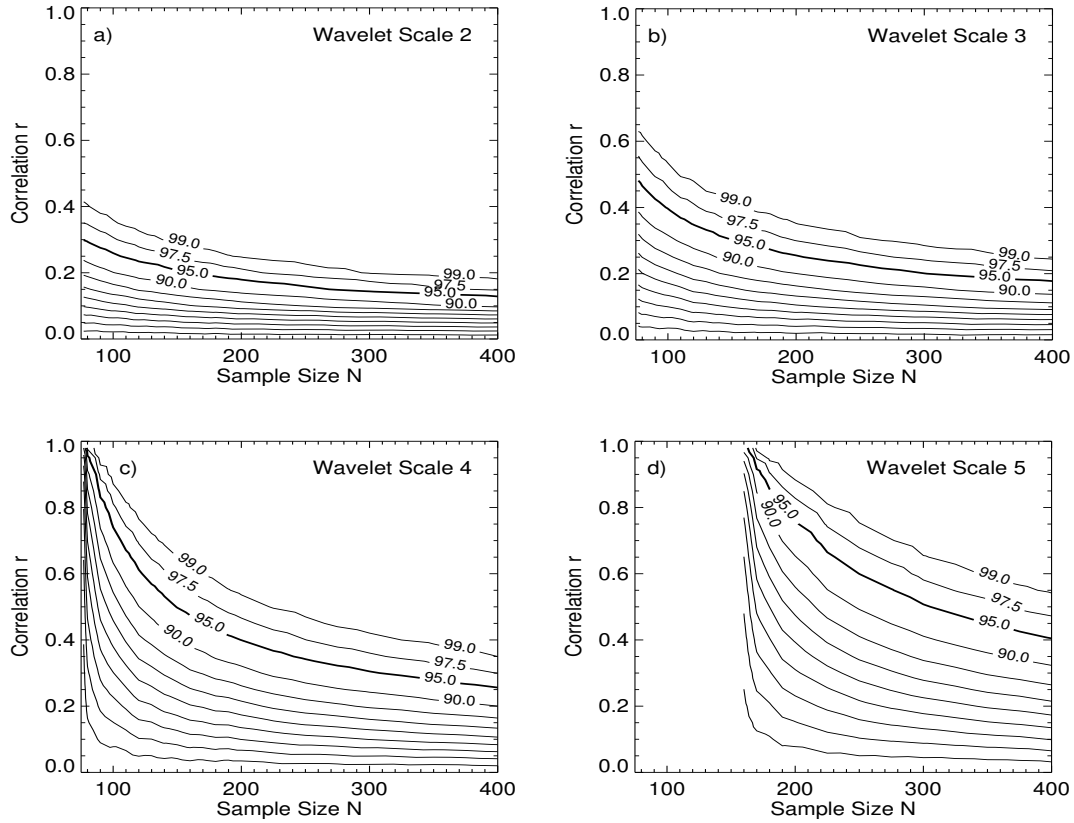


Figure B.1: *Estimated confidence levels of the wavelet correlation between independent white noise processes using the CO6 filter: a) wavelet scale 2 (W2) , b) W3, c) W4, d) W5. Lines mark the confidence levels (contour interval 5% or as labelled) as a function of the sample size* $N$.

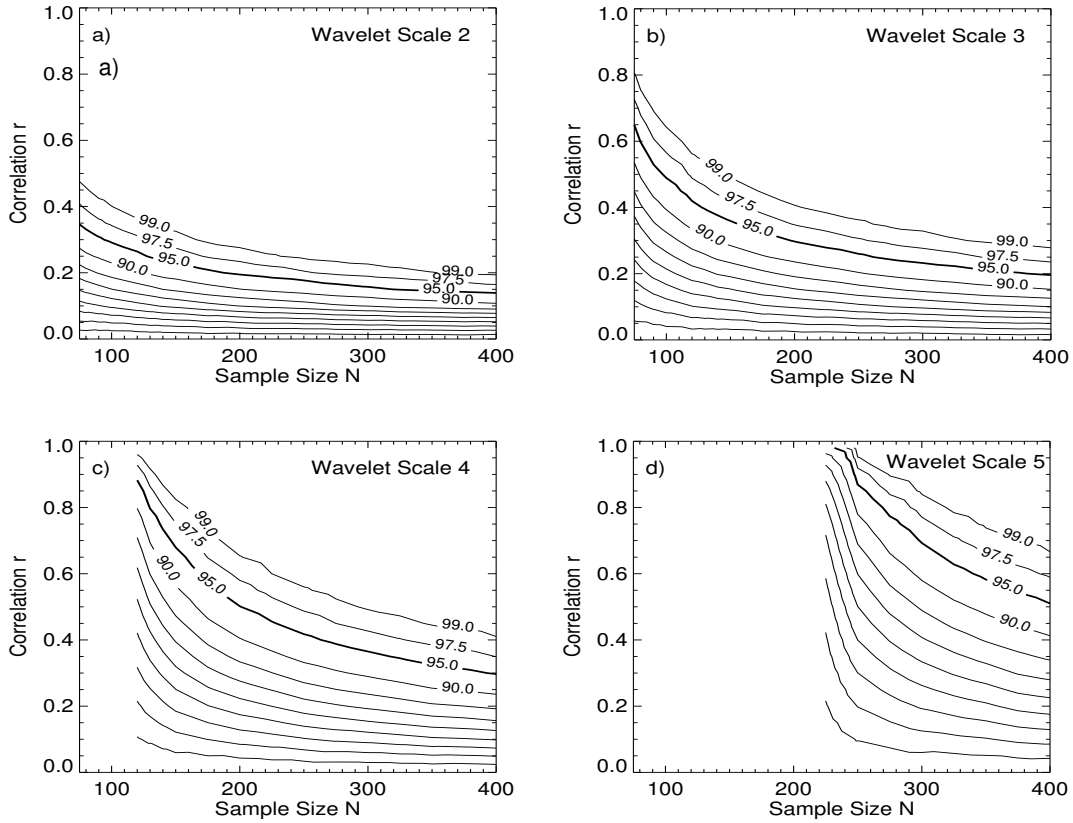


Figure B.2: *As in Fig. B.1 but for the LA8 filter.*

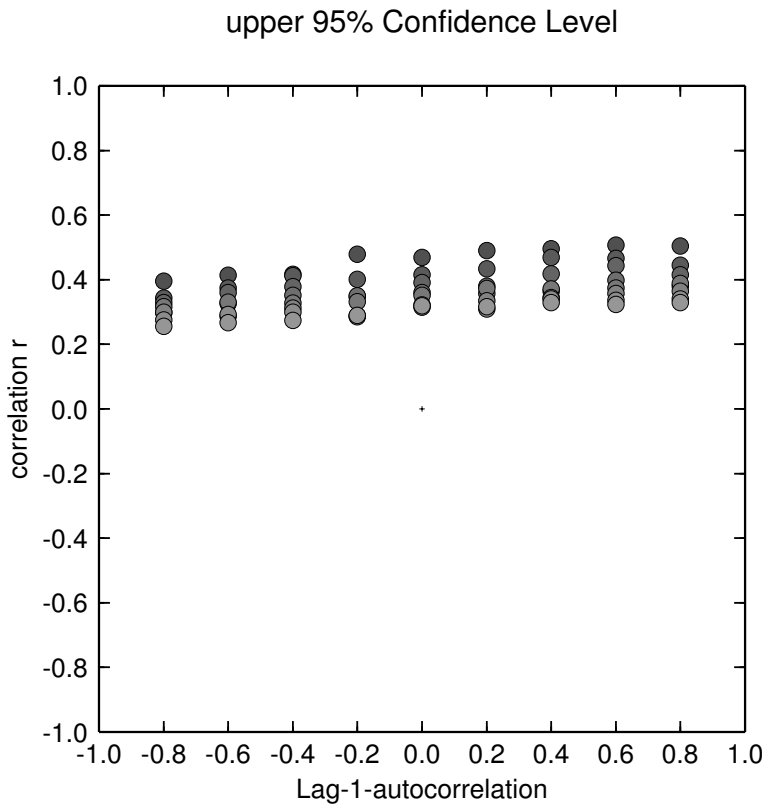


Figure B.3: *Estimated 95% confidence levels of the wavelet scale 3 correlation between independent AR(1)-processes using the CO6 filter. Note that the sample size $N$ gradually increased from 80–150 (increment 10). The darkest (lightest) colours mark the smallest (largest) sample sizes.*

# Bibliography


R. B. Alley, C.A. Shuman, D. A. Meese, A. J. Gow, K. C. Taylor, K. M. Cuffey, J. J. Fitzpatrick, P. M. Grootes, G. A. Zielinski, M. Ram, Spinelli G., and B. Elder. Visual-stratigraphic dating of the GISP2 ice core: Basis, reproducibility and application. *J. Geophys. Res.*, 102(C12): 26 367–26 381, 1997.

C. Appenzeller, J. Schwander, S. Sommer, and T. F. Stocker. The North Atlantic Oscillation and its imprint on precipitation and ice accumulation in Greenland. *Geophys. Res. Lett.*, 25(11): 1 939–1 942, 1998a.

C. Appenzeller, T. F. Stocker, and M. Anklin. North Atlantic Oscillation dynamics recorded in Greenland ice cores. *Science*, 282:446–449, 1998b.

A. Armengaud, R. D. Koster, J. Jouzel, and P. Ciais. Deuterium excess in Greenland snow: Analysis with simple and complex models. *J. Geophys. Res.*, 103(D8):8 947–8 953, 1998.

J. Bader and M. Latif. The impact of decadal-scale Indian Ocean sea surface temperature anomalies on Sahelian rainfall and the North Atlantic Oscillation. *Geophys. Res. Lett.*, 2003. accepted.

L. K. Barlow, J. C. Rogers, M. C. Serreze, and R. G. Barry. Aspects of climate variability in the North Atlantic sector: Discussion and relation to the Greenland Ice Sheet Project 2 high-resolution isotopic signal. *J. Geophys. Res.*, 102(C12):26 333–26 344, 1997.

L. K. Barlow, J. W. C. White, R. G. Barry, J. C. Rogers, and P. M. Grootes. The North Atlantic Oscillation signature in deuterium and deuterium excess signals in the Greenland Ice Sheet Project 2 ice core, 1840–1970. *Geophys. Res. Lett.*, 20(24):2 901–2 904, 1993.

T. P. Barnett, K. Hasselmann, M. Chelliah, T. Delworth, G. Hegerl, P. Jones, E. Rasmusson, E. Roeckner, C. Ropelewski, B. Santer, and S. Tett. Detection and attribution of recent climate change: A status report. *Bull. Amer. Meteor. Soc.*, 80(12):2 631–2 659, 1999.

T. P. Barnett and P. Jones. Comments on "Detection and attribution of recent climate change: A status report" — reply. *Bull. Amer. Meteor. Soc.*, 81(12):2 990–2 992, 2000.

J. J. Barsugli and D. S. Battisti. The basic effects of atmosphere-ocean thermal coupling on midlatitude variability. *J. Atmos. Sci.*, 55(4):477–493, 1998.

D. E. Black, L. C. Peterson, A. Overpeck, J. T. Kaplan, M. N. Evans, and M. Kashgarian. Eight centuries of North Atlantic ocean atmosphere variability. *Science*, 286:1 709–1 713, 1999.

R. Bleck. Numerical methods for computing moist isentropic trajectories. Final scientific report, Air Force Cambridge Res. Lab., 1967.

R. S. Bradley. *Paleoclimatology: Reconstructing climates of the Quaternary*, volume 68 of *International Geophysics Series*. Academic Press, San Diego, 2nd edition, 1999.

R. S. Bradley, M. K. Hughes, and M. E. Mann. Comments on "Detection and attribution of recent climate change: A status report". *Bull. Amer. Meteor. Soc.*, 81(12):2 987–2 990, 2000.

C. S. Bretherton, M. Widmann, V. P. Dymnikov, J. M. Wallace, and I. Blade. The effective number of spatial degrees of freedom of a time-varying field. *J. Climate*, 12:1 990–2 009, 1999.

K. R. Briffa. Interpreting high-resolution proxy climate data — the example of dendroclimatology. In H. von Storch and A. Navarra, editors, *Analysis of Climate Variability: Applications of Statistical Techniques*, pages 77–94, Berlin, 1995. Springer Verlag.

K. R. Briffa, P. D. Jones, T. S. Bartholin, F. H. Schweingruber, W. Karlén, and P. Zetterberg. Fennoscandian summers from AD 500: Temperature changes on short and long timescales. *Climate Dynamics*, 7:111–119, 1992.

K. R. Briffa and T. J. Osborn. Seeing the wood from the trees. *Science*, 284:926–927, 1999.

K. R. Briffa, T. J. Osborn, F. H. Schweingruber, I. C. Harris, P. D. Jones, S. G. Shiyatov, and E. A. Vaganov. Low-frequency temperature variations from a northern tree ring density network. *J. Geophys. Res.*, 106(D3):2 929–2 941, 2001.

K. R. Briffa, F. H. Schweingruber, P. D. Jones, T. J. Osborn, S. G. Shiyatov, and E. A. Vaganov. Reduced sensitivity of recent tree-growth to temperature at high northern latitudes. *Nature*, 391: 678–682, 1998.

D. H. Bromwich, Q. Chen, Y. Li, and R. I. Cullather. Precipitation over Greenland and its relation to the North Atlantic Oscillation. *J. Geophys. Res.*, 104(D18):22 103–22 115, 1999.

D. H. Bromwich, R. I. Cullather, Q. Chen, and B. Csathó. Evaluation of recent precipitation studies for Greenland ice sheet. *J. Geophys. Res.*, 103(D20):26 007–26 024, 1998.

P. Calanca. *The Atmospheric Water Vapour Budget over Greenland*. PhD thesis, Geographisches Institut ETH Zürich, 1994.

C. D. Charles, D. Rind, J. Jouzel, R. D. Koster, and R. G. Fairbanks. Glacial-interglacial changes in moisture sources for Greenland: Influences on the ice core record of climate. *Science*, 263: 508–511, 1994.

Q.-S. Chen, D. H. Bromwich, and B. Lesheng. Precipitation over Greenland retrieved by a dynamic method and its relation to cyclonic activity. *J. Climate*, 10:839–870, 1997.

CLIVAR. CLIVAR - A Research Programme on Climate Variability and Predictability for the 21st Century, 1997. Available at http://www.clivar.com/publications/clivar_doc_list.htm [out of print].

D. Comaniciu and P. Meer. Distribution free decomposition of multivariate data. *Pattern Analysis & Applications*, 2:22–30, 1999.

E. R. Cook. Multi-proxy reconstruction of the North Atlantic Oscillation index: a critical review and a new well-verified winter NAO index reconstruction back to AD 1400. In *The North Atlantic Oscillation*, number 134 in Geophysical Monograph Series, pages 63–79. American Geophyscial Union (AGU), Washington, 2003.

E. R. Cook, K. R. Briffa, and P. D. Jones. Spatial regression methods in dendroclimatology: A review and comparison of two techniques. *Int. J. Clim.*, 14:379–402, 1994.

E. R. Cook, R. D D'Arrigo, and K. R. Briffa. A reconstruction of the North Atlantic Oscillation using tree-ring chronologies from North America and Europe. *Holocene*, 8(1):9–17, 1998.

E. R. Cook, R. D. D'Arrigo, and M. E. Mann. A well-verified, multiproxy reconstruction of the winter North Atlantic Oscillation index since AD 1400. *J. Climate*, 15:1 754–1 764, 2002.

E. R. Cook, D. M. Meko, D. W. Stahle, and M. K. Cleaveland. Drought reconstructions for the continental United States. *J. Climate*, 12:1 145–1 162, 1999.

H. Craig. Isotopic variations in meteoric waters. *Science*, 133:1 702–1 703, 1961a.

H. Craig. Standards for reporting concentrations of deuterium and oxygen-18 in natural waters. *Science*, 133:1 833–1 834, 1961b.

T. J. Crowley. Causes of climate change over the past 1000 years. *Science*, 289:270–277, 2000.

K. M. Cuffey and E. J. Steig. Isotopic diffusion in polar firn: Implications for interpretation of seasonal climate parameters in ice-core records, with emphasis on central Greenland. *J. Glaciology*, 44(147):273–284, 1998.

R. I. Cullather and D. H. Bromwich. The atmospheric hydrologic cycle over the arctic basin from reanalyses, part I: Comparison with observations and previous studies. *J. Climate*, 13:923–937, 2000.

H. M. Cullen, R. D. D'Arrigo, and E. R. Cook. Multiproxy reconstructions of the North Atlantic Oscillation. *Paleoceanography*, 16(1):27–39, 2000.

A. Czaja and C. Frankignoul. Observed impact of Atlantic SST anomalies on the North Atlantic Oscillation. *J. Climate*, 15(6):606–623, 2002.

A. Czaja, A. W. Robertson, and T. Huck. The role of Atlantic ocean-atmosphere coupling in affecting North Atlantic Oscillation variability. In *The North Atlantic Oscillation*, number 134 in Geophysical Monograph Series, pages 147–172. American Geophyscial Union (AGU), Washington, 2003.

E. D. da Costa and A. C. de Verdiere. The 7.7-year North Atlantic Oscillation. *Quart. J. Roy. Meteor. Soc.*, 128:797–817, 2002.

E. F. Danielsen. Trajectories: Isobaric, isentropic and actual. *J. Met.*, 18:479–486, 1961.

W. Dansgaard. Stable isotopes in precipitation. *Tellus*, 14:436–468, 1964.

W. Dansgaard, S. J. Johnsen, N. Reeh, N. Gundestrup, H. B. Clausen, and C. U. Hammer. Climatic changes, Norsemen and modern man. *Nature*, 225:24–28, 1975.

C. I. Davidson, J.-L. Jaffrezo, M. J. Small, P. W. Summer, M. P. Olson, and R. D. Borys. Trajectory analysis of source regions influencing the South Greenland ice sheet during the Dye 3 gas and aerosol sampling program. *Atm. Env.*, 27A(17/18):2 739–2 749, 1993.

T. L. Delworth and R. J. Greatbatch. Multidecadal thermohaline circulation variability driven by atmospheric surface flux forcing. *J. Climate*, 13:1 481–1 495, 2000.

T. L. Delworth and T. R. Knutson. Simulation of early 20th century global warming. *Science*, 287:2 246–2 250, 2000.

P. A. Dirmeyer and K. L. Brubaker. Contrasting evaporative moisture sources during the drought of 1988 and the flood of 1993. *J. Geophys. Res.*, 104(D16):19 383–19 397, 1999.

P. D'Odorico, R. Revelli, and L. Ridolfi. On the use of neural networks for dendroclimatic reconstructions. *Geophys. Res. Lett.*, 27(6):791–794, 2000.

J. A. Eddy. The Maunder Minimum. *Science*, 192:1 189–1 202, 1976.

C. Eden and T. Jung. North Atlantic interdecadal variability: Oceanic response to the North Atlantic Oscillation. *J. Climate*, 14:676–691, 2001.

J. Esper, E. R. Cook, and F. H. Schweingruber. Low-frequency signals in long tree-ring chronologies for reconstructing past temperature variability. *Science*, 295:2 250–2 252, 2002.

M. N. Evans, A. Kaplan, and M. A. Cane. Pacific sea surface temperature field reconstruction from coral $\delta^{18}$O data using reduced space objective analysis. *Paleoceanography*, 17(10):7–1 to 7–12, 2002. 1007, DOI:10.1029/2000PA000590.

S. B. Feldstein. The recent trend and variance increase of the annular mode. *J. Climate*, 15:88–94, 2002.

D. A. Fisher. Remarks on the deuterium excess in precipitation in cold regions. *Tellus*, 43B: 401–407, 1991.

D. A. Fisher, R. M. Koerner, K. Kuivinen, H. B. Clausen, S. J. Johnsen, J.-P. Steffensen, N. Gundestrup, and C. U. Hammer. Inter-comparison of ice core $\delta(^{18}O)$ and precipitation records from sites in Canada and Greenland over the last 3500 years and over the last few centuries in detail using EOF techniques. In P. D. Jones, R. S. Bradley, and J. Jouzel, editors, *Climate Variations and Forcing Mechanisms of the Last 2000 Years*, volume I 41 of *NATO ASI Series*, pages 297–328. Springer-Verlag, New York, 1996.

D. A. Fisher, R. M. Koerner, W. S. B. Paterson, W. Dansgaard, N. Gundestrup, and N. Reeh. Effect of wind scouring on climatic records from ice-core oxygen-isotope profiles. *Nature*, 301: 205–209, 1983.

D. A. Fisher, N. Reeh, and H.B. Clausen. Stratigraphic noise in time series derived from ice cores. *Ann. Glaciology*, 7:76–83, 1985.

H. C. Fritts. *Tree Rings and Climate*. Academic Press, London, 1976.

H. E. Fuelberg, R. O. Loring Jr., M. V. Watson, M. C. Sinha, K. E. Pickering, A. M. Thompson, G. W. Sachse, D. R. Blake, and M. R. Schoeberl. TRACE a trajectory intercomparison — 2. Isentropic and kinematic methods. *J. Geophys. Res.*, 101(D19):23 927–23 939, 1996.

R. Garcia, L. Gimeno, E. Hernandez, R. Prieto, and P. Ribera. Reconstructing the North Atlantic atmospheric circulation in the 16th, 17th and 18th centuries from historical sources. *Clim. Res.*, 14:147–151, 2000.

Q. Geng and M. Sugi. Variability of the North Atlantic Cyclone activity in winter analyzed from NCEP-NCAR reanalysis data. *J. Climate*, 14:3 863–3 873, 2001.

A. Gershunov, N. Schneider, and T. Barnett. Low-frequency modulation of the ENSO-Indian Monsoon rainfall relationship. *J. Climate*, 14:2 486–2 492, 2001.

N. P. Gillett, H. F. Graf, and T. J. Osborn. Climate change and the North Atlantic Oscillation. In *The North Atlantic Oscillation*, number 134 in Geophysical Monograph Series, pages 193–209. American Geophyscial Union (AGU), Washington, 2003.

N. P. Gillett, G. C. Hegerl, M. R. Allen, and P. A. Stott. Implications of changes in the northern hemisphere circulation for the detection of anthropogenic climate change. *Geophys. Res. Lett.*, 27(7):993–996, 2000.

M. F. Glueck and C. W. Stockton. Reconstruction of the North Atlantic Oscillation 1429–1983. *Int. J. Climatol.*, 21:1 453–1 465, 2001.

R. J. Greatbatch. The North Atlantic Oscillation. *Stochastic Environmental Research and Risk Assessment*, 14(4–5):213–242, 2000.

A. Grötzner and M. Latif. A decadal climate cycle in the North Atlantic Ocean as simulated by the ECHO coupled GCM. *J. Climate*, 11:831–847, 1998.

J. Guiot. The extrapolation of recent climatological series with spectral canonical regression. *J. Climatol.*, 5:325–335, 1985.

S. K. Gulev, O. Zolina, and S. Grigoriev. Extratropical cyclone variability in the northern hemisphere winter from the NCEP-NCAR reanalysis data. *Climate Dynamics*, 17:795–809, 2001.

K. Hasselmann. Stochastic climate models: Part I. Theory. *Tellus*, 28:473–485, 1976.

M. Hilmer and T. Jung. Evidence for a recent change in the link between the North Atlantic Oscillation and Arctic sea ice export. *Geophys. Res. Lett.*, 27(7):989–992, 2000.

M. P. Hoerling, J. W. Hurrell, and T. Xu. Tropical origins for recent North Atlantic climate change. *Science*, 292:90–92, 2001.

M. P. Hoerling, J. W. Hurrell, T. Xu, G. T. Bates, and A. Phillips. Twentieth century North Atlantic climate change. Part II: Understanding the effect of Indian Ocean warming. *Climate Dynamics*, 2003. submitted.

G. Hoffmann, J. Jouzel, and S. Johnsen. Deuterium excess record from central Greenland over the last millenium: Hints of a North Atlantic signal during the Little Ice Age. *J. Geophys. Res.*, 106 (D13):14 265–14 274, 2001.

J. T. Houghton, Y. Ding, D. J. Griggs, M. Noguer, P. J. van der Linden, X. Dai, K. Maskell, and C. A. Johnson, editors. *Climate Change 2001: The Scientific Basis. Contribution of Working Group I to the Third Assessment Report of the Intergovernmental Panel on Climate Change*,

Cambridge, United Kingdom and New York, NY, USA, 2001. IPCC, Cambridge University Press.

C. J. Hsu and F. Zwiers. Climate change in recurrent regimes and modes of northern hemisphere atmospheric variability. *J. Geophys. Res.*, 106(D17):20 145–20 159, 2001.

J. W. Hurrell. Decadal trends in the North Atlantic Oscillation: Regional temperatures and precipitation. *Science*, 269:676–679, 1995.

J. W. Hurrell. Influence of variations in extratropical wintertime teleconnections on northern hemisphere temperature. *Geophys. Res. Lett.*, 23(6):665–668, 1996.

J. W. Hurrell, M. P. Hoerling, A. Phillips, and T. Xu. Twentieth century North Atlantic climate change. Part I: Assessing determinism. *Climate Dynamics*, 2003a. submitted.

J. W. Hurrell, Y. Kushnir, G. Ottersen, and M. Visbeck. An overview of the North Atlantic Oscillation. In *The North Atlantic Oscillation*, number 134 in Geophysical Monograph Series, pages 1–35. American Geophyscial Union (AGU), Washington, 2003b.

J. W. Hurrell and H. van Loon. Decadal variations in climate associated with the North Atlantic Oscillation. *Climatic Change*, 36:301–326, 1997.

IICC, 2003. International Ice-Core Cooperative, IGBP PAGES/World Data Center for Paleoclimatology, NOAA/NGDC Paleoclimatology Program, Boulder, Colorado, USA; http://www.ngdc.noaa.gov/paleo/icecore.html.

ITRDB, 2003. Contributors of the International Tree-Ring Data Bank, IGBP PAGES/World Data Center for Paleoclimatology, NOAA/NGDC Paleoclimatology Program, Boulder, Colorado, USA; http://www.ngdc.noaa.gov/paleo/treering.html.

J. Jacobeit, H. Wanner, J. Luterbacher, C. Beck, A. Philipp, and K. Sturm. Atmospheric circulation variability in the North-Atlantic-European area since the mid-seventeenth century. *Climate Dynamics*, 20:341–352, 2003. DOI:10.1007/s00382-002-0278-0.

S. J. Johnsen, W. Dansgaard, and H. B. Clausen. Climatic oscillations 1200–2000 AD. *Nature*, 227:482–483, 1970.

S. J. Johnsen, W. Dansgaard, H. B. Clausen, and C. C. Langway, jun. Oxygen isotope profiles through the Antarctic and Greenland ice sheets. *Nature*, 235:429–434, 1972.

S.J. Johnsen, W. Dansgaard, and J.W.C. White. The origin of Arctic precipitation under present and glacial conditions. *Tellus*, 41B:452–468, 1989.

P. D. Jones, K. R. Briffa, and T. J. Osborn. Changes in the northern hemisphere annual cycle: Implications for paleoclimatology? *J. Geophys. Res.*, 108(D18), 2003a. 4588,DOI:10.1029/2003JD003695.

P. D. Jones and M. Hulme. The changing temperature of 'Central England'. In *Climates of the British Isles: present, past and future*, pages 183–184. Routledge, London, 1997.

P. D. Jones, T. Jonsson, and D. Wheeler. Extension of the North Atlantic Oscillation using early instrumental pressure observations from Gibraltar and South-West Iceland. *Int. J. Climatol.*, 17:1433–1450, 1997.

P. D. Jones, T. J. Osborn, and K. R. Briffa. Pressure-based measures of the North Atlantic Oscillation NAO: A comparison and an assessment of changes in the strength of the NAO and in its influence on surface climate parameters. In *The North Atlantic Oscillation*, number 134 in Geophysical Monograph Series, pages 51–62. American Geophyscial Union (AGU), Washington, 2003b.

P. D. Jones, T. J. Osborn, K. R. Briffa, C.K. Folland, E. B. Horton, L. V. Alexander, D. E. Parker, and N. A. Rayner. Adjusting for sampling density in grid box land and ocean surface temperature time series. *J. Geophys. Res.*, 106(D4):3 371–3 380, 2001.

J. Jouzel and L. Merlivat. Deuterium and oxygen 18 in precipitation: Modeling of the isotopic effects during snow formation. *J. Geophys. Res.*, D7:11 749–11 757, 1984.

T. Jung. *The North Atlantic Oscillation: Variability and Interactions with the North Atlantic Ocean and Artic Sea Ice*. PhD thesis, Institut für Meereskunde an der Christian-Albrechts-Universität Kiel, Düsternbrooker Weg 20, D-24105 Kiel, Germany, 2000.

T. Jung, M. Hilmer, E. Ruprecht, S. K. Kleppek, S. Gulev, and O. Zolina. Characteristics of the recent eastward shift of interannual NAO variability. *J. Climate*, 16:3 371–3 3382, 2003.

J. D. Kahl, J. M. Harris, and G. A. Herbert. Intercomparison of three long-range trajectory models applied to Arctic haze. *Tellus*, 41B:525–536, 1989.

J. D. W. Kahl, D. A. Martinez, H. Kuhns, C. I. Davidson, J.-L. Jaffrezo, and J. M. Harris. Air mass trajectories to Summit, Greenland: A 44-year climatology and some episodic events. *J. Geophys. Res.*, 102(D12):26 861–26 875, 1997.

E. Kalnay, M. Kanamitsu, R. Kistler, W. Collins, D. Deavean, L. Gandin, M. Iredell, S. Saha, G. White, J. Woollen, Y. Zhu, M. Chelliah, W. Ebisuzaki, W. Higgins, Janowiak J., K. C. Mo, C. Ropelewski, J. Wang, A. Leetmaa, R. Reynolds, R. Jenne, and D. Joseph. The NCEP/NCAR 40-year reanalysis project. *Bull. Amer. Meteor. Soc.*, 77:437–471, 1996.

A. R. Kerr. A North Atlantic climate pacemaker for the centuries. *Science*, 288:1 984–1 986, 2000.

R. Kistler, E. Kalnay, W. Collins, S. Saha, G. White, J. Woollen, M. Chelliah, W. Ebisuzaki, M. Kanamitsu, V. Kousky, H. van den Dool, R. Jenne, and M. Fiorino. The NCEP-NCAR 50-year reanalysis: Monthly means CD-ROM and documentation. *Bull. Amer. Meteor. Soc.*, 82(2): 247–268, 2001.

S. Kleppek. Einfluss der NAO auf das Klima Europas anhand von Verteilungsfunktionen atmosphärischer Parameter. Master's thesis, Institut für Meereskunde an der Universität zu Kiel, Düsternbrooker Weg 20, 24105 Kiel, Germany, 2001.

R. Koster, J. Jouzel, R. Suozzo, G. Russell, W. Broecker, D. Rind, and P. Eagleson. Global sources of local precipitation as determined by the NASA/GISS GCM. *Geophys. Res. Lett.*, 13(1):121–124, 1986.

H. Kuhnert, T. Crueger, and Pätzold J. Bermua coral records of North Atlantic climate variability. [EAE03-A-03491; CL21-1MO2P-1059], presented at the EGS-AGU-EUG Joint Assembly, Nice, France., 2003.

Y. Kushnir, W. A. Robinson, I. Bladé, N. M. Hall, S. Peng, and R. Sutton. Atmospheric GCM response to extratropical SST anomalies: Synthesis and evaluation. *J. Climate*, 15:2 233–2 236, 2002.

P. J. Lamb and R. A. Peppler. North Atlantic Oscillation: Concept and an application. *Bull. Amer. Meteor. Soc.*, 68(10):1 218–1 225, 1987.

M. Latif, K. Arpe, and E. Roeckner. Oceanic control of decadal North Atlantic sea level pressure variability in winter. *Geophys. Res. Lett.*, 27(5):727–730, 2000.

M. Latif, E. Roeckner, M. Botzet, M. Esch, H. Haak, S. Hagemann, J. Jungclaus, S. Legutke, S. Marsland, U. Mikolajewicz, and J. Mitchell. Reconstructing, monitoring, and predicting decadal-scale changes in the North Atlantic thermohaline circulation with sea surface temperature. *J. Climate*, 2003. accepted.

J. Lean, J. Beer, and R. Bradley. Reconstruction of solar irradiance since 1610: Implications for climate change. *Geophys. Res. Lett.*, 22(23):3 195–3 198, 1995.

G. Leckebusch. *Meteorologiche Interpretation von Depositionen in polaren Eisbohrkernen mit Hilfe von Paläosimulationen des Klimamodells ECHAM3*. PhD thesis, Institut für Geophysik und Meteorologie der Universität zu Köln, 1999.

U. Löptien. *Über die Wechselwirkung zwischen Ozean und Atmosphäre im Zusammenhang mit der Nordatlantischen Oszillation*. PhD thesis, Institut für Meereskunde an der Universität zu Kiel, Düsternbrooker Weg 20, 24105 Kiel, Germany, 2003.

J. Luterbacher, R. Rickli, E. Xoplaki, C. Tinguely, C. Beck, C. Pfister, and H. Wanner. The Late Maunder Minimum (1675-1715) — A key period for studying decadal scale climatic change in Europe. *Clim. Change*, 49:441–462, 2001.

J. Luterbacher, C. Schmutz, D. Gyalistras, E. Xoplaki, and H. Wanner. Reconstruction of monthly NAO and EU indices back to AD 1675. *Geophys. Res. Lett.*, 26(17):2 745–2 748, 1999.

J. Luterbacher, E. Xoplaki, D. Dietrich, P. D Jones, T. D. Davies, D. Portis, J. F. Gonzalez-Rouco, H. von Storch, D. Gyalistras, C. Casty, and H. Wanner. Extending North Atlantic Oscillation reconstructions back to 1500. *Atm. Sci. Lett.*, 2:114–124, 2002a. DOI:10.1006/asle.2001.0044.

J. Luterbacher, E. Xoplaki, D. Dietrich, R. Rickli, J. Jacobeit, C. Beck, D. Gyalistras, C. Schmutz, and H. Wanner. Reconstruction of sea level pressure fields over the eastern North Atlantic and Europe back to 1500. *Climate Dynamics*, 18:545–561, 2002b. DOI:10.1007/s00382-001-0196-6.

H. Mächel, A. Kapala, and H. Flohn. Behaviour of the centres of action above the Atlantic since 1881. Part I: Characteristics of seasonal and interannual variability. *Int. J. Climatol.*, 18:1–22, 1998.

G. Manley. Central England temperatures: Monthly means 1659 to 1973. *Quart. J. Roy. Meteor. Soc.*, 100:389–405, 1974.

M. E. Mann. The value of multiple proxies. *Science*, 297:1 481–1 482, 2002.

M. E. Mann, R. S. Bradley, and M. K. Hughes. Global-scale temperature patterns and climate forcing over the past six centuries. *Nature*, 392:779–787, 1998.

M. E. Mann and P. D. Jones. Global surface temperatures over the past two millennia. *Geophys. Res. Lett.*, 30(15):CLM 5–1 – 5–4, 2003. 1820,DOI:10.1029/2003GL017814.

M. E. Mann and S. Rutherford. Climate reconstruction using 'Pseudoproxies'. *Geophys. Res. Lett.*, 29(10):139–1 – 139–4, 2002. DOI:10.1029/2001GL014554.

J. Marshall, Y. Kushnir, D. Battisti, P. Chang, A. Czaja, R. Dickson, J. Hurrell, R. McCartney, M. Saravanan, and M. Visbeck. North Atlantic climate variability: Phenomena, impacts and mechanisms. *Int. J. Climatol.*, 21:1 863–1 898, 2001. DOI:10.1002/joc.693.

L. D. Meeker and P. Mayewski. A 1400-year high-resolution record of atmospheric circulation over the North Atlantic and Asia. *Holocene*, 12(3):257–266, 2002.

D. A. Meese, A. J. Gow, R. B. Alley, G. A. Zielinski, P. M. Grootes, M. Ram, K. C. Taylor, P. A. Mayewski, and J. F. Bolzan. The Greenland Ice Sheet Project 2 depth-age scale: Methods and results. *J. Geophys. Res.*, 102(C12):26 411–26 423, 1997.

D. Meko. Dendroclimatic reconstruction with time varying predictor subsets of tree indices. *J. Climate*, 10:687–696, 1997.

D. Melzer, H. Kunz, M. Stendel, M. Barbulescu, G. Leckebusch, and A Reiner. Programmdokumentation zum „Trajektorienpaket". Institut für Geophysik und Meteorologie der Universität zu Köln, 1998.

L. Merlivat and J. Jouzel. Global climatic interpretation of the deuterium-oxygen 18 relationship for precipitation. *J. Geophys. Res.*, 84(C8):5 029–5 033, 1979.

J. T. Merrill. Isentropic airflow probability analysis. *J. Geophys. Res.*, 99(D12):25 881–25 889, 1994.

J.T. Merrill, R. Bleck, and D. Boudra. Techniques of Langrangian trajectory analysis in isentropic coordinates. *Mon. Wea. Rev.*, 114:571–581, 1986.

V. M. Metha, M. J. Suarez, J. V. Manganello, and T. L. Delworth. Oceanic influence on the North Atlantic Oscillation and associated northern hemisphere climate variations: 1959–1993. *Geophys. Res. Lett.*, 27(1):121–124, 2000.

V. L. Mitchell. An investigation of certain aspects of tree growth rates in relation to climate in the central Canadian boreal forest. Technical Report 33, Univ. of Wisconsin, Dept. Meteorol., 1967. Task NR 387-022, ONR Contract 1202(07), NFS GP-5572X, Madison.

G. North, T. R. Bell, R. Cahalan, and F. Moeng. Sampling errors in estimation of empirical orthogonal functions. *Mon. Wea. Rev.*, 110:699–706, 1982.

A. Ohmura and N. Reeh. New precipitation and accumulation maps for Greenland. *J. Glaciology*, 37(125):140–148, 1991.

T. J. Osborn and K. R. Briffa. Revisiting timescale-dependent reconstruction of climate from tree-ring chronologies. *Dendrochronologia*, 18:9–25, 2000.

T. J. Osborn, K. R. Briffa, S. F. B. Tett, P. D. Jones, and R. M. Trigo. Evaluation of the North Atlantic Oscillation as simulated by a coupled climate model. *Climate Dynamics*, 15:685–702, 1999.

H. Paeth, A. Hense, R. Glowienka-Hense, R. Voss, and U. Cubasch. The North Atlantic Oscillation as an indicator for greenhouse-gas induced climate change. *Climate Dynamics*, 15:953–960, 1999.

H. Paeth, M. Latif, and A. Hense. Global SST influence on twentieth century NAO variability. *Climate Dynamics*, 21:61–75, 2003. DOI:10.1007/s00382-003-0318-4.

W. C. Palmer. Meteorological drought. Weather Bureau Research Paper 45, U.S. Department of Commerce, 1965. 58 pp.

D. B. Percival and A. T. Walden. *Wavelet methods for time series analysis*. Cambridge Univ. Pr., Cambridge, 2000.

R. A. Petersen and L. W. Uccellini. The computation of isentropic atmospheric trajectories using a "discrete model" formulation. *Mon. Wea. Rev.*, 107:566–574, 1979.

D. H. Portis, J. E. Walsh, M. El Hamly, and P. J. Lamb. Seasonality of the North Atlantic Oscillation. *J. Climate*, 14:2 069–2 078, 2001.

D. Pozo-Vázquez, M. J. Esteban-Parra, F. S. Rodrigo, and Y. Castro-Díez. A study of NAO variability and its possible non-linear influences on European surface temperatures. *Climate Dynamics*, 17:701–715, 2001.

R. W. Preisendorfer. *Principal Component Analysis in Meteorology and Oceanography*. Elsevier, Amsterdam, 1988.

W. H. Press, B. P. Flannery, S. A. Teukolsky, and W. T. Vetterling. *Numerical Recipes in FORTRAN 77: The Art of Scientific Computing*. Cambridge Univ. Pr., Cambridge, 2nd edition, 1999.

C. J. Proctor, A. Baker, W. L. Barnes, and M. A. Gilmour. A thousand year speleothem proxy record of North Atlantic climate from Scotland. *Climate Dynamics*, 16:815–820, 2000.

N. Rimbu, G. Lohmann, T. Felis, and J. Pätzold. Arctic Oscillation signature in a Red Sea coral. *Geophys. Res. Lett.*, 28(15):2 959–2 962, 2001.

F. M. Robasky and D. H. Bromwich. Greenland precipitation estimates from the atmospheric moisture budget. *Geophys. Res. Lett.*, 21(23):2 495–2 498, 1994.

F. S. Rodrigo, D. Pozo-Vázquez, M. J. Esteban-Parra, and Y. Castro-Díez. A reconstruction of the winter North Atlantic Oscillation index back to A.D. 1501 using documentary data in southern Spain. *J. Geophys. Res.*, 106(D14):14 805–14 818, 2001.

M. J. Rodwell, D. P. Rowell, and C. K. Folland. Oceanic forcing of the wintertime North Atlantic Oscillation and European climate. *Nature*, 398:320–323, 1999.

J. C. Rogers. The association between the North Atlantic Oscillation and the Southern Oscillation in the northern hemisphere. *Mon. Wea. Rev.*, 112:1 999–2 015, 1984.

J. C. Rogers. North Atlantic storm track variability and its association to the North Atlantic Oscillation and climate variability of northern Europe. *J. Climate*, 10:1 635–1 647, 1997.

J. C. Rogers, J. F. Bolzan, and V. A. Pohjola. Atmospheric circulation variability associated with shallow-core seasonal isotopic extremes near Summit, Greenland. *J. Geophys. Res.*, 103(D10): 11 205–11 219, 1998.

E. Ruprecht, S.S. Schröder, and S. Ubl. On the relation between NAO and water vapour transport towards Europe. *Meteor. Z.*, 6:395–401, 2002.

S. Rutherford, M. E. Mann, T. L. Delworth, and R. J. Stouffer. Climate field reconstruction under stationary and nonstationary forcing. *J. Climate*, 16:462–479, 2003.

M. E. Schlesinger and N. Ramankutty. An oscillation in the global climate system of period 65–70 years. *Nature*, 367:723–726, 1994.

C. Schmutz, J. Luterbacher, D. Gyalistras, E. Xoplaki, and H. Wanner. Can we trust proxy-based NAO index reconstructions? *Geophys. Res. Lett.*, 27(8):1 135–1 138, 2000.

T. Schneider. Analysis of incomplete climate data: Estimation of mean values and covariance matrices and imputation of missing values. *J. Climate*, 14:853–871, 2001.

S. S. Schröder. Wasserdampftransport über dem Nordatlantik in Abhängigkeit von der Nordatlantischen Oszillation. Master's thesis, Institut für Meereskunde an der Universität zu Kiel, Düsternbrooker Weg 20, 24105 Kiel, Germany, 2001.

F. H. Schweingruber. *Tree rings: Basics and Applications of Dendrochronology*. Kluwer, Dordrecht, Holland, 1988.

M. C. Serreze, R. G. Barry, M. C. Rehder, and J. E. Walsh. Variability in atmospheric circulation and moisture flux over the Arctic. *Philos. T. Roy. Soc.*, A352(1699):215–225, 1995.

M. C. Serreze, F. Carse, R. G. Barry, and J. C. Rogers. Icelandic low cyclone activity: Climatological features, linkages with the NAO, and relationships with recent changes in the northern hemisphere circulation. *J. Climate*, 10:453–464, 1997.

D. T. Shindell, G. A. Schmidt, M. E. Mann, D. Rind, and A. Walpe. Solar forcing of regional climate change during the Maunder Minimum. *Science*, 294:2 149–2 152, 2001.

M. Sickmöller, R. Blender, and K. Fraedrich. Observed winter cyclone tracks in the northern hemisphere in re-analysed ECMWF data. *Quart. J. Roy. Meteor. Soc.*, 126:591–620, 2000.

B. W. Silverman. *Density Estimation for Statistics and Data Analysis*. Chapman & Hall/CRC, 1986.

W. Soon and S. Baliunas. Proxy climatic and environmental changes of the past 1000 years. *Climate Research*, 23:89–110, 2003.

C. R. Stearns, G. A. Weidner, and L. M. Keller. Atmospheric circulation around the Greenland crest. *J. Geophys. Res.*, 102(D12):13 801–13 812, 1997.

D. B. Stephenson and V. Pavan. The North Atlantic Oscillation in coupled climate models: a CMIP1 evaluation. *Climate Dynamics*, 20:381–399, 2003. DOI: 10.1007/s00382-002-0281-5.

R. T. Sutton and M. R. Allen. Decadal predictability of North Atlantic sea surface temperature and climate. *Nature*, 388:563–567, 1997.

A. Timmermann, M. Latif, R. Voss, and A. Grötzner. North Atlantic interdecadal variability: A coupled air-sea mode. *J. Climate*, 11:1 906–1 931, 1998.

K. E. Trenberth and D. A. Paolino. The northern hemisphere sea level pressure data set: Trends, errors and discontinuities. *Mon. Wea. Rev.*, 108:855–872, 1980.

S. Ubl. Variabilität von Zykloneneigenschaften über dem Nordatlantik. Master's thesis, Institut für Meereskunde an der Universität zu Kiel, Düsternbrooker Weg 20, 24105 Kiel, Germany, 2001.

U. Ulbrich and M. Christoph. A shift of the NAO and increasing storm track activity over Europe due to anthropogenic greenhouse gas forcing. *Climate Dynamics*, 15:551–559, 1999.

B.M Vinther, S. J. Johnsen, K. K. Anderson, H. B. Clausen, and A. W. Hansen. NAO signal recorded in the stable isotopes of Greenland ice cores. *Geophys. Res. Lett.*, 30(7), 2003. 1387,DOI:10.1029/2002GL016193.

M. Visbeck, E. P. Chassignet, R. G. Curry, T. L. Delworth, R. R. Dickson, and G. Krahmann. The ocean's response to North Atlantic Oscillation variability. In *The North Atlantic Oscillation*, number 134 in Geophysical Monograph Series, pages 113–145. American Geophyscial Union (AGU), Washington, 2003.

H. von Storch and F. W. Zwiers. *Statistical Analysis in Climate Research*. Cambridge Univeristy Press, Cambridge, UK, 1999.

G. T. Walker. Correlation in seasonal variation of weather, IX. *Mem. Ind. Met. Dept.*, 25:275–332, 1924.

G. T. Walker and E. W. Bliss. World weather V. *Mem. Roy. Met. Soc.*, 4(36):53–84, 1932.

H. Wanner, S. Brönnimann, C. Casty, D. Gyalistras, J. Luterbacher, C. Schmutz, D. B. Stephenson, and E. Xoplaki. North Atlantic Oscillation — concepts and studies. *Surv. Geophys.*, 22:321–382, 2001.

H. Wanner, C. Pfister, R. Brázdil, P. Frich, K. Frydendahl, T. Jónsson, J. Kington, H. H. Lamb, S. Rosenørn, and E. Wishmann. Wintertime European circulation patterns during the Late Maunder Minimum cooling period (1675–1704). *Theo. Appl. Climatol.*, 51:167–175, 1995.

WDC, 2003. World Data Center for Paleoclimatology, IGBP PAGES/World Data Center for Paleoclimatology, NOAA/NGDC Paleoclimatology Program, Boulder, Colorado, USA; http://www.ngdc.noaa.gov/paleo/data.html.

M. Werner. *Spatial and Temporal Variability of Water Isotopes in Polar Precipitation*. PhD thesis, Max-Planck-Institut für Meterorologie Hamburg, 2000.

M. Werner and M. Heimann. Modeling interannual variability of water isotopes in Greenland and antarctica. *J. Geophys. Res.*, D1:ACL1 1–12, 2002. DOI:10.1029/2001JD900253.

I. M. Whillans and P. M. Grootes. Isotopic diffusion in cold snow and firn. *J. Geophys. Res.*, 90 (D2):3 910–3 918, 1985.

B. Whitcher, P. Guttorp, and D. B. Percival. Wavelet analysis of covariance with application to atmospheric time series. *J. Geophys. Res.*, 105(D11):14 941–14 962, 2000.

J. W. C. White, L. K. Barlow, D. Fisher, P. M. Grootes, J. Jouzel, S. J. Johnson, M. Stuiver, and H. Clausen. The climate signal in the stable isotopes of snow from Summit, Greenland: Results of comparisons with modern climate observations. *J. Geophys. Res.*, 102(C12):26 425–26 439, 1997.

J. W. C. White, D. Gorodetzkey, E. R. Cook, and L. K. Barlow. Frequency analysis of an annually resolved, 700 year paleoclimate record from the GISP2 ice core. In P. D. Jones, R. S. Bradley, and J. Jouzel, editors, *Climate Variations and Forcing Mechanisms of the last 2000 Years*, volume I 41 of *NATO ASI Series*, pages 191–212. Springer-Verlag, New York, 1996.

P. Wu and C. Gordon. Oceanic influence on North Atlantic climate variability. *J. Climate*, 15: 1 911–1 925, 2002.

C. Wunsch. The interpretation of short climate records, with comments on the North Alantic and Southern Oscillation. *Bull. Amer. Meteor. Soc.*, 80(2):245–255, 1999.

E. Zorita and F. González-Rouco. Are temperature-sensitive proxies adequate for North Atlantic Oscillation reconstructions? *Geophys. Res. Lett.*, 29(14):48–1 to 48–4, 2002. 1703, DOI:10.1029/2002GL015404.

E. Zorita, F. González-Rouco, and S. Legutke. Testing the Mann et al. (1998) approach to paleoclimate reconstructions in the context of a 1000-yr control simulation with the ECHO-G coupled climate model. *J. Climate*, 16:1 378–1 390, 2003.

# Danksagung

Ich möchte mich sehr herzlich bei meinem Doktorvater Herrn Prof. Dr. Eberhard Ruprecht für die Betreuung und Förderung - die schon weit vor meiner Promotionszeit begann - bedanken. Ich danke Herrn Prof. Dr. Wolf-Christian Dullo für die bereitwillige Übernahme des Korreferates.

Insbesondere möchte ich Dr. Thomas Jung dafür danken, dass er mich an die wissenschaftlichen Arbeitsmethoden herangeführt hat und dass er in seiner uneigennützigen Art seine Statistikprogramme zur Verfügung stellt. Vielen Dank Thomas!

Axel Timmermann, Ulrike Löptien, Marco Clemens, Juerg Luterbacher und Sergey Gulev bedarf es einer besonderen Erwähnung, da sie mit ihren anregenden Diskussionen ungemein dazu beigetragen haben, dass ich nie den Spaß an der Forschung verloren habe.

Diese Arbeit wäre ohne die ständige Unterstützung von den vielen Kollegen hier am Institut - inklusive Rechenzentrum - nicht möglich gewesen. Danke!

Allen, die mir bei der Fertigstellung des Manuskripts mit Rat und Tat geholfen haben, sei hier nochmals gedankt!

Besonders herzlich möchte ich mich bei meiner Familie für die Unterstützung bedanken.

Diese Arbeit wurde im Rahmen des Sonderforschungsbereiches (SFB) 460 „Dynamik Thermohaliner Zirkulationsschwankungen” durch die Deutsche Forschungsgemeinschaft (DFG) finanziell gefördert.

**Lebenslauf** — Oliver Timm Kiel, 3. November 2003

| | |
|---|---|
| 27. November 1973 | geboren in Eutin, Kreis Ostholstein<br>deutsche Staatsangehörigkeit |
| August 1980 – Juli 1984 | Grundschule, Malente, Kreis Ostholstein |
| August 1984 – Juli 1993 | Carl-Maria-von-Weber-Gymnasium, Eutin, Kreis Ostholstein<br>Abschluss: Allgemeine Hochschulreife |
| Oktober 1993 – September 1994 | Grundwehrdienst |
| Oktober 1994 – Januar 2000 | Studium der Meteorologie<br>an der Christian-Albrechts-Universität zu Kiel<br>Abschluss: Diplom im Fach Meteorologie |
| seit Februar 2000 | wissenschaftlicher Mitarbeiter im Sonderforschungsbereich 460,<br>Gelegenheit zur Promotion mit dem Thema: *Zeitreihenanalyse und Interpretation von paläoklimatischen Zeitreihen zur Erkennung der Nordatlantischen Oszillation* |

**Erklärung**

Meine Abhandlung zur Promotion ist – abgesehen von der Beratung durch meine akademischen Lehrer – nach Inhalt und Form meine eigene Arbeit. Sie hat weder ganz noch teilweise hier oder an anderer Stelle im Rahmen eines Prüfungsverfahrens zuvor vorgelegen.

Kiel, den .....

(Oliver Timm)